Electrospinning Bicomponent Nanofibres for Platinum Ion Extraction from Acidic Solutions

by

Abraham Cilliers Willemse

Dissertation presented in partial fulfilment of the requirements for the degree of Master of Science

at the

Stellenbosch University

Supervisor: Dr Anton E. Smit
Co-Supervisor: Prof Klaus R. Koch
Department of Chemistry and Polymer Science
Faculty of Natural Sciences

March 2013

DECLARATION

By submitting this dissertation, I declare that the entirety of the work contained therein is my own, original work, that I am the owner of the copyright thereof (save to the extent explicitly otherwise stated), that reproduction and publication thereof by Stellenbosch University will not infringe any third party rights and that I have not previously in its entirety or in part submitted it for obtaining any qualification.

Abraham C. Willemse
Stellenbosch, March 2013

Even though the road is tough
and walking it is sometimes rough,
the people who make you smile
make the journey worthwhile.

This work is dedicated to those people.

ENGLISH ABSTRACT

Trace amounts of soluble Pt(II/IV) ions are not recovered using current refining processes. There are both economic and environmental incentives to recover these Pt(II/IV) ions from effluent. The work presented in this dissertation was aimed at producing functionalised electrospun nanofibre webs for the extraction of trace amounts of Pt(II/IV) ions in the form of $[PtCl_6]^{2-}$ from acidic solutions.

An insoluble, low molecular weight oligomeric compound, poly(*N*-terephthaloylthiourea)-*N*',*N*'-piperazine, was synthesised from relatively inexpensive starting reagents using a "one-pot" two step synthesis procedure. Interest in this compound lies in its ability to extract Pt(II/IV) ions from acidic, chloride-rich solutions, as may be encountered in real process solutions in platinum group metal refineries. The product was isolated and characterised with an array of techniques, including GPC, elemental analysis, ^{1}H and ^{13}C NMR, as well as FTIR, and it was found to be a mixture of various molecular weight fractions with a degree of chemical variance between oligomer chains.

The poly(*N*-terephthaloylthiourea)-*N*',*N*'-piperazine was blended with polyacrylonitrile (PAN) and electrospun using both the classical single needle approach as well as a high throughput free-surface electrospinning process, called ball electrospinning. The nanofibres consisted of the oligomer which provided the affinity for $[PtCl_6]^{2-}$ while PAN provided sufficient polymer chain entanglement which allowed the formation of fibrous structures. Two different solutions were found to produce nanofibres with the desired dimensions, namely: 6 wt% and 8 wt% PAN solution, both having a PAN to oligomer ratio of 7:3. The fibres produced by needle electrospinning and ball electrospinning had average fibre diameters of 172 ± 35 nm and 210 ± 49 nm, respectively. The ball electrospinning process had 86 times greater fibre production rates compared to needle electrospinning.

The effects of three experimental conditions on the recovery of Pt(II/IV) ions by the poly(*N*-terephthaloylthiourea)-*N*',*N*'-piperazine-containing nanofibres were determined. The conditions were: (i) the effects of specific surface area and available coordination sites over time, (ii) the effect of extraction temperature, and (iii) the effect of hydrochloric acid (HCl) concentration on $[PtCl_6]^{2-}$ extraction. Increased availability of coordination sites caused an increase in Pt ion extraction. The Pt ion extraction also increased from 0.007 g to 0.023 g for each gram of nanofibres used as the temperature was increased from 20 °C to 60 °C when using a 114 mg/L Pt stock solution. The HCl concentration had no effect on Pt ion extraction when varied between 1.0×10^{-3} M to 1 M, while increased extraction as well as fibre damage was caused at HCl concentrations greater than 1 M.

Nanofibres containing an oligomeric compound with affinity for $[PtCl_6]^{2-}$ in acidic solutions were successfully synthesised and used to extract trace amounts of Pt(II/IV) ions from solutions under various conditions.

AFRIKAANSE OPSOMMING

In huidige verfynings prosesse word spoorelemente van oplosbare Pt(II/IV) nie herwin nie. Daar is beide ekonomiese en omgewings insentiewe om hierdie Pt(II/IV) ione te verhaal uit die afval oplossings. Hierdie tesis was gemik daarop om funksionele elektrospinde nanovesel webbe te produseer vir die herwinning van Pt(II/IV) ioon spoorelemente in die vorm van $[PtCl_6]^{2-}$ uit aangesuurde oplossings.

'n Onoplosbare oligomeriese verbinding met 'n lae molukulêre gewig, poly(*N*-terephthaloylthiourea)-*N*',*N*'-piperazine, was uit relatief goedkoop begin reagense gesintetiseer deur gebruik te maak van 'n "een-pot" twee stap prosedure. Die belangrikheid van die verbinding lê in sy vermoë om Pt(II/IV) ione uit aangesuurde, chloried-ryke oplossing te onttrek, soos wat in alledaagse afval oplossings van platinum-groep metalurgiese raffinaderye ondervind kan word. Die sintese produk was geisoleer en gekarakariseer deur gebruik te maak van 'n verskeidenheid tegnieke, waaronder GPC, elementêre analise, ^{1}H en ^{13}C NMR sowel as FTIR, en daar was bepaal dat die produk bestaan uit 'n mengsel van verskeie molukulêre gewig kettings met 'n mate van chemiese variansie tussen hulle.

Die gesintetiseerde oligometriese verbinding was gemeng met poliakrielonitriel (PAN) en elektrospin deur gebruik te maak van beide die klasieke naald spin proses, sowel as 'n hoë-produksie vrye oppervlak spin proses, genaamd die bal elektrospin proses. Die nanovesels bestaan uit die oligomeer wat die affiniteit vir die $[PtCl_6]^{2-}$ voorsien terwyl die PAN genoegsame polimeer ketting verstrengeling veroorsaak het om die veselagtige struktuur te vorm. Nanovesels met die gewensde dimensies was gevorm deur die elektrospin proses toe te pas op twee verskillende oplossings, naamlik: 'n 6 massa persent PAN en 'n 8 massa persent PAN oplossing, beide met 'n PAN tot oligomeer verhouding van 7:3. Die vesels geproduseer deur die naald en bal elektrospin prosesse het 'n gemiddelde vesel deursneë gehad van 172 ± 35 nm en 210 ± 49 nm, onderskeidelik. Die bal spin proses het egter 'n 86 keer groter produksie kapasiteit van vesels gehad in vergelyking met die naald spin proses.

Die effek van drie verskillende toestande op die effektiwiteit van die nanovesels, wat poly(*N*-terephthaloylthiourea)-*N*',*N*'-piperazine bevat, om Pt(II/IV) ione te onttrek uit die oplossings was ondersoek. Die toestande was: (i) die effekte van spesifieke oppervlak area asook beskikbare ontginnings setels oor tyd, (ii) die effek van die ontginnings temperatuur, en (iii) die effek van die soutsuur (HCl) konsentrasie op die Pt ioon ontginning. 'n Toename in die beskikbaarheid van die ontginnings setels het gelei tot 'n toename in die Pt ioon ontginning. Die Pt ioon ontginning het toegeneem van 0.007 g tot 0.023 g vir elke gram van nanovesels gebruik soos die temperatuur verhoog was van 20 °C tot 60 °C wanneer 'n 114 ppm (m/v) Pt ioon oplossing gebruik was. Daar was geen effek op die Pt ioon ontginning toe die HCl konsentrasie tussen 1.0 x 10-3 M en 1 M HCl varieer was nie, alhoewel daar by konsentrasies hoër as 1M 'n verhoogde ontginning sowel as vesel skade was.

Nanovesels wat ‘n oligemetriese verbinding bevat met ‘n affiniteit vir $[PtCl_6]^{2-}$ in ‘n aangesuurde oplossing, was suksesvol gesintetiseerd en gebruik om spoorelemente van Pt(II/IV) te onttrek onder verskillende omstandighede.

ACKNOWLEDGEMENTS

I would like to thank everyone who helped me get to where I am and have supported me through this process:

My promoters, those two father figures that helped me through this academic minefield, thank you for all the guidance.

My parents, brothers, and family, as well as Marinél and her family, for all their love, support, and the well needed breaks.

My friends who kept me sane throughout this process.

All of the crazies at the Stellenbosch Nanofiber Company and PGM research group, thank you guys for all of the help, patience, and laughs. A special thanks to Haydn Kriel and Eugene Lakay for your invaluable assistance.

All of my trusted proofreaders, showing me the error(s) of my ways.

The secretaries and support staff at Stellenbosch University for keeping things running smoothly.

Lastly I would sincerely like to thank the NRF, Anglo Platinum, and Stellenbosch University for funding this work.

TABLE OF CONTENTS

TABLE OF FIGURES

LIST OF TABLES

LIST OF ABBREVIATIONS AND SYMBOLS

ΔG^o – change in Gibbs free energy

ΔH^o – standard enthalpy change

ΔS^o – standard entropy change

DMF – dimethylformamide

DMSO – dimethyl sulfoxide

FTIR – Fourier transform infrared

HCl – hydrochloric acid

K_e – equilibrium constant

M_n – number average molecular weight

M_w – weight average molecular weight

NaOH – sodium hydroxide

NaSCN – sodium thiocyanate

NMR – nuclear magnetic resonance

PAN – polyacrylonitrile

PDT – poly(dodecylthiophene)

PEO – poly(ethylene oxide)

PGM – platinum group metals

Platisorb - poly(*N*-terephthaloylthiourea)-*N*',*N*'-piperazine

PVA – polyvinyl alcohol

PVP – poly(vinylpyrrolidone)

R – universal gas constant (8.314 J K^{-1} mol^{-1})

SEC – size exclusion chromatography

SEM – scanning electron microscopy

T – temperature

TEM – transmission electron microscopy

THF – tetrahydrofuran

CHAPTER 1

INTRODUCTION AND AIMS

1.1 Introduction

Platinum is a very rare element that makes up 0.01 parts per million of the earth's crust and is only found in certain areas of the world. Of the few places where platinum is found, South Africa has the highest abundance, with more than 75 % of the world's platinum deposits located in the Bushveld Complex.[1] It is a valuable commodity that finds uses in catalytic industries, in jewellery, as well as in the electrical, glassmaking, medical and biomedical industries, to name but a few.[2–4]

Platinum forms part of the platinum group metals (PGM) along with iridium, osmium, palladium, rhodium, and ruthenium.[5] These metals are usually refined from the same ores and separated from each other in various steps of the refining process. These separations however are not perfect and as a result trace amounts of the dissolved precious metals in the effluent are not recovered. There are significant financial and environmental pressures to recover as much of these Pt(II/IV) ions as possible and to limit waste due to the ions' high value and the possibility of ground water contamination.

There have been numerous materials designed and geared toward the extraction of trace amounts of Pt(II/IV) ions from aqueous solutions.[6–20] One such material is the oligomeric poly(*N*-terephthaloylthiourea)-*N'*,*N'*-piperazine.[21] This oligomer was designed in Cape Town, South Africa and is synthesised in two steps using relatively inexpensive starting materials in a simple reaction setup. The poly(*N*-terephthaloylthiourea)-*N*',*N*'-piperazine oligomer shows great affinity for Pt(II/IV) ions, extracting more than 30 % of its own weight in Pt(II/IV) from acidic solutions.

Most affinity materials, including poly(*N*-terephthaloylthiourea)-*N*',*N*'-piperazine, are in the form of powders or resinous beads, which are potentially difficult to recover from solution after the ion extraction process. Even though powders form fine suspensions with great areas available for extraction, filtration or centrifugation is required in order to recover both these powders and the extracted metal from solution. This adds an additional step to the recovery process, as well as incurring additional costs. Fibrous affinity materials could be used to bypass this additional step in that fibrous structures, used in solution as a single membrane unit or multiple membrane layers, could more easily be removed from solution after extraction.

Nanofibres are growing in popularity due to their unique properties and wide range of possible applications. The fibres are both very long and exceptionally small (usually with diameters between 50 nm and 500 nm) with extremely large specific surface areas. Nanofibres can be formed into highly porous, very thin membranes with a variety of pore sizes which allow the membranes to have good permeability. Other nanofibre properties include a low basic weight, the ability of the fibres to retain electrostatic charges, and alignment of the polymer chains along the fibre axis.[22–25] The aforementioned properties make nanofibres applicable in many fields, including but not restricted to biomedicine, filters, sensors, tissue scaffolds, composite materials, electronics, and affinity materials.[25–27]

A few techniques are available for creating nanofibres, of which electrospinning is the most popular. The best known electrospinning technique is referred to as needle electrospinning. The process entails a reservoir from which a polymer solution flows into and through the tip of a needle or small capillary and forms nanofibres due to large electrical charges applied to the capillary or the polymer solution.

A major downside to the needle electrospinning process is that it has very limited fibre production rates, typically from 0.1 to 1 g/h.[28] This slow nanofibre production rate of needle electrospinning has hampered the potential applications locked up within these magnificent little fibres. So, while extensive research on the needle electrospinning process has been done, it has thus far been difficult to apply these findings on an economically viable scale.

To overcome the shortcoming in the needle electrospinning process, different electrospinning techniques have been created. Ball electrospinning is one such technique, where multiple nanofibres are formed simultaneously from the surface of a rotating ball which is partially submerged in a polymer solution.[29] With this technique, nanofibre membranes consisting of millions of nanofibres can be produced more rapidly than when using the conventional needle electrospinning process. Ball electrospinning therefore offers great possibilities in transforming the science done in the laboratory to an industrial scale and, ultimately, an economically viable product.

Different polymers are used to create nanofibres, depending on the production technique and the anticipated end use. Some polymers are electrospun into nanofibres as they inherently possess the functional groups or properties required for their end use. However, some polymers are more difficult to electrospin into nanofibres, either due to limitations of the electrospinning process or due to the polymer solution properties. In this case, a different polymer can first be electrospun and then these nanofibres can be modified to incorporate the desired properties.[30,31] Another possibility is to simply create a blended solution, where one component creates the nanofibre structure while the other provides the desired properties.[32]

There are some aspects that should be considered when nanofibres are used for extraction purposes. There could either be a focus on the maximum extractable amount of metal or more emphasis could be placed on the rates of extraction. In either case it is necessary to optimise the extraction process, ensuring that the conditions that are used are conducive to either maximum extraction or the optimum rate of extraction taking place. Many different factors could affect the extraction process, some of which are:

- the initial concentration of ions in solution,
- the presence and concentration of other species in solution,
- the specific surface area of the extractant, as well as
- the conditions (like temperature, pressure, agitation rate, and flow rate) at which the extraction takes place.

To date, no literature could be found on the use of nanofibres for Pt(II/IV) ion extraction. It is therefore a unique opportunity to investigate the extraction of Pt(II/IV) ions in the form of $[PtCl_6]^{2-}$ using nanofibrous affinity membranes.

1.2 Objectives of the dissertation

The following objectives were proposed at the onset of the study:

A (i) *To prepare poly(*N*-terephthaloylthiourea)-*N*',*N*'-piperazine oligomer, as reputed in the Patent Application WO 2000/53663,*[21]

(ii) *as well as conducting analytical analyses on the produced substance for characterization purposes.*

B *To examine the process of needle as well as ball electrospinning of a bicomponent solution containing poly(*N*-terephthaloylthiourea)-*N*',*N*'-piperazine oligomer and polyacrylonitrile into suitable nanofibres.*

C *To study the electrospun nanofibre webs containing the poly(*N*-terephthaloylthiourea)-*N*',*N*'-piperazine oligomer for the extraction of Pt(II/IV) ions in the form of* $[PtCl_6]^{2-}$ *from acidic solutions under varying conditions, including: varying specific surface area of the extractant, varying extraction temperature, as well as varying solution hydrochloric acid concentration.*

1.3 Outline of dissertation

The rest of the document consists of six chapters. It begins with a chapter reviewing all the relevant literature (Chapter 2 - Literature review), followed by a chapter on the chemicals and techniques used during this work (Chapter 3 - Experimental). The results and discussions are divided into Chapters 4 to 6. Chapter 4 is on the synthesis and characterization of the platinum extracting oligomer (Chapter 4 - Synthesis and characterisation of poly(*N*-terephthaloylthiourea)-*N*',*N*'-piperazine). The second results and discussion chapter focuses on the electrospinning of the bicomponent solutions (Chapter 5 – Needle and ball electrospinning of the bicomponent solutions). The final chapter of results and discussions is on the Pt(II/IV) ion extraction experiments done using the electrospun nanofibres (Chapter 6 – Extraction of hexachloroplatinate using *Platisorb*-containing nanofibres). The document ends off with a chapter of conclusions and recommendations (Chapter 7 - Conclusions and recommendations for further study) as well as appendices A and B.

CHAPTER 2

LITERATURE REVIEW

2.1 Platinum

2.1.1 Background and occurrence

Platinum is a very rare metal which has a lustrous, silver-grey appearance. Long before its discovery by the Europeans, there is evidence that the metal was already known and used by the people of Central America in decorative masks. It is first mentioned by the scientist Julius Scaliger in 1557 when he travelled with the Spanish conquistadors in Central America.[2] It was named "platina", which in Spanish means "little silver" and was seen as an undesired impurity in the silver being mined. The first papers of the discovery of platinum were submitted in 1736 from the gold mines in Colombia by Antonio de Ulloa and Charles Wood was the first to provide samples in 1741.[1]

Platinum is only found in certain areas of the world in sufficient concentrations for mining operations. Of these places, South Africa has the largest deposits with more than 75 % situated in the Bushveld Complex, while Russia also has substantial deposits in the Norilsk-Talnakh region of Siberia. These two countries currently produce more than 90 % of the world's platinum, with more than 70 % of the platinum coming from South Africa and roughly 20 % from Russia.[1] The total platinum production per region from 2006 to 2010 can be seen in Figure 2.1(a).[3]

In 1999 a report was released stating that the proven platinum reserves available in the Bushveld Complex is 203.3 million Troy ounces (6 323 tonnes), which would be sufficient for the next 40 years at the current rates of mining.[33] That being said, even if mining continued at the same pace from 1999 without increasing until the present day, only a theoretical 27 years' worth remains before the Bushveld Complex is void of platinum.

The problem with the increasingly small amount of platinum still available through mining operations is intensified by the increase in demand for this precious metal. Another report states that the demand for this precious metal will outweigh the supply sometime between 2010 and 2016.[34] This prediction is attributed to the fact that South Africa has had a decline in platinum production from 2007 to 2009 because of mine closures, lower capital expenditure, inflation, as well as a lower grade of platinum ore being mined.

2.1.2 Platinum uses

Platinum has the innate ability to adsorb large quantities of hydrogen, which makes it widely applied as a catalyst in chemical industries.[4] In fact, the largest consumers of platinum are currently the catalytic industries, as shown in Figure 2.1(b).[3] Platinum is especially widely used in modern catalytic converters in the automotive industry. A platinum-coated ceramic grid inside the automobile exhaust is responsible for converting all of the uncombusted fuels into water and carbon dioxide. Other uses of platinum in catalytic industries include the hydrogenation of liquid vegetable oils into solid forms of

vegetable oil, cracking of crude oil into gasoline, in fuel cells, and during the production of sulphuric acid.[4]

The second largest trade in which platinum is consumed is the jewellery industry. Jewellery is made from platinum because of its resistance to tarnishing and wear and tear. Some of the smaller applications in which platinum is used include electrical, glassmaking, medical and biomedical industries, as well for investment purposes.[3] Platinum is also used to form some coordination complexes with other atoms, of which the most well know is probably the cancer treatment drug called *cis*-platin ($Pt(NH_3)_2Cl_2$).[2] The main applications for platinum are shown in Figure 2.1(b), divided per industry.

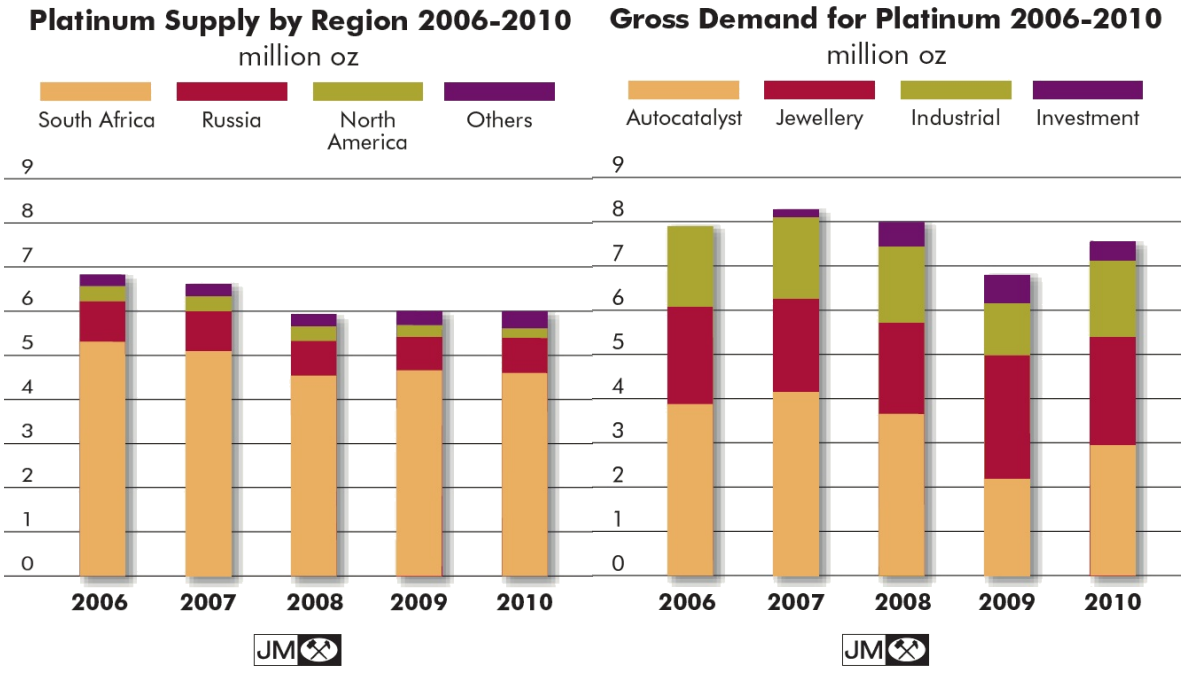

Figure 2.1 – (a) Graphs depicting the production of platinum per country from 2006 to 2010, and **(b)** the demand per industry from 2006 to 2010.[3]

2.1.3 Platinum refining process

Platinum is one of six metals which are collectively known as the platinum group metals (PGM). The other five PGM are iridium, osmium, palladium, rhodium, and ruthenium.[5] These PGM are all present in the same ore, along with other precious and base metals. It is therefore important to separate the PGM from the other metals present in the ore, as well as to ultimately isolate the platinum from the other PGM.

The ore obtained from the mining operations is crushed and milled into finer rocks to expose the PGM contained within. These smaller rock particles are added to a mixture of water and special reagents in a process called froth flotation.[35] During this process the particles containing the PGM are carried to the surface by bubbles of air which are pumped through the solution and PGM-rich froth is formed on the surface of the liquid. The froth that forms is isolated, dried, and smelted at over 1500 °C to form a matte containing the PGM as well as some other elements.[36]

The other elements are removed from the PGM; the matte is tapped while air is passed through to remove any iron and sulphur it contains, while the base metals are removed using standard electrolytic techniques.[35] All that then remains is the PGM with some gold and a small amount of silver.

The final step is to separate the platinum from the other PGM. This is done by a combination of solvent extractions, distillations and ion-exchange methods.[35] The metals that are soluble in hydrochloric acid (HCl) and chlorine gas are isolated in order: first the gold, then the palladium and finally the platinum.[37] The insoluble PGM are then separated further. This whole process is shown in Figure 2.2 in the form of a flow chart.

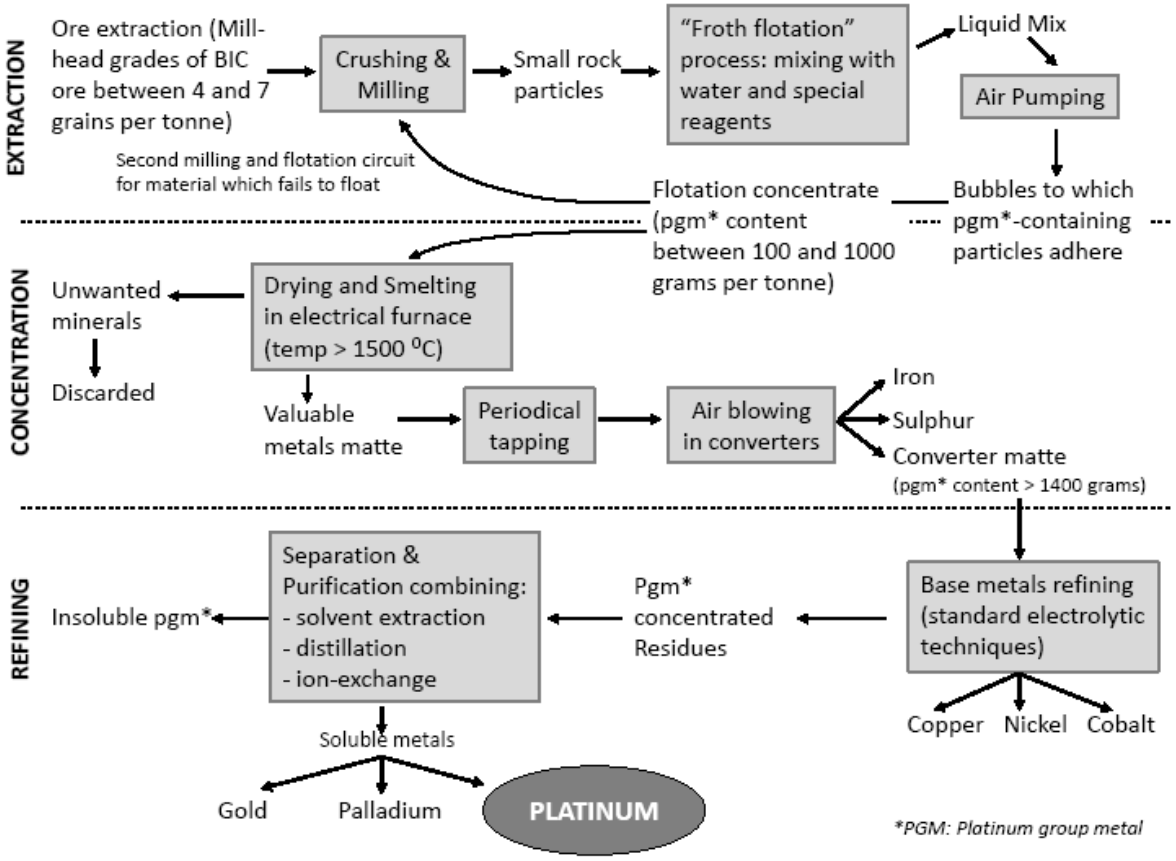

Figure 2.2 – The process of producing platinum from the ore to the pure metal. Image is redrawn from reference 37.

The strong chlorine concentration in the solution due to the HCl and chlorine gas treatment causes the platinum to predominantly form hexachloro- anions, including hexachloroplatinate $[PtCl_6]^{2-}$.[38] Trace amounts of this water soluble $[PtCl_6]^{2-}$ is not recovered during the refining process and remains in the effluent, representing a significant financial loss to the mining company as well as being a possible environmental concern if introduced into the ground water surrounding the processing plant. Both are important reasons to try and separate these trace amounts of dissolved platinum from the effluent solution.

One method that is currently used to recover more of the platinum ions is to reintroduce the effluent into the recovery process at the smelter.[39] The problem is that this method is both time consuming and expensive. Another possible method to recover these trace amounts of $[PtCl_6]^{2-}$ from the effluent is to use affinity materials. These materials could be used to selectively capture the Pt(II/IV) ions before being removed from the effluent solution, effectively isolating and removing the precious metal from solution as well.

2.2 Affinity materials

2.2.1 Background

Affinity is a phenomenon in chemistry where specific atoms, ions or molecules have a propensity to interact, form bonds, or aggregate with each other. Affinity materials are therefore substances that have a tendency to interact, *via* ion-exchange or non-bonding interactions, or to form direct coordination bonds with other molecules.

A huge range of analytes have been and are currently being extracted using affinity materials, ranging all the way from foodstuff to radioactive material.[40,41] Affinity materials can be a cost effective means of selectively removing the desired particles from solution.[42,43] These materials can be designed to exhibit a high loading capacity, be selective for a single particle type, and be robust enough to withstand chemical attack as well as high flow rates during use.

2.2.2 Materials with an affinity for Pt(II/IV) ions

Many articles have been published on the extraction of Pt(II/IV) ions from solution. Table 2.1 shows a list with references, which is in no way exhaustive, of some of the Pt(II/IV) ion affinity materials as well as the unit mass of Pt(II/IV) ions removed from solution per unit mass of material used (g/g).

Table 2.1 - List of some of the extractants used for the extraction of Pt(II/IV) ions from solution, as well as their extraction efficiency in mass per mass.

Extractant material	**Pt(II/IV) ions extracted (g/g)**
Fe_3O_4 nanoparticles [6]	0.013
Tris(2,6-dimethoxyphenyl)phosphine modified polystyrene [7]	0.015
Primary amine modified cross-linked lignophenol [8]	0.043
Amine-treated activated carbon (Norit RO 0.8) [9]	0.055
Amberlite IRC 718 [10]	0.066
Ethylenediamine modified cross-linked lignophenol [8]	0.105
Dimethylamine modified cross-linked lignophenol (DMA-CLP) [11]	0.121
Lysine modified cross-linked chitosan [12]	0.129
Thiourea modified chitosan microspheres [13]	0.130
Cyphos IL-101 (tetraalkylphosphonium chloride salt) [14]	0.177
Bayberry tannin immobilized on collagen fibre [15]	0.222
Poly(vinylbenzylchloride-acrylonitrile-divinylbenzene) modified with tris(2-aminoethyl)amine [16]	0.245
Poly(vinylpyridine) modified with dithizone [17]	0.250
Imidazol containing resin [18]	0.310
Glutaraldehyde- cross-linked chitosan [19]	0.310
Poly(*N*-terephthaloylthiourea)-*N*',*N*'-piperazine [21]	0.321
1-(2-aminoethyl)piperazine resin [20]	0.480

The species have a number of different affinity moieties with which anionic precious metal complexes like $[PtCl_6]^{2-}$ interact, including amines, hydroxyl groups, quaternary phosphonium cations, sulphur groups and thiourea moieties. Amines are readily protonated in acidic solutions, becoming attractive targets for the anionic Pt(II/IV) complexes *via* ion-pairing.[8,9,20,44] Both magnetite and tannins employ hydroxyl groups to extract Pt(II/IV) ions from solution, while quaternary phosphonium cations forms ion-pairs with the oppositely charged Pt(II/IV) anions.[6,7,15]

N,*N*-dialkyl-*N*-aroyl- or -acyl-thiourea compounds (for instance poly(*N*-terephthaloylthiourea)-*N*',*N*'-piperazine) have also been shown to complex with Pt(II) chloride ions in solution *via* either only a sulphur atom or a sulphur and oxygen atom pair complexation mechanism.[45–47] This complexation between the Pt(II/IV) ions and the thiourea compounds can be used as an affinity separation method if the complex that forms can be isolated from solution. A simple structure of one of these complexes is shown in Figure 2.3 showing the proposed complexation between the Pt(II/IV) ion and the coordination site of the molecule.[47]

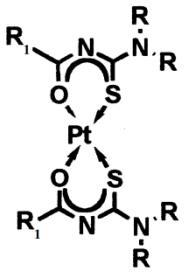

Figure 2.3 – Simple structure of a *N,N*-dialkyl-*N*-aroyl- or -acyl-thiourea compound.[47]

Especially good Pt(II/IV) ion extraction is achieved when using imidazol-containing resin, glutaraldehyde-crosslinked chitosan, poly(*N*-terephthaloylthiourea)-*N*',*N*'-piperazine, and 1-(2-aminoethyl)piperazine resin.[18-21] All of these affinity materials achieve an extraction of more than 30 % mass Pt(II/IV) ions per mass of affinity material used.

Poly(*N*-terephthaloylthiourea)-*N'*,*N'*-piperazine is of particular interest to this study as the product has been designed in Cape Town, South Africa. An International Patent Application was filed on the synthesis, characterisation and extraction efficiency of poly(*N*-terephthaloylthiourea)-*N*',*N*'-piperazine.[21] The general chemical structure described in the patent application is shown in Figure 2.4, "*wherein R_1 is selected from linear and branched alkyl and alkenyl groups, C_6 aromatic rings, substituted C_6 aromatic rings, fused aromatic rings, substituted fused aromatic rings, and aralkyl groups, or is absent; R_2 is selected from linear and branched alkyl and alkenyl groups, C_6 aromatic rings, substituted C_6 aromatic rings, linked aromatic rings, fused aromatic rings, substituted fused aromatic rings, and aralkyl groups; each X is independently H, alkyl or phenyl or X-N-R_2-N-X form a ring in which R_2 is alkyl or substituted alkyl and the two X groups together are alkyl or substituted alkyl; and m is an integer greater than or equal to two.*"[21]

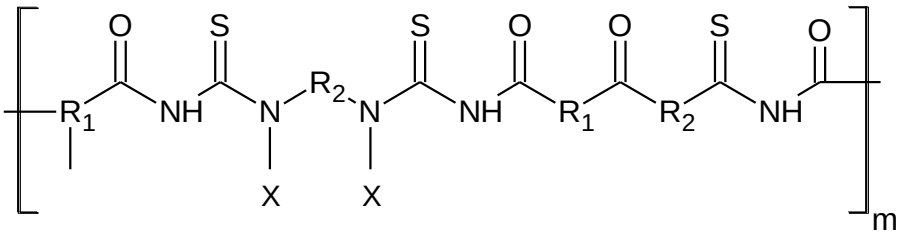

Figure 2.4 – General structure of the proposed extractant material, redrawn from the patent application.[21]

Poly(*N*-terephthaloylthiourea)-*N'*,*N'*-piperazine is chosen as the affinity material for the extraction of Pt(II/IV) ions during this work for four reasons:

- Poly(*N*-terephthaloylthiourea)-*N'*,*N'*-piperazine has been synthesised in Cape Town, South Africa, making it a locally designed product.

- The poly(*N*-terephthaloylthiourea)-*N',N'*-piperazine shows excellent extraction capabilities, extracting 0.321 g of Pt(II/IV) ions per gram of oligomer used under optimised conditions.
- The synthesis is a "one-pot" two step procedure which eliminates tedious reactions and expensive reaction setups.
- The sorbent can be produced by using relatively inexpensive starting materials, which allows it to be used as a single-use extraction material without the need to desorb the Pt(II/IV) ions after extraction.

The characterisation of the poly(*N*-terephthaloylthiourea)-*N',N'*-piperazine oligomer is described in more detail in Chapter 4.

2.2.3 Different macroscopic forms of affinity materials

Affinity materials can come in different macroscopic forms, including but not restricted to powders, beads, gels, and fibres.[13,48,49] In an experimental context it has been found that powders and beads are more difficult to handle and remove from solution after extraction than membranes. Powders and beads need to be removed from solution *via* filtration, centrifugation, or another separation method after the extraction process. This is in contrast to membranes (whether consisting of interwoven fibres, nonwoven fibres, solution cast media, etc.) which are easier to remove from the solution after extraction as a single unit. Ease of use is therefore an important reason to use membranes rather than powders or beads as affinity materials.

Three main methods of creating membranes have been described in literature, the first of which is the solution cast method.[50] Solution casting is when dissolved media, consisting of the affinity material dissolved in a suitable solvent, is dispersed onto a surface. The solvent is then evaporated off the surface and the thin film that remains forms the membrane. The thickness of the membrane can be increased by dispersing more media onto the evaporation surface or by overlaying multiple membranes on top of each other.

The second method of creating an affinity membrane is to chemically modify an existing textile substrate.[51] The textile substrate is first produced and then a post processing modification step is added to impart the desired functionality. In this way the substrate remains intact and the desired affinity is incorporated onto the substrate's surface. This method of functionalising an existing textile membrane has previously been used to create fibrous ion exchangers for metal ion extraction.[30]

The method of post-process modification can be used on fibres with smaller diameters than those of conventional macroscopic textiles. In a similar way to fibrous ion exchangers,[30] nanofibres can also be modified to incorporate coordination sites. One example of these nanofibres is where polyacrylonitrile (PAN) is first electrospun into a nanofibre web and then treated with hydroxylamine hydrochloride

and sodium carbonate to form amidoxime-modified PAN nanofibres.[31] This post-electrospinning chemical treatment adds the amidoxime functional groups that are desired for metal ion extraction.

A final method for creating affinity membranes is to use a blend between the desired affinity material and a suitable fibre forming material prior to spinning. The blended solution can then be spun to produce fibres which incorporate the desired functionality. This method of creating affinity membranes removes the post processing functionalization step. It has also been shown to work on the electrospinning process, producing functionalised nanofibres. One such example involves the electrospinning of a solution containing wool keratose (WK) and silk fibroin (SF).[32] The WK imparts the functionality while the SF acts as the fibre forming component during the electrospinning process.

2.3 Nanofibres

2.3.1 Nanofibre properties

Nanofibres typically have fibre diameters between 50 nm and 500 nm. The fibres are both very long and have extremely large specific surface areas. Nanofibres can be formed into very thin membranes which are highly porous with a variety of pore sizes. These pores allow the nanofibre membranes to have good permeability. Other nanofibre properties include a low basic weight, the alignment of the polymer chains along the fibre axis, and the ability of the fibres to retain electrostatic charges.[22–25]

One of the possibilities is to modify the nanofibres' surfaces to incorporate a certain desired functionality. The combination of the inherently large surface area with affinity causes an increase in the surface reactivity of the material produced.[6] This property of large specific surface area therefore enables nanofibre membranes (when containing immobilised functional groups that impart the desired functionality) to be very efficient affinity materials.

Decreasing the fibre size to the nanometre range can also have a compounding effect on some of the existing polymer properties. One example is when polymers that are only slightly hydrophobic are electrospun to form extremely hydrophobic nanofibres. The same goes for the inverse, where slightly hydrophilic polymers form extremely hydrophilic nanofibres.[52]

2.3.2 Nanofibre production techniques

Nanofibres can be prepared by different techniques, including fine hole extrusion, multi-component fibre spinning, the "islands-in-the-sea" method, and electrospinning. The first technique, fine hole extrusion, is similar to melt-blowing macroscopic fibres, in that a molten polymer is forced through an extrusion die to form the fibres.[53] Modified dies with very fine holes are however required and each hole is surrounded by up to eight air jets that forces air to flow parallel to the polymer melt to stretch it

into a fine fibre. Depending on the polymer flow rate, air flow rate and extrusion hole size, nanofibres with diameters of as small as 100 nm can be produced.[54]

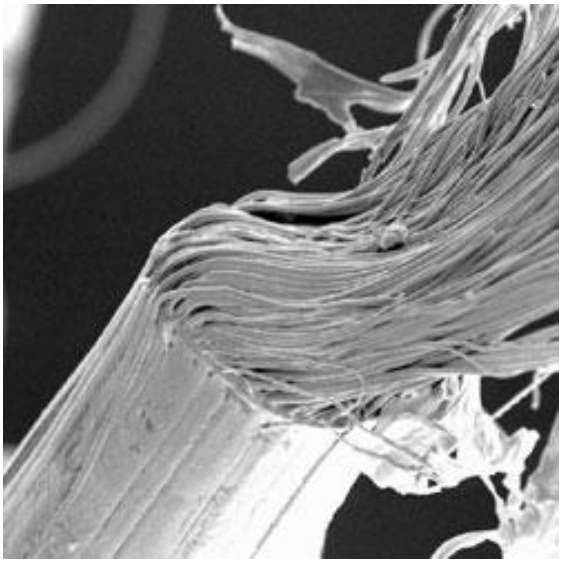

Figure 2.5 – 600 polypropylene fibres in a "sea" of polyvinyl alcohol (PVA). PVA is removed with boiling water, leaving only the polypropylene fibres with an average fibre diameter of 500 nm.[56]

Another method of preparing fibres with small diameters is by spinning a multi-component fibre, consisting of two or more incompatible polymers, into segments which can be split from each other to produce fibres with much thinner diameters than the parent fibre.[55] The segments are disentangled from one another by means of contact with either heated water or steam, forming a nonwoven web of very thin fibres.

The third method, "islands-in-the-sea", is a specialised multi-component fibre spinning process where the desired small fibres are spun within a larger fibre. The larger fibre fulfils the role of the "sea" which is removed after spinning and drawing to produce the small "island" fibres, shown in Figure 2.5. This is done by choosing a polymer for the "sea" partition that is soluble in a solvent that does not dissolve the "island" polymer.[56] The desired fibres are usually in the micrometre range, but nanofibres have also been created.[57]

Even though fine hole extrusion, multi-component spinning and the "islands-in-the-sea" techniques have the ability to produce fibres in the nanometre range, the most common technique used for creating nanofibres is electrospinning, described in detail below.

2.4 Electrospinning

Most literature reviewed states that the first patent on the electrospinning process was by Formhals in 1934,[58] disregarding those of both Cooley and Morton.[59,60] Cooley and Morton both patented, in 1902, the process that is today known as electrospinning. While only recently rediscovered, the past 15 years has seen a steady stream of publications on the electrospinning process.[61] Since then electrospinning has given rise to many different processes which vary from the original technique. Some of these, including free surface electrospinning and needleless electrospinning, are discussed later in this chapter.

The most basic electrospinning setup consists of only three parts: a polymer solution/melt focused at a specific point (for example a capillary tip), a high voltage power source, and a collector or electrode onto which the fibres are deposited. A polymer is dissolved in a suitable solvent to form a solution, or if insoluble it may be melted to form a polymer melt. The polymer solution or melt is then placed in a container from which it can slowly flow, such as a syringe or glass pipette. An electric potential is applied to the polymer solution by the high voltage power source.

The surface tension of the polymer solution at the air-liquid interface needs to be overcome by the electrical potential in order for electrospinning to take place.[61] As the electrical potential builds up on the solution surface, it starts to counteract the surface tension forces. There are two types of electrostatic forces which are exerted on the polymer droplet. Both the electrostatic repulsions between the charges on the droplet surface and the Coulombic forces caused by the external field forces the droplet to deform and elongate.[25] At a critical point of applied electrical voltage, called the critical potential, the polymer solution deforms into a conical shape referred to as the Taylor cone.[62,63] When sufficient voltage is applied to surpass the critical potential, the voltage overcomes the surface tension and a thin liquid jet erupts from the Taylor cone. This process is referred to as jet initiation.[64]

Figure 2.6 shows the Taylor cone formation and subsequent jetting from a pendant drop. After jetting has been initiated (28th millisecond in Figure 2.6), a steady state is reached where the pendant drop relaxes into a rounded shape. The jet from the Taylor cone travels from the like-charged polymer solution towards an oppositely charged or grounded collector. The jet initially travels in a straight line towards the collector, often referred to as steady-state jet motion.[65,66]

As the liquid jet travels through the air, past the steady-state jet motion segment, it starts to undergo what are referred to as jet instabilities or bending instabilities. This is mainly caused by the charge repulsions that build up on the fibre surface.[67] These like-charges on the liquid jet repel each other according to Coulomb's Law which results in the largest possible distance separating them.[68] Both a schematic depiction and stroboscopic image (shown in Figure 2.7) of this deformation shows the liquid jet when it twists and turns as the jet travels through the air, also called whipping or wagging.

As the polymer jet whips through the air, solvent continuously evaporates from the jet surface, causing the jet's volume to decrease, and in effect, the charge density on the jet to increase.[69] This dries the jet, causing further bending instability and whipping as the jet travels towards the collector.[65] Multiple orders of bending instability have been observed (shown in Figure 2.7(a) as first, second and third bending instability). When primary bending instability sets in, the jet deviates from travelling straight towards the collector and forms coil-like structures. As the charge repulsions along the jet are further increased and if the distance to the collector is long enough, secondary bending instability sets in.[70,71] Secondary coil-like structures form along the already coiling jet. All of this bending and stretching takes place very rapidly and high-speed video equipment is required to visualize the process.[72,73]

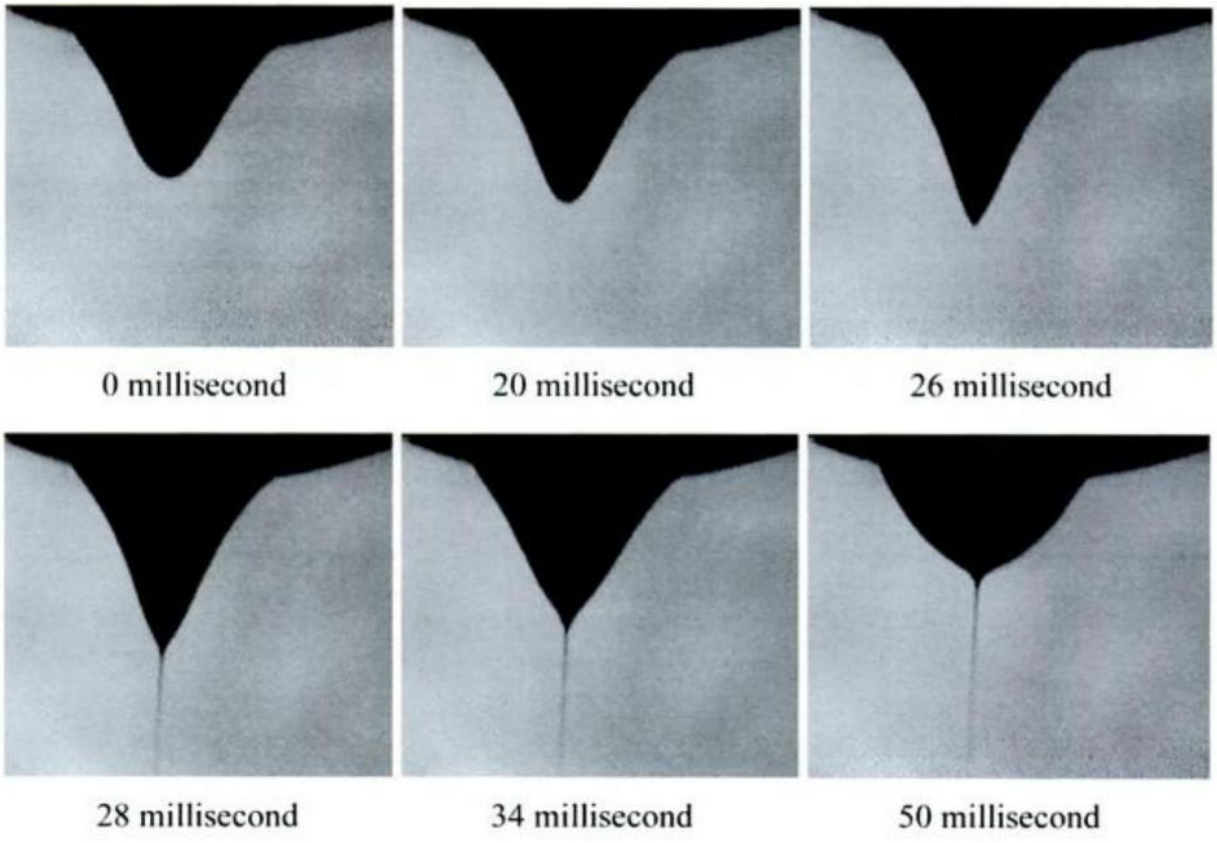

Figure 2.6 – Taylor cone formation, jet initiation and droplet relaxation into a steady state are all observed in the span of a few milliseconds.[74] The pendant solution droplet deforms with increasing applied electric potential (0 ms to 26 ms) until a Taylor cone forms and a jet ejects from the surface of the droplet (28 ms). After the jet forms the droplet relaxes into a rounded shape. The polymer solution used in this case is 3 wt% polyethylene oxide in water that flows through a 300 µm hole and is subjected to an electric field of 0.5 kV/cm.

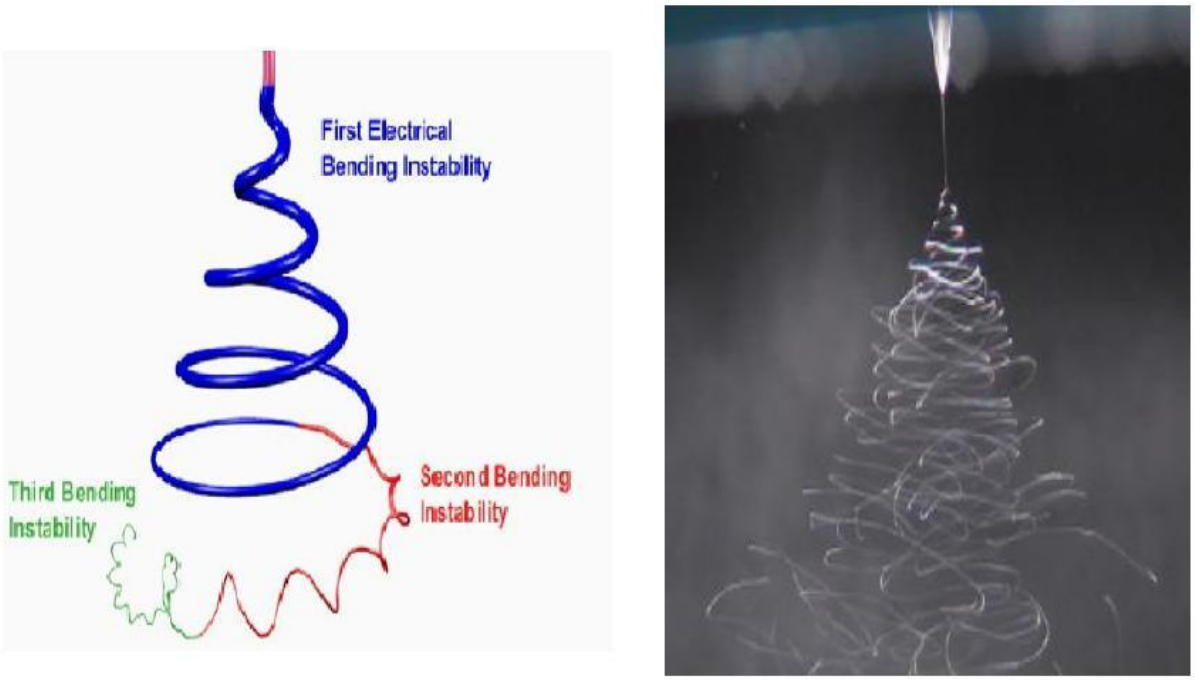

Figure 2.7 – Whipping of the jet during electrospinning shown as **(a)** schematic and **(b)** stroboscopic image.[75]

Finally the dried polymer fibres are deposited on a collector. At this stage they are no longer referred to as jets, but rather nanofibres or microfibres, depending on their diameters. The properties of the fibres produced by electrospinning depend largely on the characteristics of the polymer being spun, polymer solution properties and the electrospinning parameters during production.

2.4.1 Parameters affecting the electrospinning process

Generally three different sets of parameters affect the electrospinning process:

- the system parameters, which are the physiochemical properties of the spin solution,
- the operational parameters, which describe the electrospinning conditions, and
- the external factors, which are the ambient conditions surrounding the electrospinning setup.

The main system parameters are solution viscosity, conductivity and surface tension.[76] Other system parameters include the dielectric constant of the solution, the molecular weight of the polymer, the molecular weight distribution, and the architecture of the polymer in solution (e.g. branched or unbranched polymer molecules). The operational parameters include the effective spinning distance, applied electric field, solution feed rate, as well as the type of collector used.[77] The external factors which affect the electrospinning process include the humidity, temperature and solvent vapour surrounding the electrospinning setup.[78] All of these have to be considered and/or optimised before and during electrospinning to ensure the successful formation of the desired nanofibres.

2.4.1.1 Conductivity, surface tension and viscosity

The electrical conductivity, surface tension and viscosity of the solution are critical when it comes to bead formation on the fibres and the fibre diameters obtained by the electrospinning process.

Conductivity of the solution

The higher the conductivity of a polymer solution, the easier it is for electrical charges to flow through the solution. During electrospinning, the electrical charge needs to be sufficiently high to overcome the surface tension of the polymer solution at the liquid air interface.[22] When this is the case, the liquid jets from the surface of the solution and electrospinning takes place.

Basic salts (e.g. sodium chloride and calcium chloride) have been used in previous studies to increase the conductivity of polymer solutions so that electrospinning can initiate at a lower electric field strength.[77,79] This in turn results in the formation of thicker fibres as the increase in conductivity caused an increased mass flow of the polymer solution during the electrospinning process.[80]

Surface tension of the solution

Surface tension affects the electrospinning solution both prior to Taylor cone formation and jet initiation, as well as during the whipping of the polymer jet. The forces exerted on the polymer solution by the applied electrical charge need to be strong enough to overcome the surface tension forces in order for Taylor cone formation and subsequent jetting to occur. When surface tension is the dominant force during jetting and whipping, the polymer solution will form the smallest possible specific surface area as it travels towards the collector. This causes beads to form on the nanofibres, since beads have a lower surface to volume ratio than fibres.[77,81]

Viscosity of the solution

Viscosity is the third main force that acts on the liquid jet during electrospinning. The viscosity of the spin solution may be changed by varying the polymer concentration in solution, where increasing the ratio of polymer to solvent causes the viscosity to increase.[82]

When the viscosity is too high, polymer chain entanglement on a molecular level inhibits the solution from flowing and deforming fast enough, which in turn stops the solution from undergoing Taylor cone formation.[83] When the viscosity is too low there is not sufficient chain entanglement for continuous fibres to form when an electrical potential is applied to the solution. When this is the case, droplets are formed instead of fibres in a process called electrospraying.[84] A middle ground needs to be reached where the viscosity is sufficient to facilitate polymer chain entanglement during electrospinning without electrospraying or beading occurring (if beads are undesired), but not too high to hamper Taylor cone formation and the subsequent jetting.

Changing the viscosity within the minimum and maximum electrospinnable range affects the fibre diameters of the nanofibres formed. An increase in the solution viscosity causes an increase in the fibre diameters obtained by the electrospinning process.[23,76,85] This is due to two effects. The first is simply that a smaller portion of the jet consists of solvent and therefore less of the jet volume is volatilised during the whipping and jetting process. Secondly, thicker fibres are formed because polymer chain entanglements also increase as viscosity increases. This increase in chain entanglement causes less solution flow during the whipping process, effectively producing thicker fibres.

Balancing the conductivity, surface tension and viscosity

To review the effects that conductivity, surface tension and viscosity have on the formation of beads: decreasing the surface tension and/or increasing either the conductivity or viscosity of the solution causes fewer beaded structures.[86] It is found that as the polymer concentration (and thus the viscosity) increases, the average fibre diameter of the fibres obtained from electrospinning also increases.[23,76,85] An increase in conductivity causes thicker fibres as an increase in mass flow during the electrospinning process is observed.[80]

All three parameters; solution viscosity, conductivity and surface tension, must be considered when it comes to the formation of beads on the fibres and creating nanofibres with the desired fibre diameters. These three solution parameters should be recorded before electrospinning and optimized in the case of undesired electrospinning results.

2.4.1.2 Effective spinning distance

The effective spinning distance, also called the tip-to-collector distance, is the distance between the point of electrospinning initiation where the Taylor cone forms and the collector where the electrospun fibres are deposited. Both the drying of the electrospun jets as well as the fibre diameters are affected by the spinning distance. As the polymer jets whip while travelling towards the collector, the solvent evaporates and dry nanofibres are formed and deposited on the collector. When the spinning distance is very short, the solvent does not have sufficient time to evaporate completely and wet fibres are deposited on the collector.[87] Shorter spinning distances also lead to thicker fibres because the distance that the polymer jets has to stretch and elongate is limited.[76] The effective spinning distance therefore needs to be chosen in such a way to ensure complete drying of the fibres as well as enough time for the fibres to stretch and elongate to form thinner fibres (when desired).

2.4.1.3 Electric field strength

The electric field strength is dependent on the voltage applied to the polymer solution and the collector as well as the distance between these two charged points. To increase the electric field in which electrospinning takes place, one could either increase the voltage applied to the polymer solution or the collector, or decrease the distance between the point of jet initiation and the collector.

Sufficient electrical potential is required to ensure that the solution surface tension is overcome and electrospinning initiates.[88] Fibre diameters decrease with increasing electric field strength until they reach a minimum diameter, after which the fibre diameters start increasing when additional voltage is added.[89] This is seen in Figure 2.8 with the spin distance (or "gap") of 50 mm, where the fibre diameters first decrease with applied voltage of 5 kV to 10 kV and then increase when the voltage increases to 15 kV.

Care should be taken to ensure that the surroundings of the electrospinning setup are non-conductive or thoroughly isolated. If the surrounding area is conductive, some/all of the charge applied to the system to facilitate the electrospinning process can be conducted away. This is dangerous, costly and the reported results would not be accurate as some of the applied voltage does not go into the electrospinning process, but is rather dissipated to the surroundings.

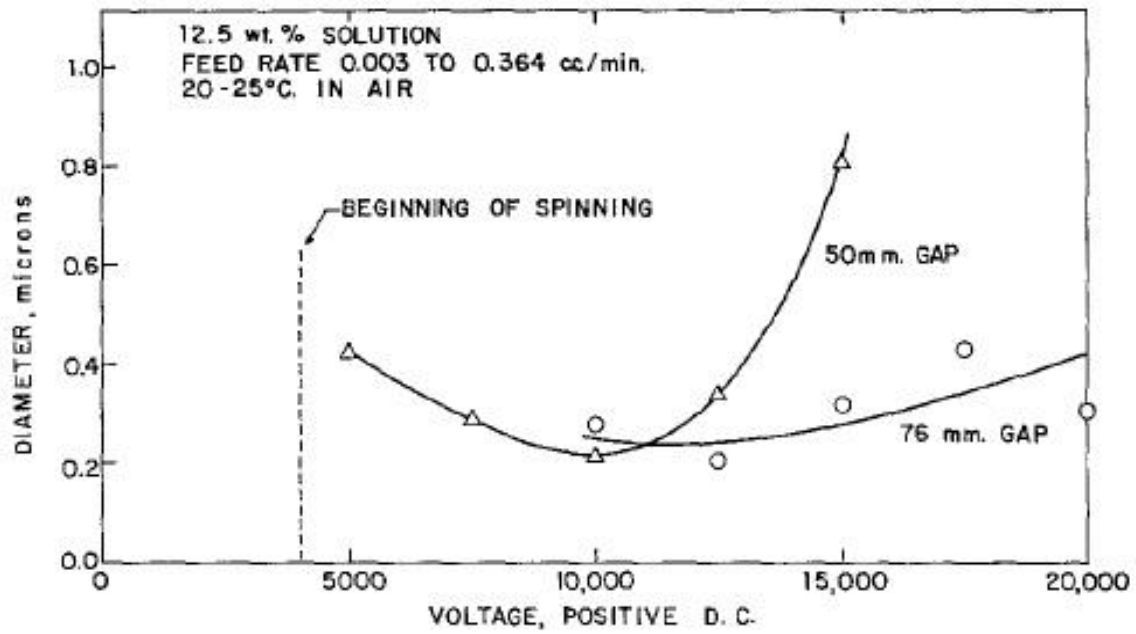

Figure 2.8 – Effect of electric field strength on fibre diameter for acrylic dissolved in DMF. The solution flow rate as well as polymer solution concentration are shown in the top of the figure.[89]

2.4.1.4 Collector design

Different collector designs are used as platforms on which electrospun fibres are deposited, including static and rotating collectors.[90] A static collector is most often used for the electrospinning process, usually consisting of a flat piece of aluminium foil. The conductive foil is oppositely charged to the polymer spin solution or grounded.

A rotating drum collector can be used to overcome backbuilding (discussed in more detail in Chapter 3, section 3.2.4). By rotating, the collector flattens the fibres against the surface of the drum, allowing enough time for the fibres to lie down or release loose superficial fibres from the collector by centrifugal forces. The rotating drum is also a good collector to impart alignment into the nanofibre web as it is formed, while some tests show that the take-up speed of the collector can be used to control the fibre diameters of the electrospun fibres.[91–93]

2.4.1.5 Humidity

The humidity in the atmosphere can be measured in two forms: absolute humidity and relative humidity. Absolute humidity is the mass of moisture per unit volume of air while relative humidity is a calculated value giving the amount of moisture in the air relative to the maximum amount of moisture that the air could hold at that specific temperature and pressure. With relative humidity it is therefore important to record the temperature as well as the pressure. Absolute humidity is reported as kg/m^2 while relative humidity is reported as a percentage.

There is an optimum humidity range within which electrospinning occurs. A study using PAN dissolved in dimethylformamide (DMF) found that when the relative humidity is less than 5 % the suspended polymer drop dries out after only one or two minutes and when the relative humidity is greater than 60 % the fibres that form are not dry.[89] These wet fibres form a tangled mass above the collector. It is important to note that different polymer and solvent combinations could have different upper and lower humidity ranges.

It has been found that the relative humidity at which fibres are electrospun affects their diameters in both water based and organic solutions.[94] A decrease in fibre diameter was observed as the relative humidity increased above 60 % when water based polyvinyl alcohol (PVA) solution was electrospun. Contrary to this, fibres electrospun from organic solvents such as DMF, tetrahydrofuran (THF), and toluene generally showed a fibre diameter increase as relative humidity increased.

2.4.1.6 Temperature

Temperature is one of the external factors that affects the electrospinning process and needs to be controlled or monitored closely. This is due to temperature having the potential to alter electrospinning in two very distinct ways: by affecting all three of the primary solution properties (viscosity, conductivity, and surface tension) and by affecting solvent evaporation during electrospinning.

Firstly, an increase in temperature decreases both the viscosity and surface tension, but causes an increase in the conductivity.[95] It has been found that a temperature increase from room temperature to 88.7 °C when using a solution of PAN in DMF causes a decrease in fibre diameter from between 190 and 240 nm to between 65 and 85 nm.

The second effect that temperature has on the electrospinning process is that it facilitates solvent evaporation. Figure 2.9 shows the results of a temperature study done on poly(vinylpyrrolidone) (PVP) in ethanol at two different PVP concentrations and two different spinning distances.[96] At the lowest temperature the solvent evaporates much slower, the jet takes longer to solidify and elongation and whipping continues for a longer period of time. At the highest temperature the change in the viscosity, conductivity and surface tension is the dominant force and the resultant fibres have smaller diameters.

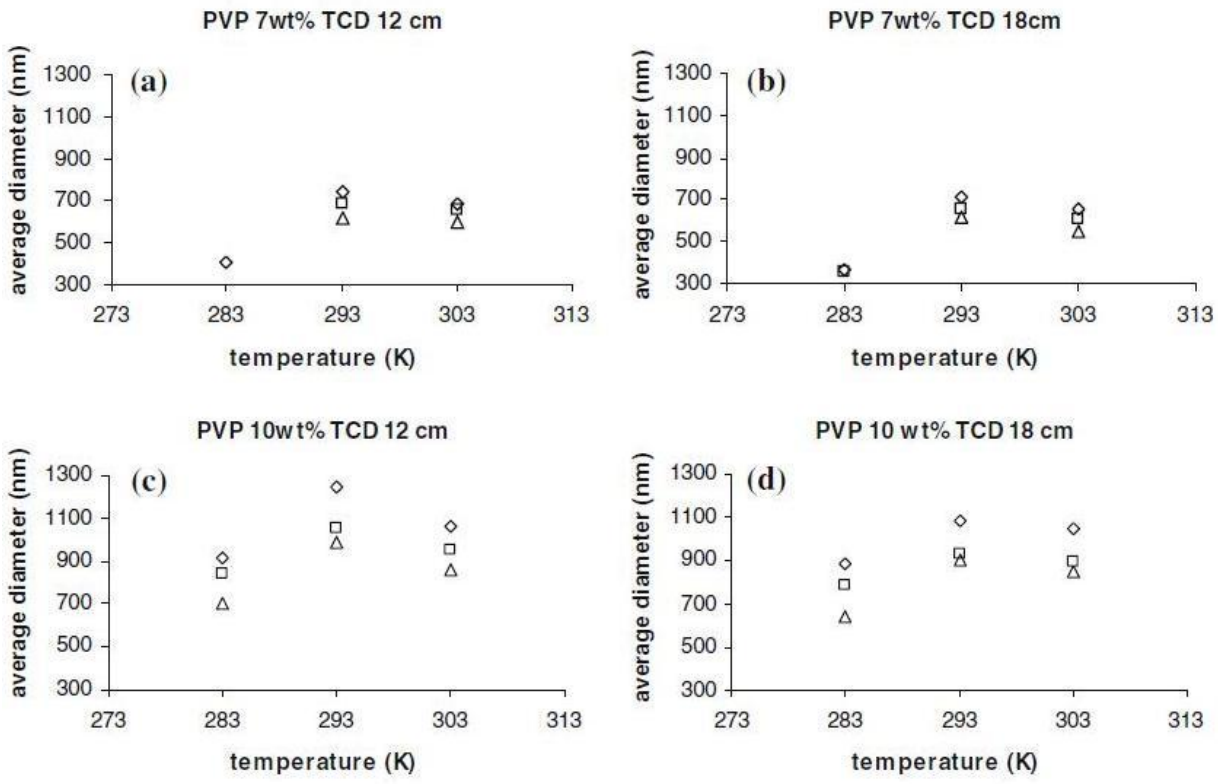

Figure 2.9 – The effect of temperature on the fibre diameters of PVP in ethanol. Both 7 wt% **(a** and **b)** and 10 wt% **(c** and **d)** polymer solutions are spun at 12 cm **(a** and **c)** and 18 cm **(b** and **d)** spinning distances. The polymer flow rate was set to 3 mL/h for all the experiments while the applied voltage was 10 kV when spinning over 12 cm and 15 kV when spinning over 18 cm.[96]

2.4.1.7 Solvent evaporation during electrospinning

The solvent that evaporates from the polymer jet as it travels towards the collector as well as the solvent that evaporates off the polymer solution surface or droplet from which electrospinning takes place is referred to as the solvent vapour. Depending on the amount of solvent vapour present in the fibre forming area, the polymer jets dry faster or slower.[97] The jets will dry slower as the atmosphere around the electrospinning setup becomes saturated with solvent vapour during the electrospinning process, making it more difficult for solvent to evaporate off subsequent polymer jets, and *vice versa*.

Another solvent phenomenon is observed when co-solvents are used to create porous electrospun fibres. The most volatile co-solvent evaporates from the surface of the liquid jet first, creating pores along the length of the fibre.[98]

2.4.2 The needle electrospinning technique

Needle electrospinning is the most basic of all the electrospinning processes. It is the process often used for parameter studies as it requires relatively small amounts of polymer solution and forms a single jet which is easier to study than when high throughput techniques are used. These techniques, described later, require larger amounts of polymer solution and form multiple jets during the electrospinning process.

The needle electrospinning setup is very similar to the setup discussed at the beginning of the electrospinning section of the chapter. At the most basic level it only consists of three parts: a polymer solution focused at a specific point, a high voltage power source and a collector or electrode where the fibres are collected. For needle electrospinning, the polymer solution is housed in a syringe or a pipette with a small tip or orifice from which the spin solution can flow. The needle tip or polymer solution itself is charged by the high voltage power source, while either gravity or a pump can be used to achieve a continuous feed of polymer solution to the tip of the syringe where electrospinning takes place.[69,99]

The collector used during needle electrospinning usually has a flat or rounded surface, like a plate or a rotating drum. However, variations of the needle to plate spinning setup have been reported, including needle to needle, plate to needle and plate to plate electrospinning.[100] A needle tip penetrating the plate supplies the polymer solution in the cases where a plate is used as the point of electrospinning initiation.

The syringe containing the polymer solution is either placed directly above, directly below, at an angle, or horizontal with regards to the collector.[85,101] The findings of a study on the difference between upward, downward, and horizontal electrospinning are that upward electrospinning has the largest fibre diameters with the smallest size distribution and the downward electrospinning has the smallest fibre diameters with the largest size distribution.[102] The resultant fibre diameters and size distribution of horizontal electrospinning was found to be between that of upward and downward needle electrospinning.

The needle electrospinning setup has been modified by using a dual syringe setup to create core-shell nanofibres in a process called co-axial electrospinning.[103] The setup used is graphically shown in Figure 2.10(a) and consists of two syringes of different sizes with the small syringe placed inside the larger one. An electrode is inserted into both syringes to ensure that the polymer solutions experience the same electrical charge. In Figure 2.10(b) a transmission electron microscopy (TEM) image of a resultant cone-shell fibre created by the dual syringe spinneret system is shown.

Co-axial electrospinning can also be used to create nanofibres from polymer solutions that are not electrospinnable on their own. One example of this is when using low molecular weight poly(dodecylthiophene) (PDT) as the core and poly(ethylene oxide) (PEO) as the shell. The PDT's

molecular weight is too low for it to be electrospun alone, so PEO is used as a template to form the shell fibres with the PDT forming the inner, core nanofibre. If it is desired, the shell polymer can then be removed to yield a pure PDT nanofibre, something that could not be achieved *via* electrospinning of the PDT alone.[103] Core-shell fibres can also be created where the core and the shell consists of the same polymer. Recently the co-axial spinning of poly(lactic acid) fibres consisting of a semi-crystalline poly(L-lactic acid) core and an amorphous poly(D,L-lactic acid) shell was demonstrated.[104]

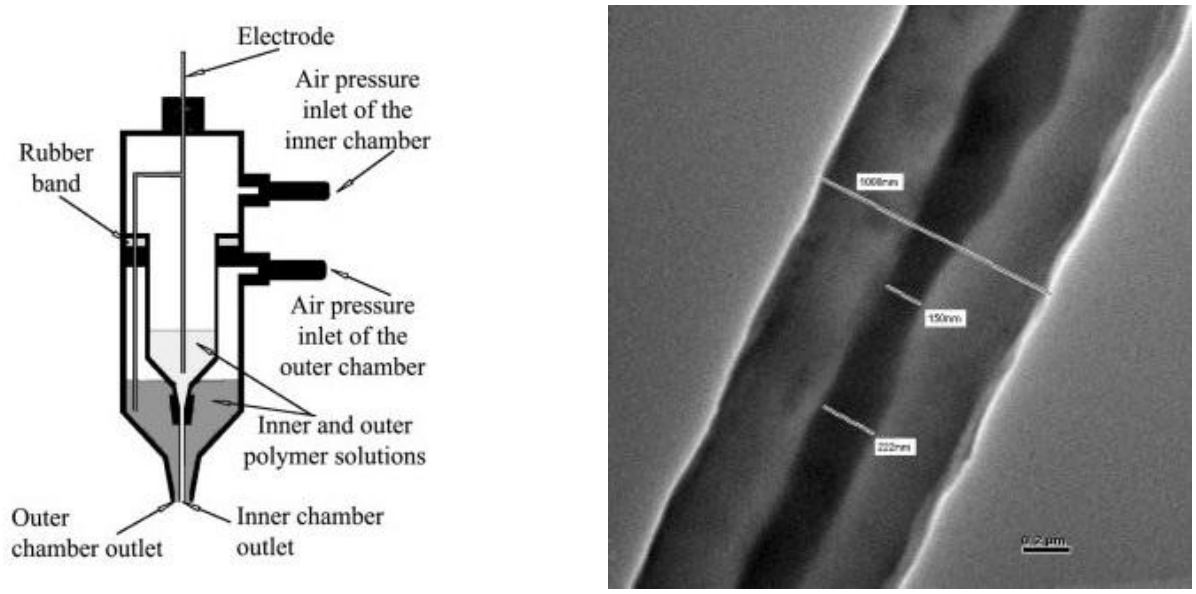

Figure 2.10 – **(a)** Duel syringe spinneret setup for the creation of novel nanofibres as well as **(b)** an unstained TEM image of a nanofibre spun with a PEO shell and a PDT core.[103]

One of the problems experienced when using needle electrospinning is that the process has very low nanofibre production rates. A typical production rate of 0.1 to 1 g/h can be achieved using needle electrospinning, depending on the various system and operational parameters of the polymer solution.[28] This slow fibre production rate severely limits the potential commercial applications of electrospun nanofibre membranes.

2.4.3 Scaling up electrospinning: multiple needle, free surface and needleless electrospinning

Different multiple needle electrospinning configurations, free surface electrospinning and needleless electrospinning setups have been reported in literature and described in a few review papers.[25,105–107] These electrospinning processes are specifically designed to increase the fibre production capacity of the electrospinning process. Multiple needle electrospinning as well as four of the free surface and needleless electrospinning processes are briefly discussed.

2.4.3.1 Multiple needle electrospinning

One way of increasing the electrospinning process' fibre production capacity is to simply use more needles. This is achieved by placing needles or pipettes used for electrospinning next to each other, increasing the production capacity far beyond that of a single needle or pipette. The final production capacity of the multiple needle process is dependent on both the amount of needles used as well as their configuration.

Different amounts and arrangements of needles have been used, for instance the square and the straight line configurations shown in Figure 2.11. The jets from neighbouring needles repel each other due to the charges they carry and decreasing the distance between nozzles cause the repulsive forces to increase.[71] Different spin solutions can also be used in the same multiple needle setup.[108]

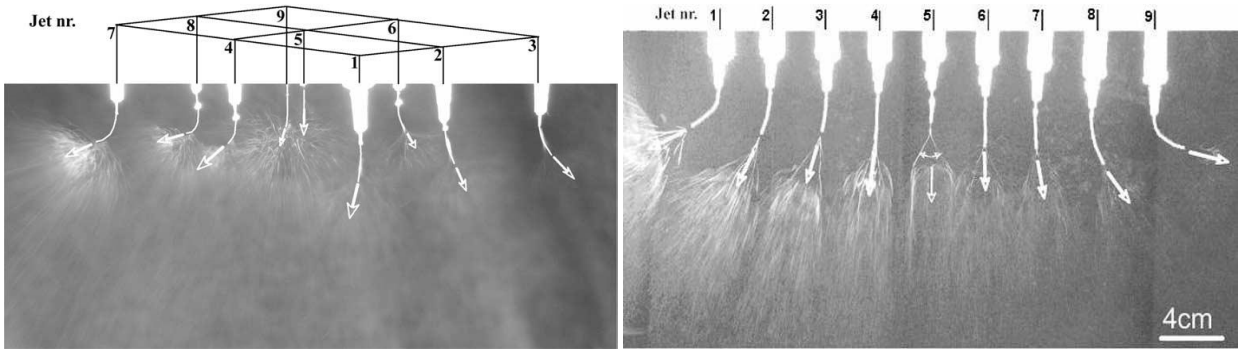

Figure 2.11 – **(a)** A square configuration nine-jet multiple needle electrospinning setup where the syringes are placed 5 cm apart. **(b)** A straight line nine-jet multiple needle electrospinning setup where the syringes are placed 4 cm apart. In both images arrows are added to show the direction in which the individual electrospinning jets form. The solution consisted of 3 wt% PEO dissolved in water.[71]

One of the problems observed with multiple needle electrospinning is that the process creates non-uniform electric fields, which in turn causes non-uniform nanofibre membranes.[28] The jets on the outer edges of the electrospinning process have a larger area to undergo whipping and stretching, causing variations in the nanofibres obtained by this process. Another problem when using the multiple needle electrospinning setup is the blockage of the needles by precipitated polymer solution.

2.4.3.2 Electrospinning from a magnetic liquid

This needleless electrospinning technique employs a magnetic liquid to create localized point charges in the polymer solution to be electrospun.[109] A schematic diagram of the setup is shown in Figure 2.12. When the magnetic field is applied, the magnetic liquid forms spike-like structures in the bath. The polymer solution covering the magnetic liquid takes on these shapes and produces localized points from which electrospinning initiates. When sufficient potential is applied, in the reported case a positive voltage of 32 kV applied to the polymer solution while the collector was grounded, the spin solution forms Taylor cones at these spikes.[109] Spinning from a 38.5 cm^2 dish towards a flat collector

produces only 2 to 70 jets, while many more jets are produced when spinning to a collector with teeth pointing toward the spin solution, such as a saw blade.

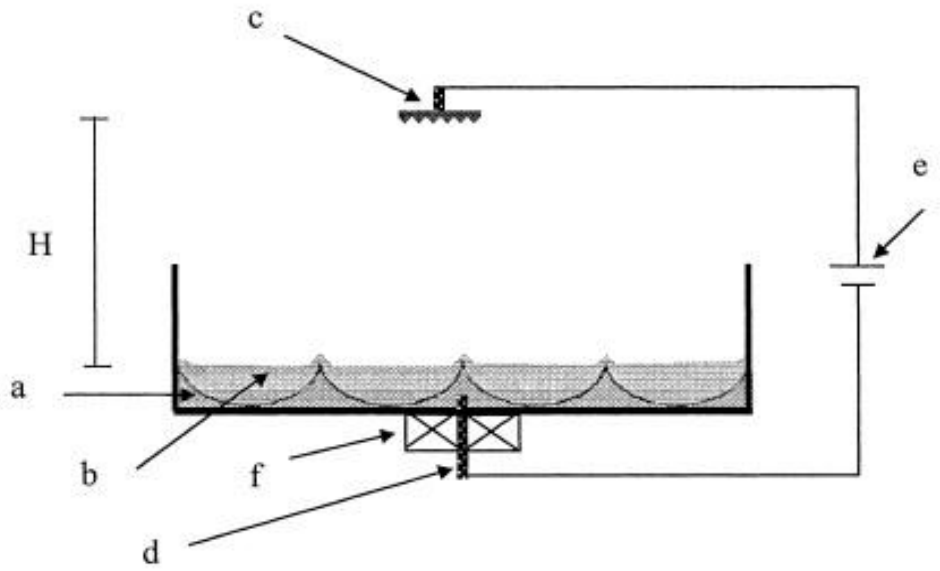

Figure 2.12 – A schematic diagram showing the needleless electrospinning process using a magnetic liquid. The bottom of the bath holds a layer of magnetic liquid (a) that is in turn covered by the polymer solution to be electrospun (b). An electrode (d) is submerged in the magnetic liquid to charge the polymer solution while a permanent magnet or electromagnet (f) ensures the spiking of the magnetic liquid. The counter electrode (c) is above the polymer solution and acts as the collector for the nanofibres, while a high voltage power supply (e) is used to create the electric field in which electrospinning takes place.[107]

2.4.3.3 Bubble electrospinning

Bubble electrospinning is a process where, instead of spinning from the surface of a solid entity such as a needle tip, the jets form on the surface of a polymer bubble, shown in Figure 2.13(a). It is a high throughput needleless electrospinning process that has only recently been developed and patented. According to a European Patent Office, the first patent describes bubble electrospinning as being a process where high voltage is applied to continuously generated polymer bubbles to facilitate electrospinning.[110]

Gas is blown into the bottom of the polymer bath and its low density makes it rise through the solution until the gas forms half spherical bubbles on the surface of the polymer. A number of different types of gas has been used for this, including atmospheric air, CO_2, N_2 or inert gasses.[111] The collector is positioned above the polymer bubbles, so electrospinning takes place bottom to top when a high voltage is applied to the polymer solution.[112]

2.4.3.4 The Nanospider™ process

Elmarco is a company that uses the patented Nanospider™ technology.[113] The technology is based on a polymer bath with a pivoted rotating electrode that is partly submerged in the polymer solution. A potential of between 30 and 120 kV is applied to the electrode and then transferred to the polymer solution on the electrode surface.[114] This voltage is strong enough to overcome the surface tension forces of the spin solution, which causes Taylor cones to form and electrospinning to initiate (Figure 2.13(b)).

The Nanospider™ technology has been used to create a range of nanofibres, including but not restricted to polyurethane nanofibres for filters, polyvinyl alcohol nanofibres as part of noise absorption filters, and many different inorganic nanofibres including TiO_2 nanofibres for dye sensitized solar cells.[114–116]

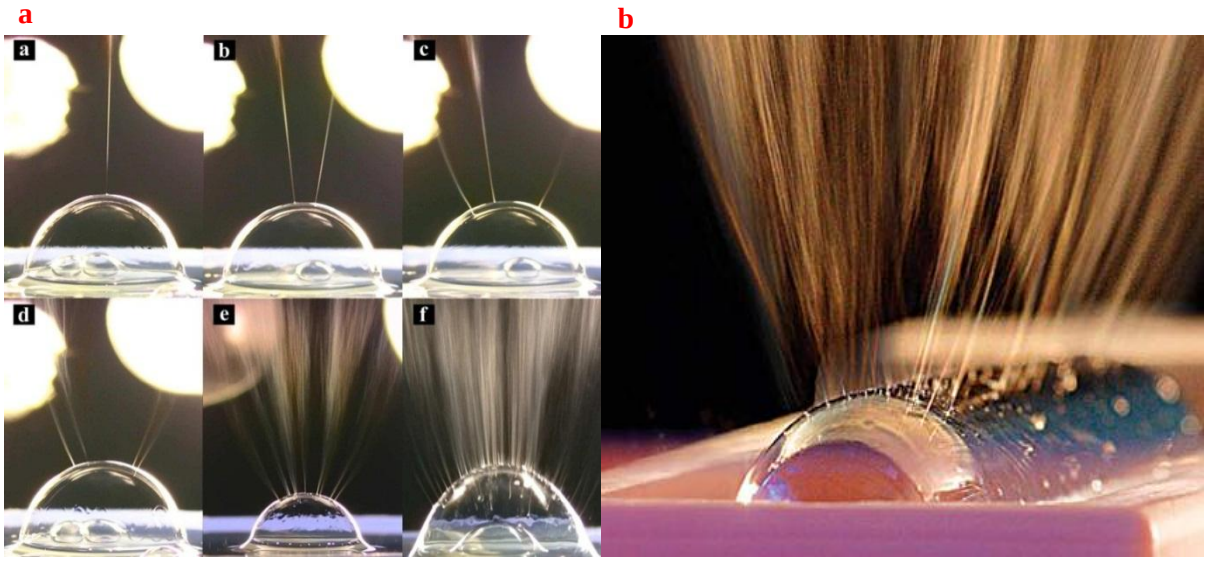

Figure 2.13 – (a) Photographs of the repulsion effect that an increasing amount of jets on the same bubble (from a to f) have on each other. Their raised configuration with regard to the rest of the polymer solution creates a shorter distance between the top of the bubble and the collector. This in turn causes a larger concentration of charge at the top of the bubble and more of the electrospun jets initiate or migrate to that area. Reprinted with permission from A.E Smit. **(b)** The Nanospider process' rotating electrode during electrospinning, with multiple jets forming on the electrode surface.[114]

2.4.3.5 Ball electrospinning

The final high throughput electrospinning process being discussed is that of ball electrospinning. Ball electrospinning is an upward needleless electrospinning process used to create multiple nanofibres from multiple simultaneously formed polymer jets. It is based on the principle of polymer jets forming on the surface of an electrically charged sphere. The process of ball electrospinning was developed at Stellenbosch University and since then a patent application has been filed on the process.[29] Figure 2.14 is the setup from the ball electrospinning patent with numbers indicating the different components.

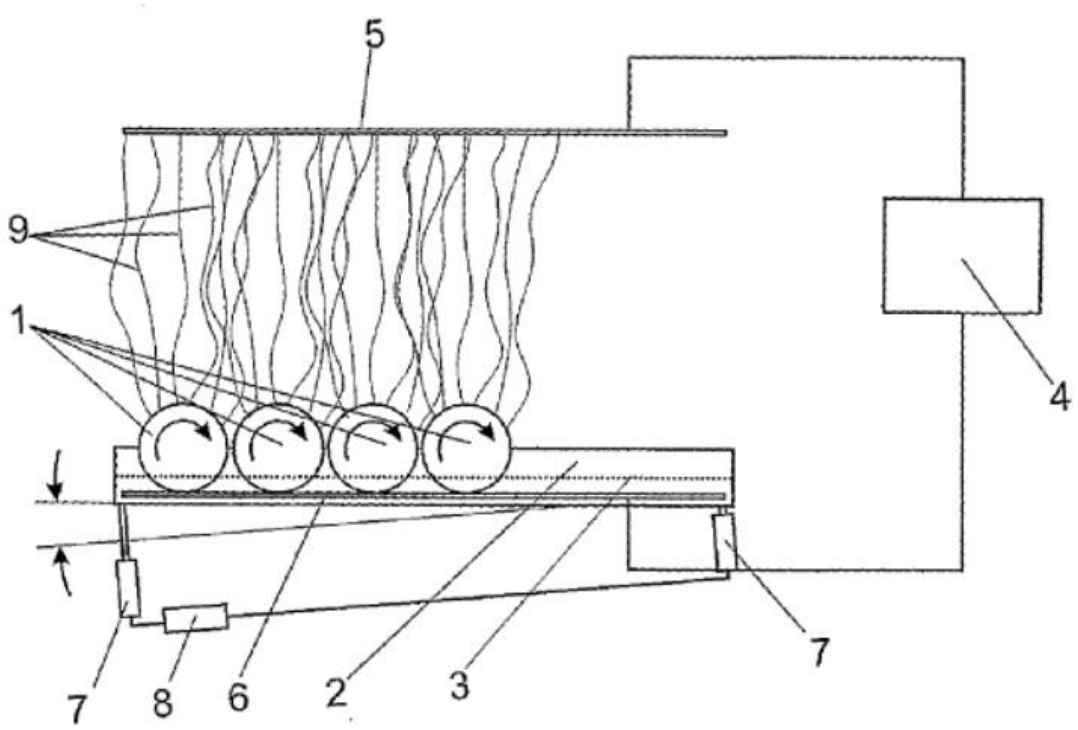

Figure 2.14 – The ball electrospinning setup as shown in the patent, where multiple balls are used to create electrospun nanofibres. Multiple loose rotating balls (1) in a solution container (2) houses the polymer solution (3) to be electrospun. An electric field is created between the balls (1) and a collector (5) by means of a high voltage power supply (4). A contact plate (6) supports the balls while the trough is moved by one of a few different methods, including by means of pistons (7). The motion can be controlled by using an automatic valve assembly (8). When sufficient electrical charge is applied to the balls, electrospinning jets (9) eject from the surface of the balls and are deposited on the collector as nanofibres.[29]

Taylor cones formed during the ball electrospinning process are stabilised into jets when two conditions are met.[117] The first condition is that the jets are mechanically strong enough to stabilise the Taylor cones. Sufficient polymer chain entanglement is therefore required as low molecular weight or low viscosity solutions would not form stable Taylor cones. The second condition is that the polymer spin solution continuously feeds the jets on the spinning surface. This means that the spin solution has to have sufficiently low viscosity to be able to flow and continuously feed the jet with fresh polymer from the surrounding solution. This is facilitated by the ball rotating in solution to continuously supply solution from the bath to the points of electrospinning.

The ball surface area is large relative to the surface area available on the tip of a needle, therefore multiple jets form when the electric potential is high enough (the potential required depends on the system parameters, operational parameters and external factors). These jets increase fibre formation drastically as multiple jets forming multiple fibres spring forth from each individual ball. A trade-off for all these fibres being produced is that ball electrospinning requires much higher applied voltages to initiate electrospinning than conventional needle electrospinning.[118]

2.4.4 Applications and uses for nanofibres

Even though renewed research into nanofibres has only recently started in earnest, a wide range of applications are already available for these fibres, with a few review articles listing some of them.[25–27] The main properties that make these fibres so sought after have already been mentioned, and include their very long fibre length and small diameters coupled with their extremely large specific surface area. The nanofibres can be formed into very thin and highly porous membranes that have a variety of membrane pore sizes with good permeability. They can also have the ability to retain electrostatic charges, have a low basic weight, and aligned polymer chains along the fibre axis.[22–25]

Nanofibres have been found to be useful in various medical applications. They are well suited as tissue engineered scaffolding materials that support a variety of cells and exhibit cell attachment and growth.[27] Nanofibres are also used as wound dressings because their large surface areas can contain many antimicrobial agents that provide protection for the user while the pores in the structure allow unrestricted breathing.

The use of electrospun nanofibres for chemical supports has been investigated. The chemicals imbedded in the nanofibres include catalysts and enzymes.[119,120] Nanofibres are also used to keep chemicals out, like the layers placed in military garments designed to shield the wearer from chemical warfare agents.[121] Some nanofibre materials have been designed to react to external stimuli and to produce an output. These nanofibre sensors can be used as tools in bioindustrial, medical and environmental analysis, to name but a few.[26,122]

There are a wide variety of electric and electronic applications where nanofibres are concerned. Electrospinning is an easy method for creating one-dimensional polymer field-effect transistors, which in turn forms the basic building blocks of logic circuits and display switches.[123,124] Electrospun nanofibres are also used as the first step in creating carbon nanofibre webs that can be applied as electrodes for super capacitors.[124]

Composite building materials have begun to incorporate nanofibres. Large surface areas allow a greater degree of adhesion between the nanofibres and the composite matrix. It has been shown that incorporating polybenzimidazole nanofibres into epoxy-based composites increase the final product's Young's modulus, fracture toughness and fracture energy.[125] Nanofibres are also used in the creation of transparent epoxy-based composites because they have diameters that are smaller than the wavelength of visible light, effectively making them invisible in the matrix.[126]

Some nanofibre properties however limited their use as standalone materials, including their low basic weight and the fact that they mostly consist of thin layers with only limited mechanical strength. Nanofibre filters are therefore usually composites that consist of a substrate or substrates which ensure the filter had sufficient mechanical strength while the nanofibre layer or layers provide filtration efficiency or other desired properties. The very high filtration efficiency achieved can be ascribed to

the small size of the nanofibres as well as the small pore sizes and pore distribution.[127] In this regard, nanofibres are mostly used as air/gas filters, but they have also been used in liquid filtration.[48]

In conclusion, nanofibres are well suited for applications in the fields of medicine and biomedicine, pharmacy, catalysis, sensors, composites, ceramics, electronics, photonics, and filters, to name but a few.[25] Nanofibres also form great affinity membranes and are ideally suited for the extraction and potential separation/recovery of a variety of chemical species due to their large specific surface areas and functionalisable surfaces. Moreover, the pores formed within these nanofibre web structures are interconnected, which creates a three-dimensional network structure that allows the entire surface area to be available for extraction.[128]

CHAPTER 3

EXPERIMENTAL

3.1 Synthesis and characterization

3.1.1 Reagents used

The three reagents used for the synthesis of the poly(*N*-terephthaloylthiourea)-*N*',*N*'-piperazine were:

- terephthaloyl chloride flakes ($C_8H_4Cl_2O_2$) (Sigma-Aldrich®, 99+ % assay),
- sodium thiocyanate (NaSCN) (Merck, 98.5 % assay), and
- piperazine ($C_4H_{10}N_2$) (Sigma-Aldrich®, *ReagentPlus*®, 99 % assay).

Both the terephthaloyl chloride and NaSCN were dried for 12 hours in a vacuum oven at approximately 60 °C prior to weighing. The terephthaloyl chloride and NaSCN were transferred to a glove box for weighing because of the chemicals' hygroscopic nature.[129] Weighed terephthaloyl chloride and NaSCN were then placed in separate containers, sealed with paraffin film and stored in a desiccator until use. Piperazine sublimates when dried in a vacuum oven, so it was weighed into a container using a bench top scale, sealed with paraffin film and stored in a desiccator until use. The reagents were proven to be sufficiently pure using proton (^{1}H) and carbon (^{13}C) nuclear magnetic resonance spectroscopy (NMR) (see Appendix A).

3.1.2 Synthesis process

Glassware was cleaned in a base bath, rinsed and dried in an oven prior to use. Acetone (uniLAB®, 98.0 % assay) was distilled over 3 Å molecular sieves prior to use to ensure all water was removed. Nitrogen gas (N_2) was passed through drying agent to ensure no moisture was introduced during the reaction. The synthesis followed a "one-pot" two step synthesis procedure, similar to the synthesis described by Douglass and Dains.[130]

Some changes were made to the reaction process described in the patent application.[21] Firstly, the terephthaloyl chloride was placed in the round bottom flask while the thiocyanate salt was placed in the dropping funnel, as NaSCN was easier to dissolve in refluxing acetone than the terephthaloyl chloride. Secondly, the synthesis batch size was much larger than described in the patent application. Therefore, filtration instead of centrifugation was used to recover the product after the completion of the synthesis. Lastly, NaSCN instead of potassium thiocyanate was the thiocyanate salt used because it was readily available.

Figure 3.1 shows the reaction setup used for the poly(*N*-terephthaloylthiourea)-*N*',*N*'-piperazine synthesis while the synthesis procedure is described in a step-wise manner below:

Step 1:

- The setup shown in Figure 3.1 was continuously flushed with dried N_2.
- 2 mol (203.0 g) terephthaloyl chloride was placed in a 6 L round bottom flask.
- The terephthaloyl chloride was completely dissolved in ± 1 L distilled acetone to form a colourless solution.
- 4 mol (162.2 g) NaSCN was transferred to the frit inside the dropping funnel.
- The terephthaloyl chloride and acetone solution was mechanically stirred and heated until refluxing (± 60 °C).
- The NaSCN slowly dissolved in the refluxing acetone and was added drop-wise to the round bottom flask below. As the reaction progressed, the solution in the round bottom flask became slightly more viscous and changed to a lemon yellow colour.
- Refluxing was continued for ± 30 min after all NaSCN was added to the round bottom flask.
- Refluxing was stopped and the solution was allowed to cool. Stirring continued to ensure a homogeneous dispersion and N_2 flushing continued to ensure no moisture was introduced to the setup.

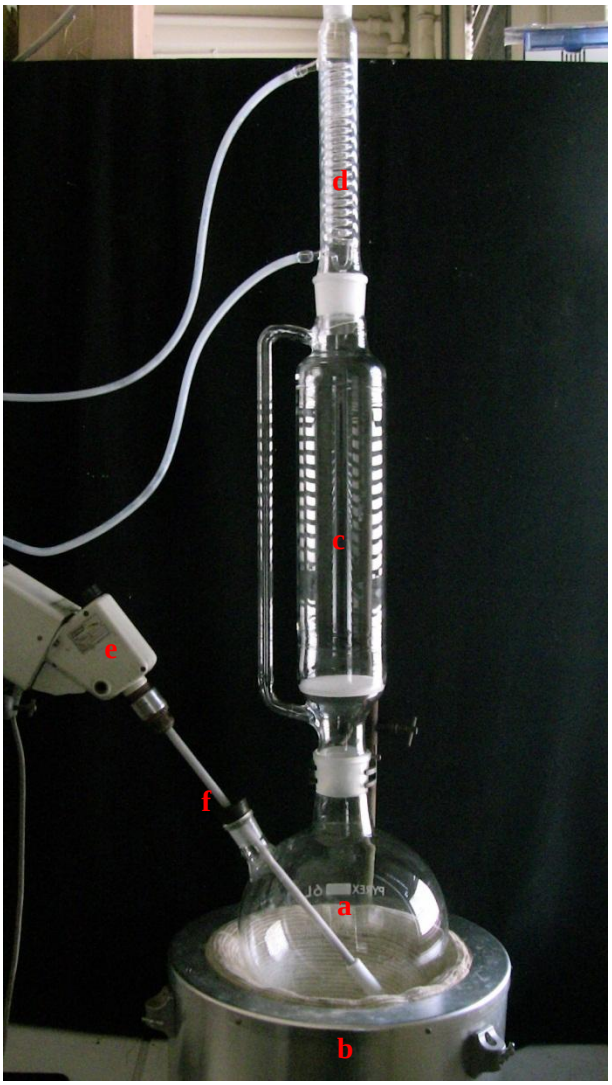

Figure 3.1 – The reaction setup used for the synthesis of poly(*N*-terephthaloylthiourea)-*N'*,*N'*-piperazine consisted of a 6 L round bottom flask (a) positioned in a heating jacket (b). Above the round bottom flask was a dropping funnel with a size one frit (c), while a reflux condenser (d) was placed above the dropping funnel. At the top of the dropping funnel (not shown) was an inlet to introduce the dried N_2 gas. Mechanical stirring was introduced through a second neck in the round bottom flask *via* a motor (e) and chemically inert bladed stirrer (f).

Step 2:

- 2 mol (86.1 g) piperazine was transferred to the frit inside the dropping funnel.
- ± 500 mL additional acetone was added to the solution in the round bottom flask.

- The round bottom flask was heated until the acetone refluxed (± 60 °C). The piperazine formed a white film on the inside of the dropping funnel where it came into contact with the acetone vapours.
- Piperazine dissolved more rapidly than the NaSCN and was added drop-wise to the round bottom flask below. A pale yellow solid formed where the dissolved piperazine came into contact with the lemon yellow solution in the round bottom flask. These solid lumps made stirring the solution increasingly difficult as the reaction progressed. A viscous mixture was subsequently formed.
- The reaction was stirred and refluxed for 30 min after all the piperazine had been added to the round bottom flask.
- Refluxing was stopped and the reaction setup was allowed to cool.
- Stirring and flushing with N_2 gas was stopped.

Step 3:

- The viscous poly(*N*-terephthaloylthiourea)-*N*',*N*'-piperazine mixture was transferred to a beaker containing ± 2 L of Milli-Q water and allowed to stand in a fumehood for 12 h so some acetone could evaporate.
- The viscous mixture was filtered using a Buchner funnel and no.41 Whatman® filter paper. The filtrate was a lemon yellow liquid.
- 1 L acetone was used to wash the product while stirring for ± 60 min.
- The acetone was filtered off using a funnel and filter paper. The filtrate was again a lemon yellow liquid.
- In this way the solid product was washed alternating between 1 L Milli-Q water and 1 L acetone for ± 60 min each time and filtered after each washing cycle. This was done until the filtrate was colourless (requiring seven cycles of each Milli-Q H_2O and acetone).

The end product was a fine powder with an off-yellow colour. The powder was dried overnight in a vacuum oven to remove any residual acetone and water before weighing or analysis. A number of analysis techniques were used to elucidate the structure, molecular weight and chemical composition of the solid produced by the synthesis, including proton (^{1}H) and carbon (^{13}C) nuclear magnetic resonance spectroscopy (NMR), Fourier transform infrared spectroscopy (FTIR), gel permeation chromatography (GPC) and elemental analysis (EA).

3.1.3 Proton (^{1}H) and carbon (^{13}C) nuclear magnetic resonance spectroscopy (NMR)

A Varian Inova 400 MHz NMR spectrometer and Varian Inova 600 MHz NMR spectrometer were used for the NMR analysis. Deuterated dimethyl sulfoxide (Sigma-Aldrich®, 99.9 atom % D DMSO-d_6) was used to prepare the NMR solutions. ^{1}H NMR was done on terephthaloyl chloride and

piperazine, while ^{13}C NMR analysis was done on all three the starting reagents (terephthaloyl chloride, NaSCN and piperazine) to determine their purity. ^{1}H NMR and ^{13}C NMR analysis for the poly(*N*-terephthaloylthiourea)-*N*',*N*'-piperazine were also done in an attempt to elucidate the structure.

3.1.4 Fourier transform infrared spectroscopy (FTIR)

A Nexus™ 670 FTIR spectrometer from Thermo Nicolet was used for FTIR analysis. Potassium bromide (KBr, puriss p.a. for IR-spectroscopy) was used to create KBr pellets containing the poly(*N*-terephthaloylthiourea)-*N*',*N*'-piperazine for analysis. FTIR analysis of the poly(*N*-terephthaloylthiourea)-*N*',*N*'-piperazine was done in an attempt to elucidate the structure.

3.1.5 Gel permeation chromatography (GPC)

The GPC analysis was performed on instrumentation consisting of a Shimadzu LC-10AD pump, a Waters 717Plus autosampler, a column system fitted with a 50 x 8 mm guard column in series with three 300 x 8 mm, 10 µm particle size GRAM columns (2 x 3000 Å and 100 Å) obtained from PSS, a Waters 2487 dual wavelength UV detector and a Waters 410 differential refractive index (DRI) detector all in series. The instrument was calibrated with PMMA standards (Polymer Laboratories) and the analysis was done using dimethyl acetamide as the solvent system. GPC was done on the poly(*N*-terephthaloylthiourea)-*N*',*N*'-piperazine so that the number average molecular weight (M_n) and weight average molecular weight (M_w) could be determined from the retention volume.

3.1.6 Elemental analysis

A Leco® TruSpec® Micro was used for elemental analysis. The instrument was calibrated using sulfamethazine standards. Elemental analysis was done on the poly(*N*-terephthaloylthiourea)-*N*',*N*'-piperazine to determine the elemental composition, including percentages carbon, hydrogen, nitrogen and sulphur.

3.2 Needle and ball electrospinning

3.2.1 Preparation of electrospinning solutions

The solutions used for electrospinning consisted of three parts:

- synthesised poly(*N*-terephthaloylthiourea)-*N*',*N*'-piperazine oligomer,
- polyacrylonitrile (PAN) fibres (tows consisting of 12000 filaments, gifted by Bluestar Fibres Company Limited), and
- DMSO (C_2H_6OS) (Merck, ≥ 99 % assay).

Both the PAN and DMSO were used as received. The solutions used for electrospinning were reported as having a wt% PAN as well as a ratio of PAN to poly(*N*-terephthaloylthiourea)-*N*',*N*'-piperazine oligomer. The wt% PAN referred to was the dry weight of PAN relative to the weight amount of solvent. The calculation of the wt% PAN is shown in Equation 1. The ratio of PAN to poly(*N*-terephthaloylthiourea)-*N*',*N*'-piperazine referred to the dry weight of PAN relative to the dry weight of oligomer added to the spin solution.

$$\frac{(weight\ of\ PAN\ in\ g)}{(total\ weight\ of\ solution\ in\ g)} = wt\%\ as\ a\ fraction \qquad [1]$$

3.2.2 Composition of the electrospinning solutions

Two different solutions were used to create all the electrospun nanofibre webs during this work. The wt% PAN was chosen as 6 wt% and 8 wt%, while both solutions had a ratio of PAN to poly(*N*-terephthaloylthiourea)-*N*',*N*'-piperazine of 7:3. The mass of each component required for making these solutions are shown in Table 3.1.

Table 3.1 – Mass of each component required to create the 6 wt% and 8 wt% PAN solutions with a PAN to poly(*N*-terephthaloylthiourea)-*N*',*N*'-piperazine ratio of 7:3 using DMSO as solvent.

	6wt% Solution	**8wt% Solution**
PAN added (g)	6.00	8.00
poly(*N*-terephthaloylthiourea)-*N*',*N*'-piperazine added (g)	2.57	3.43
DMSO added (g)	91.43	88.57
Total weight (g)	100	100

3.2.3 Needle electrospinning setup

Electrospinning was done in a bottom to top configuration where the needle tip was pointing vertically up towards the collector. This configuration was used for both needle and ball electrospinning processes to ensure the processes were comparable in this regard. The needle electrospinning setup is shown in Figure 3.2.

A hydraulic pump (Pump 33 double syringe pump from Harvard Apparatus) with a flow rate of 5 µL/min was used to ensure a steady feed of polymer solution during needle electrospinning. Disposable 1 mL syringes were used as a solution reservoir and disposable hypodermic needle tips with an internal diameter of 0.45 mm were used to create the point where electrospinning occurred. The power source was a high voltage power source by Matsusada Precision (model number: UNIT AU-80P1.87-LC), capable of supplying 80 kV positive charge. The rotating collector was made in-house (circumference 46 cm, length 32 cm) and was operated at a surface speed of 200 m/min.

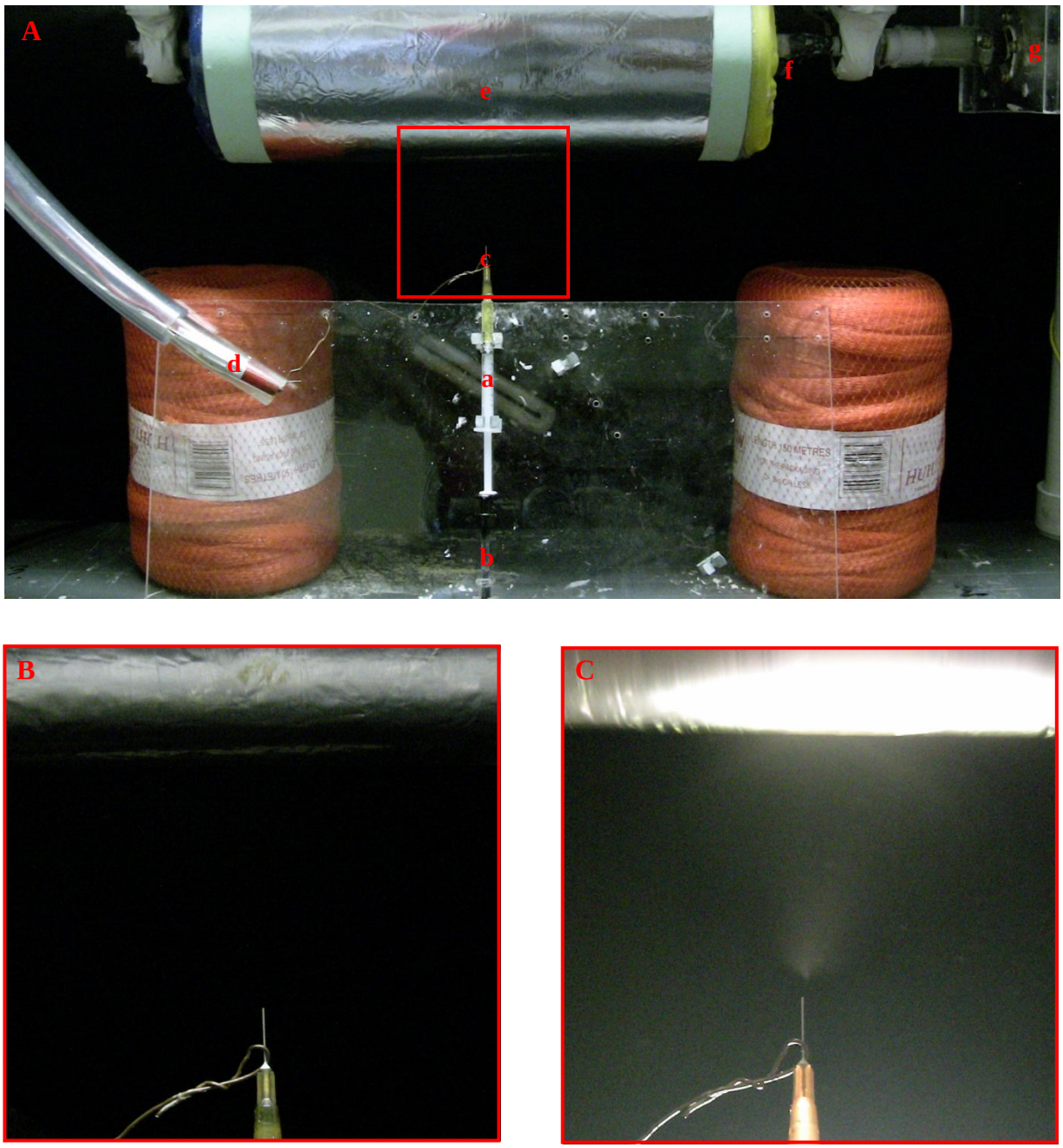

Figure 3.2 – **(A)** An image of the needle electrospinning setup with its components, while **(B)** and **(C)** are magnified images of the process while not electrospinning and during electrospinning, respectively. The setup consisted of a disposable 1 mL syringe (a) which contained the spin solution, connected to a hydraulic pump (b). A metallic tip (c) was fixed to the syringe which in turn was connected to the positive electrode of the high voltage power source (d). A rotating collector (e) was positioned above the needle and was grounded by a conductive wire (f). The collector was rotated by an electrical motor (g) at a surface speed of 200 m/min.

3.2.4 Ball electrospinning setup

Ball electrospinning was performed using a setup designed by the Electrospinning and Nanofibre Yarns Group within the Department of Chemistry and Polymer Science at the University of Stellenbosch. The setup is shown in Figure 3.3.

The solid glass ball used during ball electrospinning had a diameter of 26 mm and was rotated at 3.5 rpm. The same high voltage power source and collector as in the needle electrospinning process were used, with the collector rotating at a surface speed of 200 m/min. The polymer solution in the reservoir ((c) in Figure 3.3(A)) was topped up as required to maintain a steady solution level (usually every 3 to 5 min).

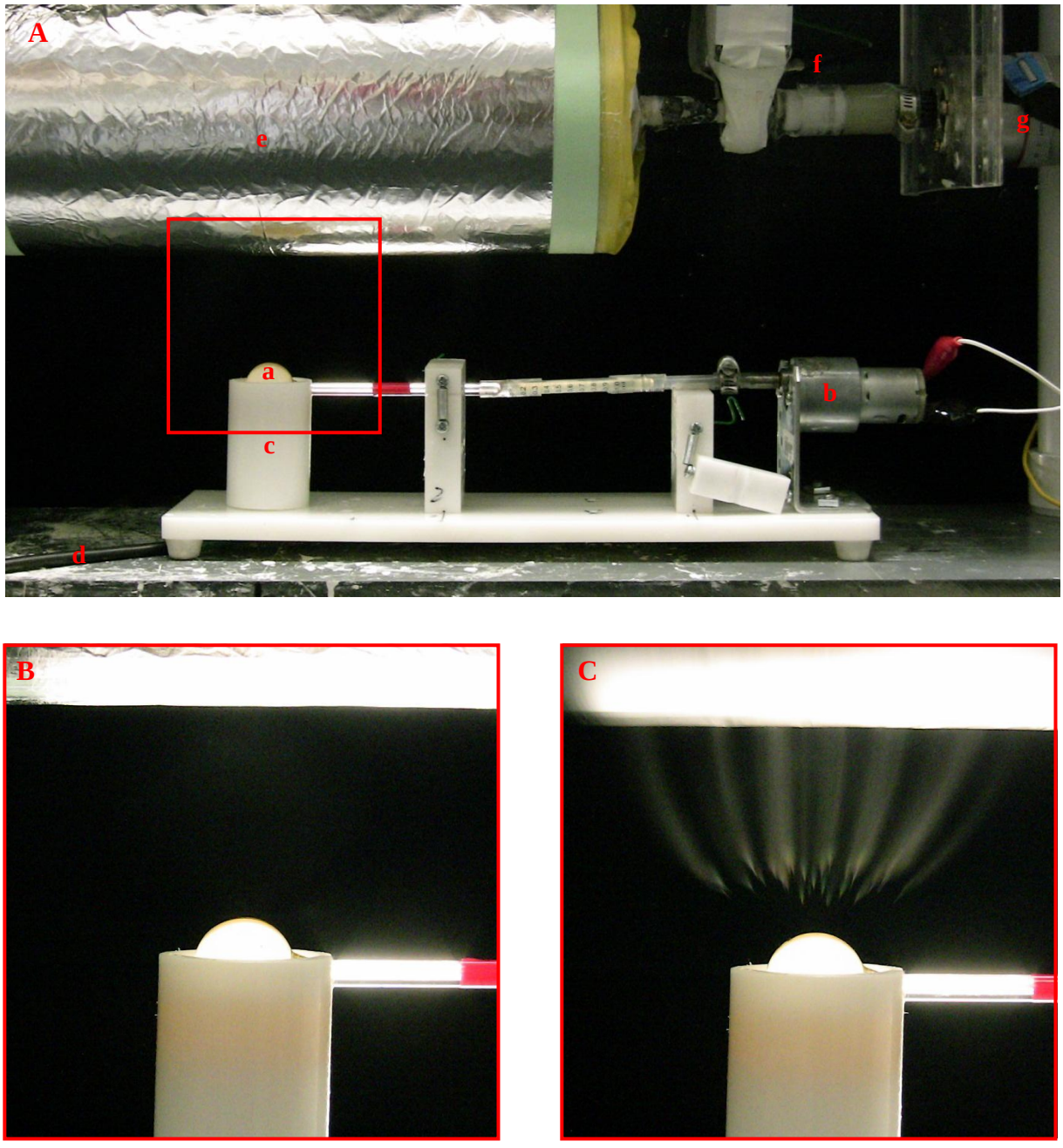

Figure 3.3 – **(A)** An image of the ball electrospinning setup with its components, while **(B)** and **(C)** are magnified images of the process while not electrospinning and during electrospinning, respectively. The setup consisted of a glass ball (a) which was rotated at 3.5 rpm by an electrical motor (b). The stand on which the motor was mounted, as well as a cup which acted as a spin solution reservoir (c) were made from a chemically inert and non-conductive material. In the bottom of the spin solution reservoir was a metal rod that was connected to the positive electrode of the high voltage power source (d). A rotating collector (e) was positioned above the ball electrospinning setup. The collector was grounded by a conductive wire (f). The collector was rotated by an electrical motor (g) at a surface speed of 200 m/min.

Backbuilding is occasionally observed when using high throughput electrospinning processes such as ball electrospinning.[131] Backbuilding is described as polymer jets targeting other jets or raised nanofibres on the collector surface rather than forming flat nanofibre webs on the collector.

Some nanofibres that hit the collector were not immediately flattened against the surface of the collector. This caused localized raised surfaces on the collector which were more attractive targets for incoming jets (electric field strength was higher when the same voltage was applied over a smaller distance). Incoming polymer fibres therefore targeted these raised fibres. This fibre on fibre deposition was repeated (Figure 3.4(a) to (c)) until there was a strand of polymer building from the collector towards the ball by means of incoming polymer jet deposition. A second, more systematic set of images showing the process of backbuilding is shown in appendix B.

Ball electrospinning over greater distances (7 cm and more during this work) caused the jets to consecutively target raised fibres on the collector and backbuilding was observed. The nanofibres were therefore spun over the largest effective spinning distance to ensure the driest possible nanofibres, while keeping the distance short enough to ensure backbuilding was not observed.

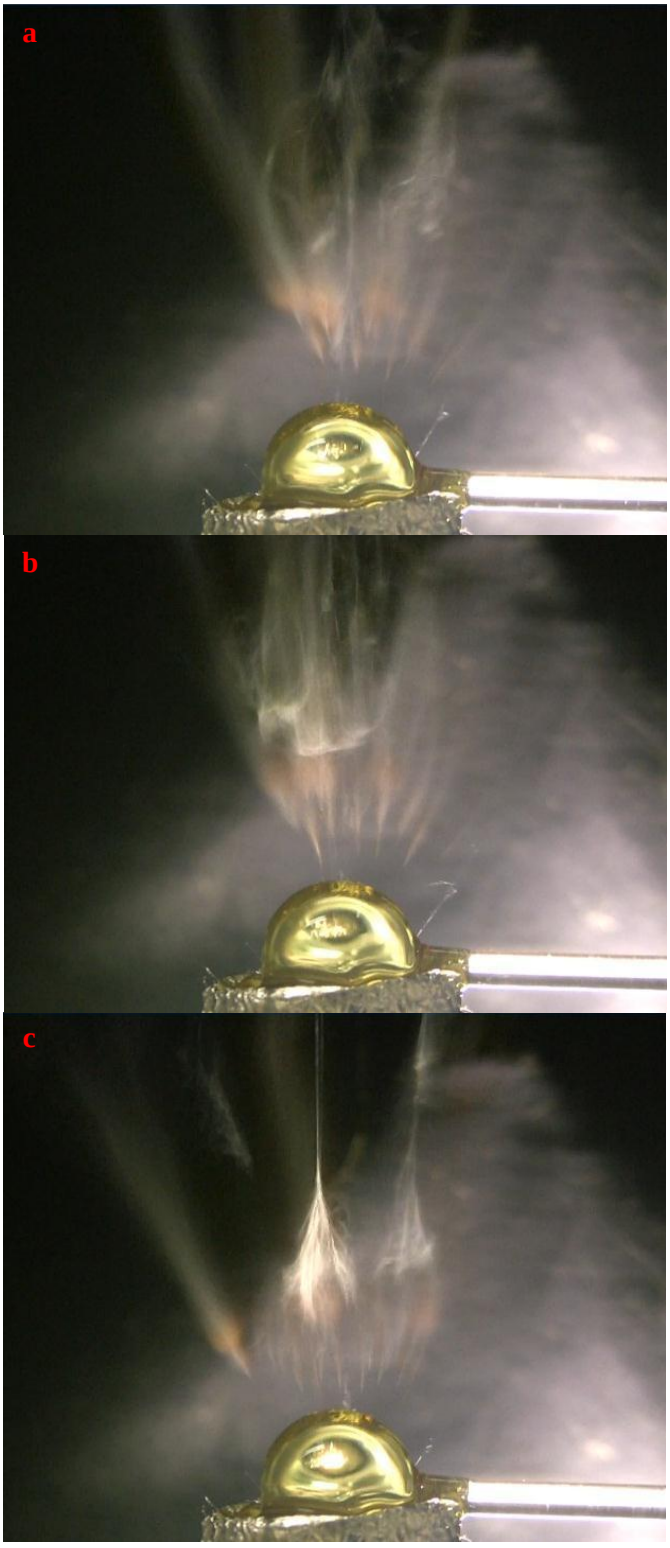

Figure 3.4 – Sequence of images (from (a) to (c)) of backbuilding during ball electrospinning.

The nanofibres deposited on the collector were wet, as complete drying did not take place during the whipping and stretching of the polymer jets while traveling such small distances. To ensure that no

residual solvent affected the subsequent extraction experiments, all the nanofibre webs were washed with distilled water at room temperature no more than 60 seconds after electrospinning was completed. They were washed for roughly 30 minutes and then allowed to dry at room temperature.

3.2.5 Solution property measurements

Each solution's conductivity, viscosity and surface tension was measured before electrospinning. Solution conductivity was measured with an EC215 Conductivity Meter from Hanna Instruments and reported in µS/cm. Solution viscosity was measured with a Brookfield DV-E Viscometer (Model RVTD) using a number 21 cone spindle and shear rate of 50 rpm while the solution chamber was at 25 °C. Viscosity values were reported in cP. Solution surface tension was measured with a Krüss tensiometer (model K6) using a platinum-iridium ring. Surface tension values were reported in mN/m.

3.2.6 Electrospinning conditions for the comparison between needle and ball electrospinning

The 6 wt% PAN solution with a ratio of PAN to poly(*N*-terephthaloylthiourea)-*N*',*N*'-piperazine of 7:3 was chosen for the comparison between the needle and ball electrospinning processes. The effective spinning distance was 5 cm, the solution flow rate was 5 µL/min, and a positive voltage of 8 kV was applied to the solution during needle electrospinning. The effective spinning distance was 5 cm, the ball rotation speed was 3.5 rpm and a positive voltage of 35 kV was applied to the solution during ball electrospinning. For both of these processes the collector was grounded. The fibres produced by the two electrospinning techniques were weighed after being washed in distilled water and dried at room temperature for 12 hours.

3.2.7 Conditions for ball electrospinning 6 wt% PAN and 8 wt% PAN solutions

Fibres with different specific surface areas were produced to determine the effect that electrospun nanofibres' specific surface area had on the extraction of Pt ions. To investigate this a 6 wt% PAN and an 8 wt% PAN solution, both with a ratio of 7:3 of PAN to poly(*N*-terephthaloylthiourea)-*N*',*N*'-piperazine (see Table 3.1) were ball electrospun. The 6 wt% PAN solution was electrospun over an effective spinning distance of 5 cm while the applied voltage was set to positive 35 kV. The 8 wt% PAN solution was electrospun over an effective spinning distance of 6 cm while the applied voltage was set at positive 35 kV. A grounded rotating collector was used in both cases. The fibres produced by the two electrospinning techniques were weighed after being washed in distilled water and dried at room temperature for 12 hours.

3.2.8 Analysis of the nanofibre webs produced by electrospinning

A Leo® 1430VP scanning electron microscope (SEM) was used to obtain images of the nanofibre webs formed by the needle and ball electrospinning processes. A Nova™ NanoSEM was used to acquire high resolution images of the electrospun nanofibres. The fibre diameters were analysed using SEM Image Studio software. A minimum of 200 fibre diameters were measured from each nanofibre web to ensure representative average fibre diameter and standard deviation values.

3.3 Extraction of hexachloroplatinate

Sodium hexachloroplatinate(IV) hexahydrate salt ($Na_2[PtCl_6]\cdot 6H_2O$) was used to make 3 L stock solution with a Pt ion concentration of 100 mg/L. The amount of platinum salt required to make the stock solution was determined by using the platinum molar mass fraction. The molar mass of $Na_2[PtCl_6]\cdot 6H_2O$ is 561.9 g/mol while the molar mass of platinum is 195.1 g/mol. Using these molar masses, the platinum molar mass fraction was calculated and is shown in the equation: $\frac{M_r\ Na_2\ PtCl_6\cdot 6H_2O}{M_r(Pt)} = 2.88$. For every gram of Pt ions required in the solution, 2.88 g of $Na_2[PtCl_6]^{2-}\cdot 6H_2O$ had to be added.

The extraction of Pt ions by the poly(*N*-terephthaloylthiourea)-*N*',*N*'-piperazine oligomer and oligomer-containing nanofibres was investigated in a hydrochloric acid (HCl) matrix. The HCl was bought from Sigma-Aldrich® (Fluka® Analytical, ≥ 32 %). The matrix concentration chosen for the extraction of Pt ions was 1 M HCl (except during the investigation of the effect of HCl concentration on Pt extraction, discussed in Chapter 6, section 6.4). To prepare a 3 L solution with a Pt ion concentration of 100 mg/L and HCl concentration of 1 M, 288.0 mg of $Na_2[PtCl_6]\cdot 6H_2O$ and 297.9 mg concentrated HCl was needed. The rest of the 3 L solution was made up using Milli-Q water.

All of the investigations were in the form of batch extraction experiments. Each batch extraction experiment was repeated three times and for each extraction 50 mg nanofibres or 15 mg of poly(*N*-terephthaloylthiourea)-*N*',*N*'-piperazine powder as well as 10 mL acidified $[PtCl_6]^{2-}$ stock solution was used. All extractions were conducted in size eight polytops under continuous shaking. The polytops were sealed with paraffin film to ensure no solution loss due to leakage.

3.3.1 Inductively coupled plasma atomic emission spectroscopy (ICP-AES)

The ICP instrument used was a Spectro Arcos model FHS12. For each solution analysed, the argon and chloride concentrations were monitored to ensure a stable background, while several platinum wavelengths were recorded. The values given by the platinum 265.95 nm wavelength was used to

represent the Pt(II/IV) ion concentrations reported for this study. For each ICP analysis 10 mL of solution was used and triplicate measurements were taken for every solution analysed.

3.3.2 Effect of specific surface area and available coordination sites on Pt(II/IV) ion extraction

The samples used for this investigation consisted of fibres spun using a 6 wt% PAN solution, fibres spun using a 8 wt% PAN solution and pure poly(*N*-terephthaloylthiourea)-*N*',*N*'-piperazine powder. The mass of oligomer-containing nanofibres used for each experiment was 50 mg while the mass of pure poly(*N*-terephthaloylthiourea)-*N*',*N*'-piperazine used was 15 mg. This was due to only 30 % of the electrospun nanofibres consisting of poly(*N*-terephthaloylthiourea)-*N*',*N*'-piperazine (ratio of 7:3 PAN to oligomer), which constituted 15 mg of the total 50 mg sample. The PAN and *Platisorb* were intimately blended before electrospinning, so it was reasonable to assume that all 15 mg of the *Platisorb* was incorporated into the nanofibre webs. Each sample therefore (whether 50 mg nanofibres or 15 mg poly(*N*-terephthaloylthiourea)-*N*',*N*'-piperazine powder) contained 15 mg of the oligomer.

The volume of $[PtCl_6]^{2-}$ solution used for each analysis was 10 mL, while the concentration of Pt ions and HCl in the solution were 118.9 mg/L and 1 M, respectively. Contact time was varied while samples were mounted horizontally on an auto shaker, shaken at 250 rpm. The contact times were 30 min, 1, 2, 3, 4, 5, 7, 9, 12, 18, 24, 30, 36, 42, 48, 54, 60, 66, 72, 78, 84, 90, 96, 102, 108, 114 and 120 hours.

Each solution (done in triplicate) was removed at the designated time and filtered using disposable syringes and syringe filters (Millipore Millex-HV PVDF Filter, 0.45 µm, 33 mm). The solutions containing the poly(*N*-terephthaloylthiourea)-*N*',*N*'-piperazine powder were first centrifuged for 10 min and then filtered using disposable syringes and syringe filters. The solutions containing the nanofibres were allowed to stand while the powder samples were being centrifuged to ensure comparable contact times. The supernatants were then analysed using ICP-AES to determine the concentration of Pt ions remaining in each solution.

3.3.3 Temperature dependence Pt(II/IV) ion extraction investigation

The effect of temperature on the Pt ion extraction using nanofibres was investigated using 50 mg samples of ball electrospun nanofibres produced from the 6 wt% PAN solution with a PAN to oligomer ratio of 7:3. The temperatures investigated were 20, 25, 30, 35, 40, 50, 55, and 60 °C, while the concentration of Pt ions was 114.0 mg/L in a 1 M HCl matrix.

The auto shaker was mounted inside an atmospherically controlled chamber within which the temperature could be regulated. The instrument used for this was an Ecotron by Infors HT. The samples were placed vertically on the auto shaker rotating in a circular motion at 250 rpm. Each

solution (done in triplicate) was removed after 24 hours and filtered using disposable syringes and syringe filters (Millipore Millex-HV PVDF Filter, 0.45 µm, 33 mm). The Pt concentration in the supernatant solutions was then analysed using ICP-AES.

3.3.4 Extraction of Pt(II/IV) ions as a function of the hydrochloric acid concentration

Ball electrospun nanofibre webs (50 mg) using the 6 wt% PAN solution with a PAN to oligomer ratio of 7:3 were used for each batch extraction experiment to determine the effect of HCl matrix concentration on the extraction of Pt ions. The various HCl concentrations selected for investigation were 0.001, 0.1, 0.5, 1, 3, and 6 M, while the concentration of Pt ions in the stock solution was 118.9 mg/L.

The horizontally mounted samples were shaken at 250 rpm on an automated shaker for 24 hours. Each solution (done in triplicate) was filtered using disposable syringes and syringe filters (Millipore Millex-HV PVDF Filter, 0.45 µm, 33 mm) and the Pt concentration in the supernatant solutions was then analysed using ICP-AES.

CHAPTER 4

*SYNTHESIS AND CHARACTERISATION OF POLY(*N-*TEREPHTHALOYLTHIOUREA)*-N',N'-*PIPERAZINE*

Objective A:

(i) *To prepare poly(*N-*terephthaloylthiourea)*-N',N'-*piperazine oligomer, as reputed in the Patent Application WO 2000/53663,*[21]

(ii) *as well as conducting analytical analyses on the produced substance for characterization purposes.*

4.1 Synthesis procedure for poly(*N*-terephthaloylthiourea)-*N*',*N*'-piperazine

4.1.1 Synthesis procedure based on the synthesis by Douglass and Dains

The synthesis of poly(*N*-terephthaloylthiourea)-*N*',*N*'-piperazine followed a similar method to the *N*,*N*-dialkyl-*N*'-acylthiourea synthesis suggested by Douglass and Dains.[130] A simple "one-pot" method is proposed for the ligand synthesis that usually gives good yields. The first step in the Douglass and Dains synthesis is the addition of an ammonium, potassium or sodium thiocyanate to an acyl halide to form the intermediate thiocyanate and isothiocyanate compounds, shown as the first step in Figure 4.1. The thiocyanate and isothiocyanate intermediates are in equilibrium, but it has previously been shown that only the isothiocyanate intermediate reacts during the second step of the synthesis: the addition of primary or secondary amines,[39] shown as step 2 in Figure 4.1. The desired *N*,*N*-dialkyl-*N*'-acylthiourea compound is then obtained.

Step 1:

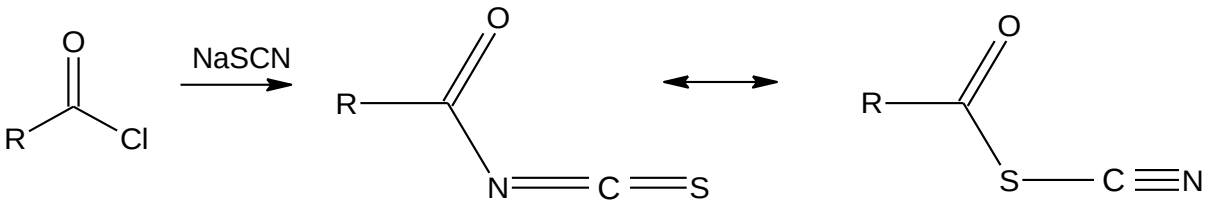

Step 2:

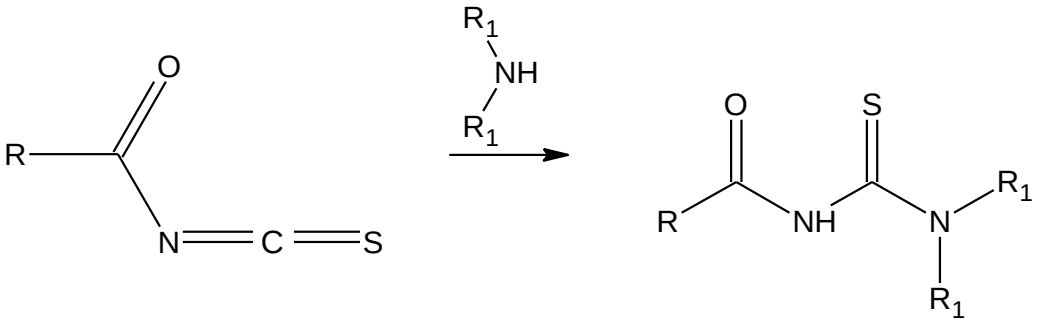

Figure 4.1 – Representation of the reaction described by Douglass and Dains. Redrawn from reference 39, where R is either an alkyl or aryl and R_1 is an alkyl.

The difference from the synthesis proposed by Douglass and Dains was that terephthaloyl chloride was used as acyl chloride and piperazine was used as the amine during the poly(*N*-terephthaloylthiourea)-*N*',*N*'-piperazine synthesis. Instead of only one equivalent of thiocyanate reacting, as is the case with the single acyl chloride used in the Douglass and Dains synthesis, two thiocyanate ions reacted with the terephthaloyl moiety. A stoichiometric ratio of one part terephthaloyl chloride to two parts thiocyanate was therefore required to produce the di-isothiocyanate substituted terephthaloyl intermediate.

Piperazine was subsequently added to the reaction during the second step. Each of the secondary amine groups of the piperazine molecule could react with the di-isothiocyanate substituted terephthaloyl intermediate produced during the first step of the synthesis. The chain grew in this way and an oligomer formed *via* condensation polymerisation.

4.1.2 Product yield

A product yield of 65.5 % was achieved after the synthesis of poly(*N*-terephthaloylthiourea)-*N*',*N*'-piperazine. This was less than the yield of 76.2 % reported in the patent application.[21] The lower yield is attributed to the larger scale at which the synthesis was conducted as well as the additional washing steps. The synthesis reaction in the patent application only used 0.04 mol of both terephthaloyl chloride and piperazine and 0.08 mol NaSCN, while the synthesis reaction for this dissertation used 2 mol of both the terephthaloyl chloride and piperazine and 4 mol NaSCN. Less contact between reagents was obtained, resulting in less product forming and more unreacted reagent being washed away. Similar decreased yield due to scale-up has also been reported elsewhere.[132,133]

The large amount of synthesised product had to be divided up and washed in smaller batches to ensure complete removal of any unreacted components. The product described in the patent application was "washed three times with water and then twice with acetone".[21] However, during the washing of the synthesised product it was found that the water and acetone still retained a murky yellow colour after the prescribed amount of wash cycles. Product washing was continued until the wash liquids remained clear (alternating between Milli-Q water and acetone for seven consecutive washing cycles) to ensure the removal of as much of the unreacted components as possible. Small amounts of product were lost on the filter paper and the sides of the funnel during each of the wash cycles. This further reduced the product yield.

4.2 Investigation of smaller molecules with similar functionality to that of poly(*N*-terephthaloylthiourea)-*N*',*N*'-piperazine

It is important to investigate the chemistry behind the poly(*N*-terephthaloylthiourea)-*N*',*N*'-piperazine synthesis in more detail. Two bipodal *N*'-aroylthiourea compounds were chosen from work done at the University of Cape Town.[134] They observed side reactions during the bipodal *N*'-aroylthiourea compound synthesis procedures. The desired bipodal ligand structures (left) as well as the side-products that could form during the synthesis (right) are shown in Table 4.1.

Table 4.1 – **(a1** and **a2)** Synthesis products obtained when preparing two different bipodal *N*'-aroylthioureas, as well as the accompanying side-products formed **(b1**, **c1**, **b2** and **c2)**. These structures are re-drawn from those in reference 134 and IUPAC names were generated using MarvinSketch v.5.11.4, available from http://www.chemaxon.com.

(a1) *N*,*N*'-bis(piperidine-1-carbothioyl)benzene-1,4-dicarboxamide 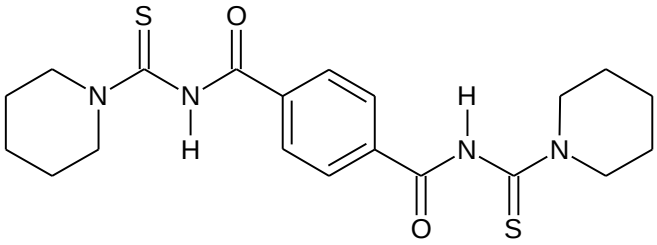	**(b1)** 4-(piperidine-1-carbonyl)-*N*-(piperidine-1-carbothioyl)benzamide 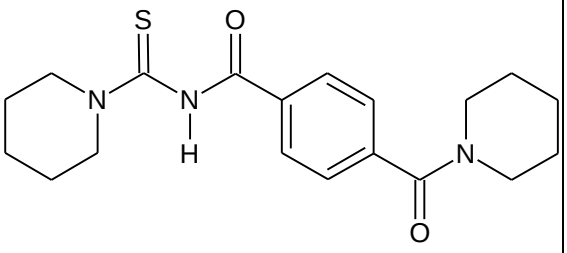 **(c1)** 1-[4-(piperidine-1-carbonyl)benzoyl] piperidine 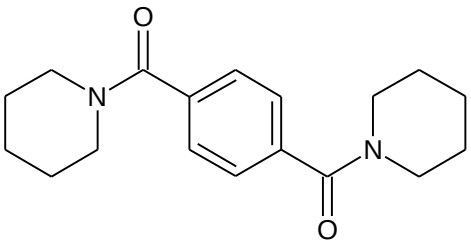
(a2) *N*-{4-[(phenylformamido)methanethioyl] piperazine-1-carbothioyl}benzamide 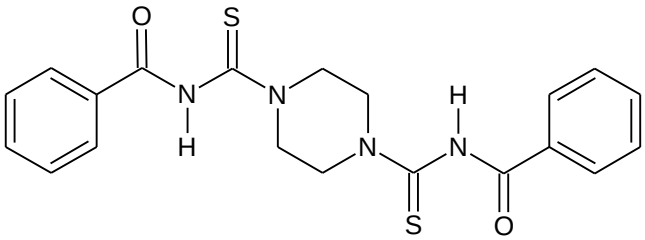	**(b2)** *N*-(4-benzoylpiperazine-1-carbothioyl) benzamide 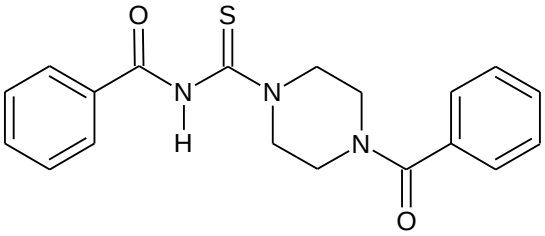 **(c2)** 1,4-dibenzoylpiperazine 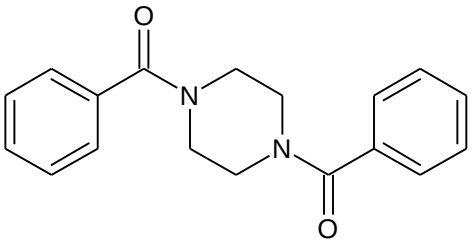

From the side-product structures it follows that some (in the case of side-products b1 and b2) or all (in the case of side-products c1 and c2) of the thiocyanate ions did not react during the first step of the synthesis to form isothiocyanate intermediates. Figure 4.2 illustrates the second step of the synthesis of

N,*N*'-bis(piperidine-1-carbothioyl)benzene-1,4-dicarboxamide (a1 in Table 4.1), along with the reactions leading to the possible side-products.

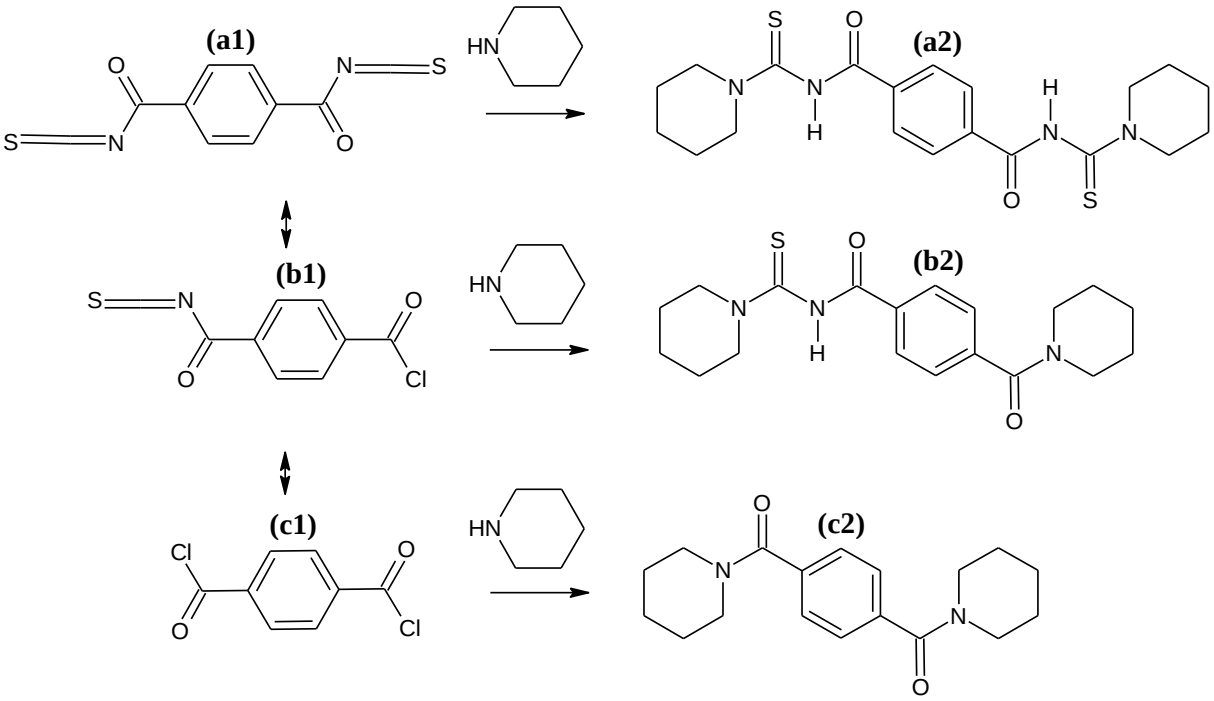

Figure 4.2 – The second step in the synthesis of *N*,*N*'-bis(piperidine-1-carbothioyl)benzene-1,4-dicarboxamide after **(a1)** both the chlorides ions were substituted to form a di-isothiocyanate intermediate, **(b1)** one of the chlorides was substituted to form a single isothiocyanate intermediate, and **(c1)** none of the chlorides were substituted and no isothiocyanate intermediate moieties were formed. The resultant products are shown as **(a2)**, **(b2)**, and **(c2)**, respectively.

The two to one molar ratio of thiocyanate to aroyl chloride caused the equilibrium to shift to the right during the first step of the reaction and more of the di-substituted isothiocyanate intermediate product (a1) would have formed. However, unreacted aroyl chloride moieties (b1 and c1) may have been present in the reaction vessel when the secondary amine was added during the second step of the synthesis process. This meant that some of the secondary amines reacted with the isothiocyanate intermediate, forming synthesis products (a), while others reacted with the acyl chloride, forming the by-products (b2) and (c2).

4.3 Characterisation of Poly(*N*-terephthaloylthiourea)-*N*',*N*'-piperazine

The complete structure of the poly(*N*-terephthaloylthiourea)-*N*',*N*'-piperazine should have a repeat unit shown in Figure 4.3(a) when a reagent molar ratio of 1:2:1 of terephthaloyl chloride to sodium thiocyanate to piperazine is used. However, the empirical molecular formula proposed in the patent application when using the reagent molar ratio of 1:2:1 of terephthaloyl chloride to sodium thiocyanate to piperazine was $C_{27}H_{27}N_7O_4S_3$,[21] leading the author to formulate the repeat unit shown in Figure

4.3(b). This empirical molecular formula and repeat unit makes provision for one in every four of the proposed thiourea moieties in the oligomer structure to not be formed.

(a)

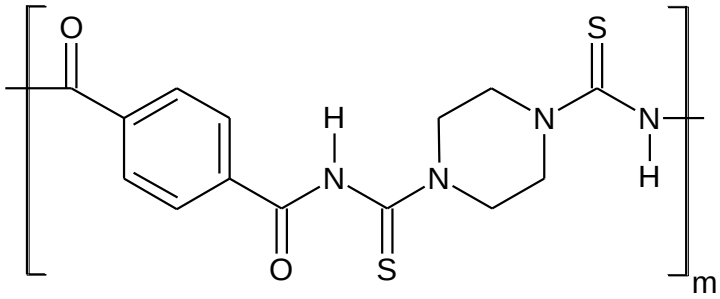

(b)

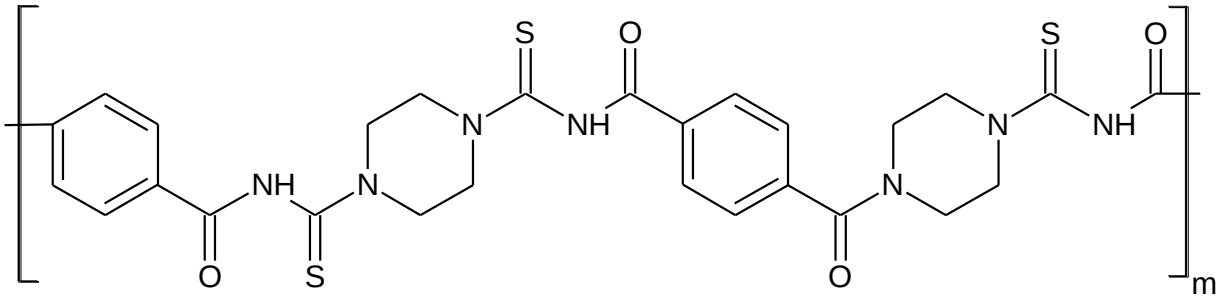

Figure 4.3 – **(a)** The repeat unit of the poly(*N*-terephthaloylthiourea)-*N*',*N*'-piperazine oligomer if the synthesis progresses as postulated when using a reagent molar ratio of 1:2:1 of terephthaloyl chloride to sodium thiocyanate to piperazine. **(b)** The structure proposed by the author when using the empirical molecular formula of $C_{27}H_{27}N_7O_4S_3$, supplied in the patent application as the molecular formula of the repeat unit.[21]

4.3.1 Elemental analysis and proposed repeat unit of the oligomer

The elemental analysis results in Table 4.2 show how well the mass percentages of carbon, nitrogen, hydrogen and sulphur obtained from the synthesised poly(*N*-terephthaloylthiourea)-*N*',*N*'-piperazine compared to the reported values as well as the elemental composition range proposed in the patent application. The elemental analysis of the synthesised poly(*N*-terephthaloylthiourea)-*N*',*N*'-piperazine showed that the amounts of carbon, hydrogen and nitrogen all fell within the range proposed in the patent application, while the sulphur fell one mass percent outside of the proposed range. The low mass percentage sulphur obtained from the elemental analysis confirms, to a certain extent, the absence of some of the thiourea groups from the oligomer chain, as seen from the repeat unit in Figure 4.3(b). However, other possible repeat units or even combinations of repeat unit possibilities are shown in Figure 4.4, along with their molecular formulas, molecular weights and elemental compositions as determined using ACD/ChemSketch, (available from http://chemsketch.en.softonic.com).

Table 4.2 – Chemical composition of the poly(*N*-terephthaloylthiourea)-*N*',*N*'-piperazine oligomer as determined by elemental analysis, as well as an elemental composition range provided by the patent application.[21]

	Elemental analysis results for this dissertation	**Range proposed for general compound reported in patent application**
%C	50.6	50.0 – 55.0
%H	4.6	4.0 – 5.0
%N	16.0	15.0 – 17.0
%S	13.0	14.0 – 18.0

(a) Molecular formula: $C_{28}H_{28}N_8O_4S_4$

Molecular weight: 668.9 g/mol

Elemental composition: 50.3 %C, 4.2 %H, 16.8 %N, 19.2 %S

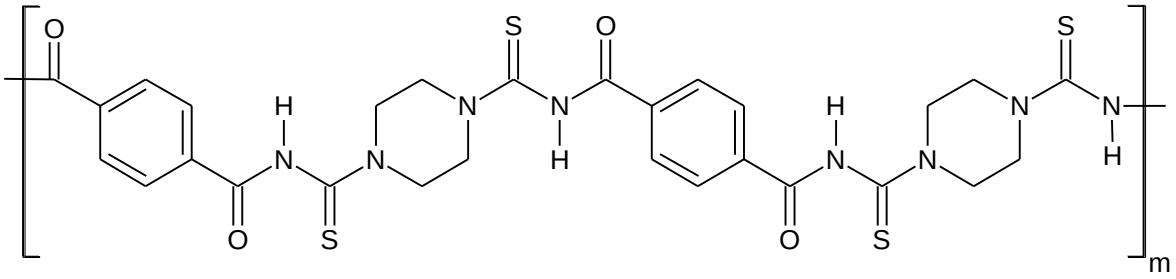

(b) Molecular formula: $C_{27}H_{27}N_7O_4S_3$

Molecular weight: 609.8 g/mol

Elemental composition: 53.2 %C, 4.5 %H, 16.1 %N, 15.8 %S

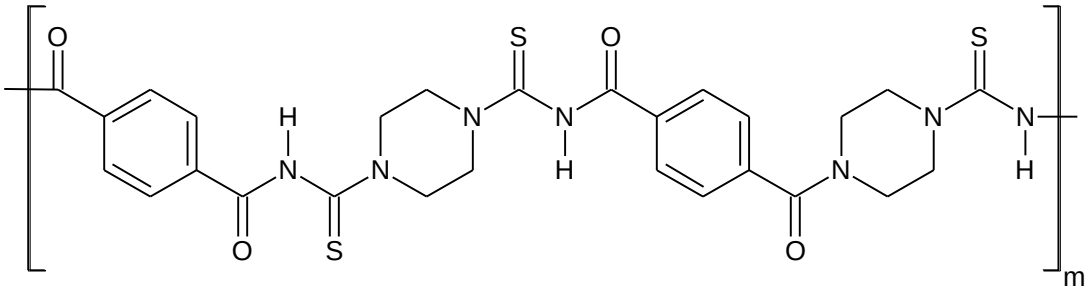

(c) Molecular formula: $C_{26}H_{26}N_6O_4S_2$

Molecular weight: 550.7 g/mol

Elemental composition: 56.7 %C, 4.8 %H, 15.3 %N, 11.7 %S

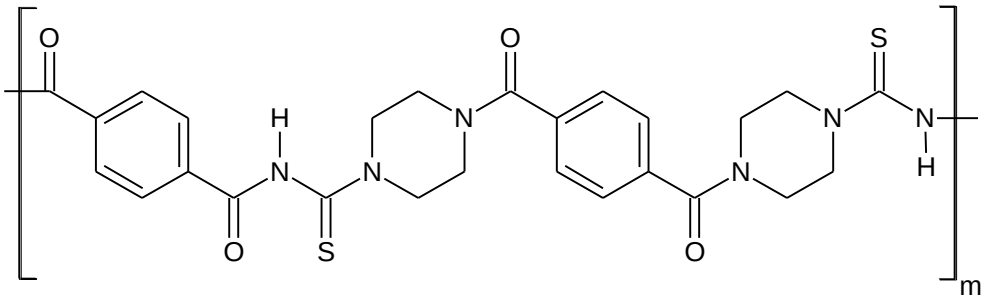

(d) Molecular formula: $C_{25}H_{25}N_5O_4S$

Molecular weight: 491.6 g/mol

Elemental composition: 61.1 %C, 5.1 %H, 14.3 %N, 6.5 %S

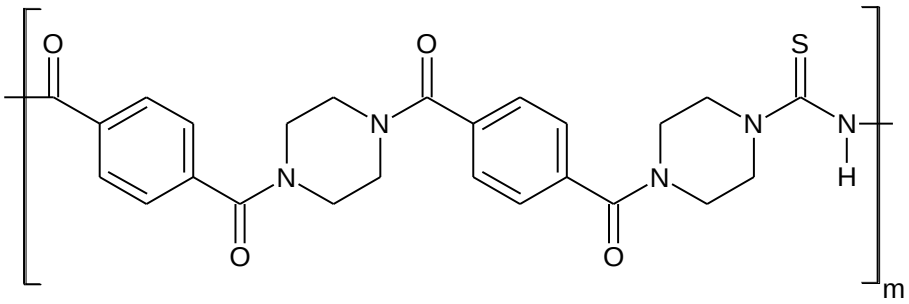

(e) Molecular formula: $C_{24}H_{24}N_4O_4$

Molecular weight: 432.5 g/mol

Elemental composition: 66.7 %C, 5.6 %H, 13.0 %N

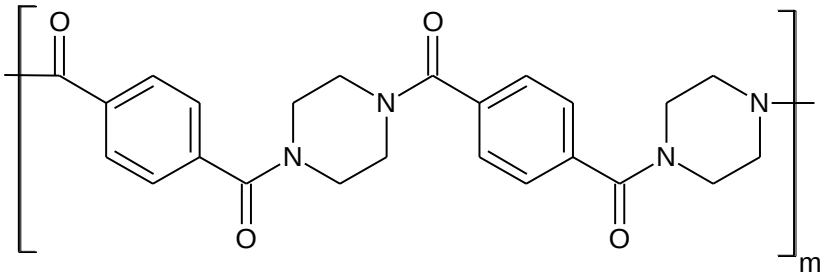

Figure 4.4 – The molecular formula, molecular weight, elemental composition and structure of five possible repeat units formed during the synthesis of poly(*N*-terephthaloylthiourea)-*N*',*N*'-piperazine. The absent thiourea moieties were arbitrarily chosen and their position could vary for structures **(b)**, **(c)** and **(d)**.

None of the compositions calculated for the repeat units in Figure 4.4 were the same as the elemental composition determined for the synthesised oligomer (50.6 %C, 4.60 %H, 16.0 %N, 13.0 %S). However, when using a combination of repeat units (a), (b) and (c) it is possible to get reasonably good correlation between the elemental composition of the synthesised oligomer and those calculated from the repeat units.* The repeat unit structures of (b) and (c) showed one and two unformed thiourea moieties, respectively. The elemental analysis results therefore indicates that, on average, one out of four thiourea moieties were absent when compared to the oligomer structure for complete reaction of all of the reagents, as shown in Figure 4.3(a).

* Note: It is important to recognize that the end groups of the oligomer would have an impact on its elemental composition as well as the resultant molecular weight. The possible end groups of the oligomer chain are a piperazine unit or a carboxylic acid moiety formed on the terephthaloyl structure. However, investigating the possibilities of the different end groups as well as the effect that they had on the oligomer's elemental composition and molecular weight falls outside the scope of this study.

For simplicity the oligomer will be referred to as *Platisorb* for the remainder of the work. Pure poly(*N*-terephthaloylthiourea)-*N*',*N*'-piperazine is not easily produced and for the purposes of this work it does not have to be. *Platisorb* is therefore the term used for the heterogeneous poly(*N*-terephthaloylthiourea)-*N*',*N*'-piperazine oligomers.

4.3.2 Analysing *Platisorb* with GPC

GPC was the technique used to determine the *Platisorb* oligomer's molecular weight. The number average molecular weight (M_n) and weight average molecular weight (M_w) values obtained were 3705 g/mol and 6427 g/mol, respectively.

The M_n and M_w values were used to determine the polydispersity index (PDI) of the oligomer chains. PDI is a measure of the variation in molecular weight and the closer to one the PDI is the less variation exists between the molecular weights of the oligomer chains. By using Equation 4 as well as the M_n and M_w values obtained from the GPC analysis, the oligomer's PDI was calculated as 1.73. This means that there is quite a large variation in the average molecular weight between the different *Platisorb* chains.

$$PDI = \frac{M_w}{M_n} \qquad [4]$$

It was also possible to determine the number of repeat units in the average oligomer chain by using the M_n of the oligomer and the molecular mass of a single repeat unit. M_n rather than M_w was used for this calculation as M_n is more sensitive to lower molecular weight species.[135] For this calculation the molecular weight of a single repeat unit was required and for that the repeat unit has to be known. An average molecular weight of 609.8 g/mol was obtained when using the molecular weights of repeat units (a), (b) and (c) in Figure 4.4, shown to be the repeat units that best fit the elemental composition obtained for the synthesised oligomer. When dividing the M_n of 3705 g/mol by the molecular weight of 609.8 g/mol, 6.08 was obtained. The average *Platisorb* oligomer chain therefore consists of roughly six repeat units. It is however important to note that the PDI value is high, which means that the chain lengths vary considerably around this average value.

4.3.3 Characterisation of *Platisorb* by FTIR spectroscopy

FTIR was used to verify some of the molecular functional groups present in the *Platisorb* structure by investigating characteristic bending and stretching vibrations. The IR spectrum, ranging from 900 cm^{-1} to 4000 cm^{-1}, is shown in Figure 4.5, where only the most important peaks are highlighted from the complex spectrum, labelled (a) to (g).

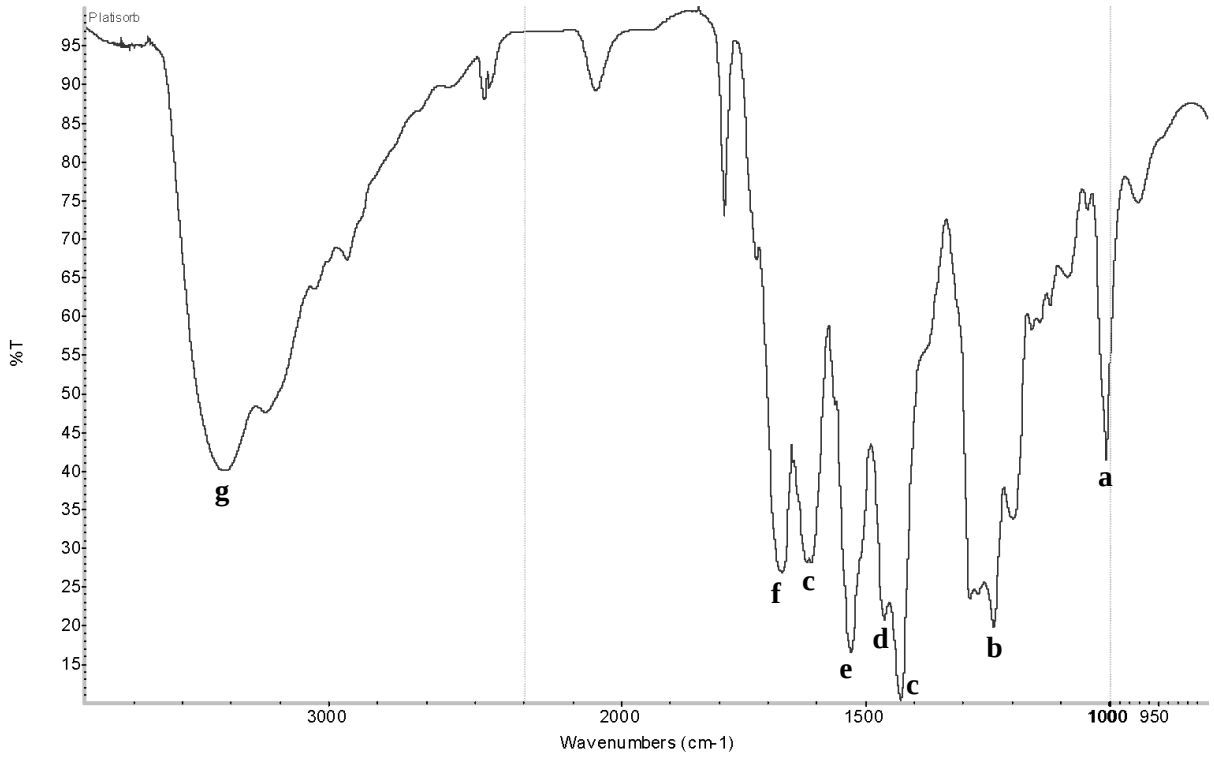

Figure 4.5 – Infra-red spectrum obtained for the *Platisorb* oligomer. The sample was prepared using the KBr pellet press method.

The first absorption band was found at 1005 cm^{-1} (a) when going from right to left across the IR spectrum. This strong band was created by the thiocarbonyl stretching vibration. The next characteristic band was created by the secondary amine N-C stretch vibration, at 1237 cm^{-1} (b). Both the strong bands with designation (c), around 1427 cm^{-1} and 1620 cm^{-1}, were indicative of the aromatic stretching vibrations of the C=C bonds. An absorption band originating from methylene bending vibrations was seen at 1461 cm^{-1} (d), as well as a secondary amine N-H bending vibration around 1530 cm^{-1} (e). There was also a strong band observed around 1672 cm^{-1} (f) which was assigned the C=O bending vibrations, belonging to the carbonyl as well as the possible carboxylic acid moieties. Carboxylic acid might have formed as an end group due to the high reactivity of terephthaloyl chloride to water.[136] The final, very broad set of absorption bands with the maximum intensity at 3426 cm^{-1} was assigned to overlapping peaks belonging to secondary amine N-H stretching vibrations and aromatic C-H vibrations (g).

The infra-red spectrum of the oligomer gives reasonable support for the proposed *Platisorb* structure, as bending and stretching vibration bands are shown for the piperazine ring (N-C stretch as well as methylene bend), the six membered aromatic ring (stretching vibrations of the aromatic C=C and aromatic C-H bonds), as well as the groups linking these two structures (S=O stretching vibration, C=O bending vibration, and secondary amine N-H bending vibration peaks).

4.3.4 Characterisation of *Platisorb* by ^{1}H and ^{13}C NMR spectroscopy

^{1}H and ^{13}C NMR spectroscopy were used to elucidate the structure of the synthesised *Platisorb* oligomer. The complexity of the oligomer made it difficult to assign all the peaks to specific protons or carbons and to define the complete structure from the NMR spectra, so different ranges and/or sets of peaks were identified as being indicative of specific moieties present in the oligomeric structure. Figure 4.6 shows a *Platisorb* repeat unit with assignments made for the different proton signals in the ^{1}H NMR spectrum shown in Figure 4.7.

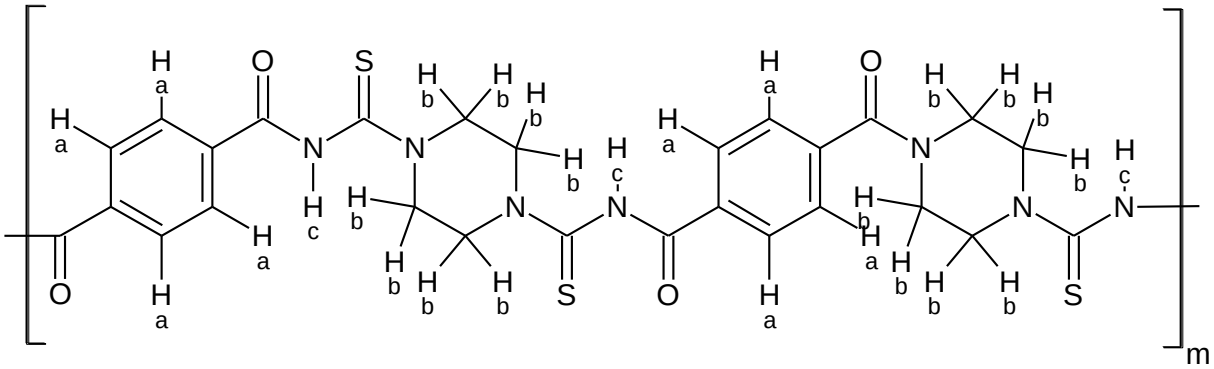

Figure 4.6 – The *Platisorb* repeat unit with differently labelled protons.

The ^{1}H NMR spectrum shows seven different sets or individual peaks, while only three sets of proton types were expected to be present in the *Platisorb* oligomer:

- the protons of the aromatic ring (H_a),
- the protons of the piperazine carbons (H_b), and
- the amines protons (H_c).

The other four peaks were assigned to the reference material (TMS) at 0 ppm, residual acetone in the system at 2.07 ppm, the DMSO-d_6 solvent peaks at 2.50 ppm and water at 3.08 ppm.

The broad multiplets observed between 2.50 ppm and 4.50 ppm (excluding the DMSO-d_6 solvent peak and water peak at 2.50ppm and 3.08 ppm, respectively) were assigned to the protons of the piperazine moiety (H_b). The multiplets in the region 7.00 ppm to 8.50 ppm were indicative of aromatic protons, and were assigned to the protons on the aromatic ring (H_a). Lastly, the broad peak with a maximum around 10.0 ppm was assigned to the amine protons (H_c). An expansion of this broad amine ^{1}H NMR peak is also shown in the top left of Figure 4.7. The integrals of the different sets of peaks were as follows: $H_a = 3.7$, $H_b = 5.3$, $H_c = 1$.

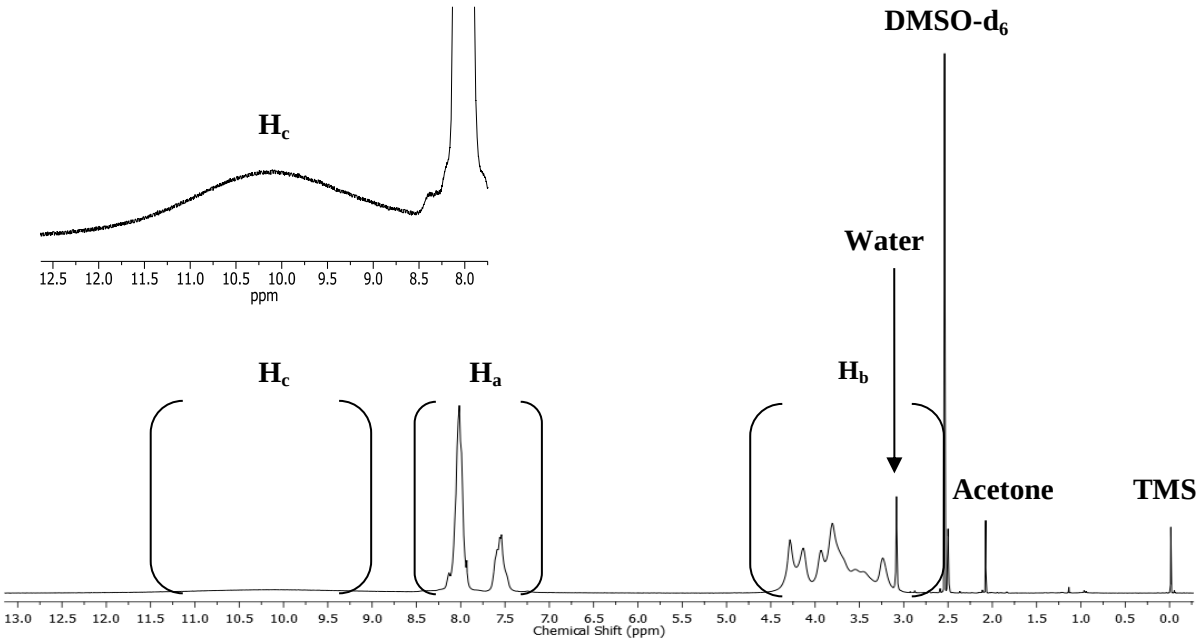

Figure 4.7 – ^{1}H NMR spectrum of the *Platisorb* oligomer.

The proton-decoupled ^{13}C NMR spectrum (Figure 4.8 top) consisted of five different regions of ^{13}C peaks. The first intense set of peaks around 39.5 ppm belonged to the carbons of the solvent DMSO-d_6. The region of peaks directly adjacent the solvent peaks between 40.0 ppm and 52.5 ppm were assigned to the piperazine carbons (a), while the peaks between 125 ppm and 140 ppm were indicative of the different aromatic carbons (b). The three peaks between 163 ppm and 170 ppm and the peaks around 177 ppm and 180 ppm were assigned to the carbonyl carbons (c) and thiocarbonyl carbons (d) of the acyl thiourea moiety of the *Platisorb*, respectively.

The ^{1}H and ^{13}C NMR also give reasonable support for the proposed *Platisorb* structure. However, the complete structure of the oligomer could not be elucidated with the four techniques used. Preliminary tests (not shown here) using the oligomer for the extraction of $[PtCl_6]^{2-}$ from acidic solutions proved successful, so the *Platisorb* was used as is or in electrospun nanofibre form for all the extraction experiments conducted for the rest of the thesis.

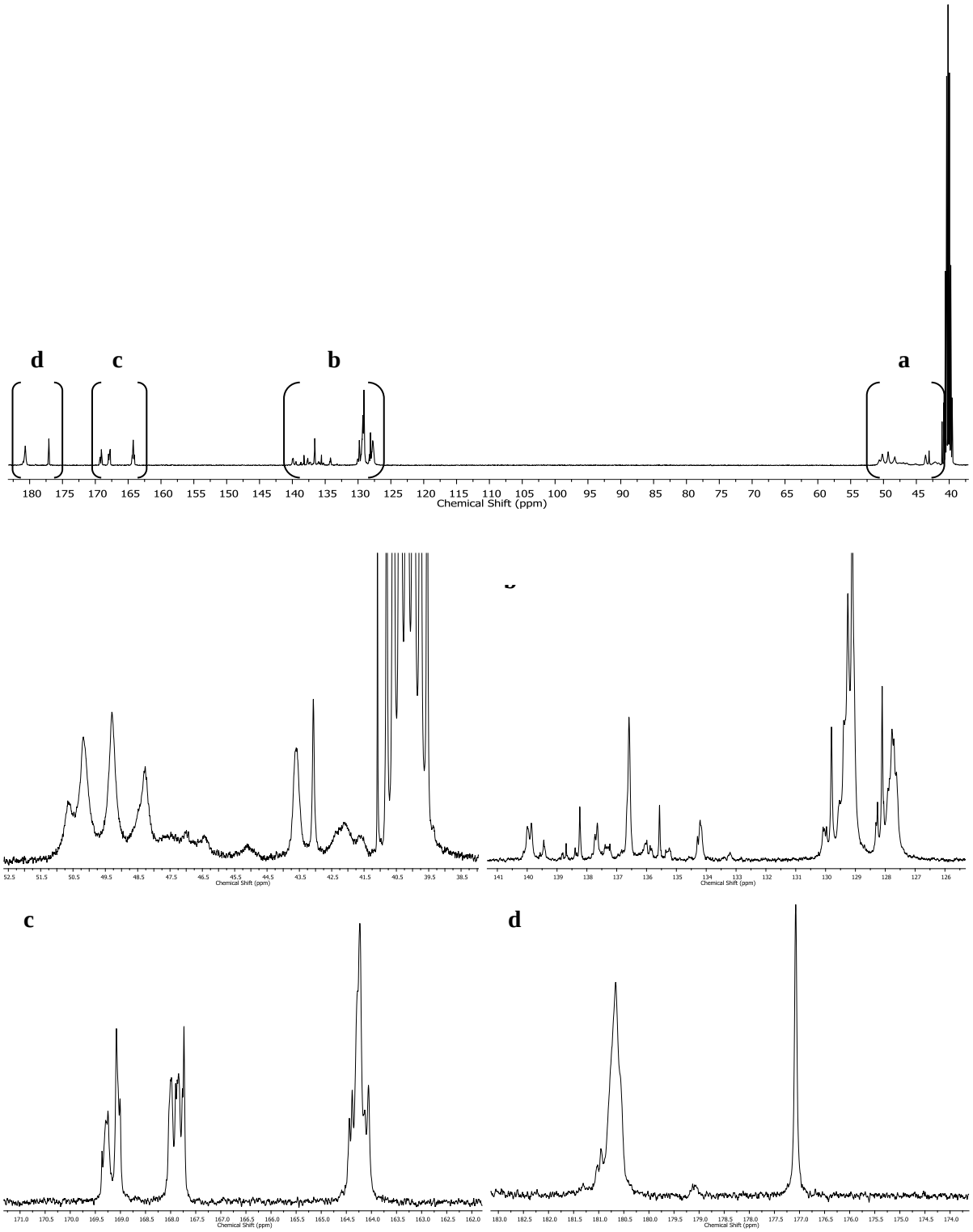

Figure 4.8 – The top image is the complete proton-decoupled ^{13}C NMR spectrum of the *Platisorb* oligomer. Expanded images shown below are labelled (a) to (d), corresponding to the peak regions similarly labelled in the top image.

CHAPTER 5

NEEDLE AND BALL ELECTROSPINNING OF THE BICOMPONENT SOLUTIONS

Objective B:

*To examine the process of needle as well as ball electrospinning of a bicomponent solution containing poly(*N*-terephthaloylthiourea)*-N*',*N*'-piperazine oligomer and polyacrylonitrile into suitable nanofibres.*

5.1 A comparison between needle electrospinning and ball electrospinning

Single needle electrospinning is seen as the classic approach to electrospinning and has been studied intensively in the past. However, for this work the more recently developed high throughput ball electrospinning process was chosen due to its ability to create the large amounts of nanofibres required for the $[PtCl_6]^{2-}$ extraction experiments.[29] It was therefore desirable to do a comparison between these two processes.

A direct comparison between needle and ball electrospinning was not possible due to the difference in applied voltage that the processes required for jet initiation. The increased voltage required for ball electrospinning was brought about by the increased number of jets that formed on the ball surface and because the potential was not concentrated at a specific point, as was the case with needle electrospinning.

The differences between needle and ball electrospinning were examined by observing the physical process, absolute fibre production rates and fibre diameters of the nanofibres produced. This was done by electrospinning a 6 wt% PAN solution with a ratio of 7:3 of PAN to *Platisorb* while allowing each electrospinning process to proceed for 30 minutes before the fibres obtained were washed and weighed.

5.1.1 Visual comparison of the electrospinning processes

Sequences of images were taken during the needle and ball electrospinning processes at a rate of three frames per second. These images, in Figures 5.1 and 5.2, show the number of jets and jet stabilities during both the electrospinning processes.

A single, stable jet formed on the tip of the needle during the needle electrospinning process. The jet followed an upward path towards the collector, undergoing whipping and stretching as it travelled through the air. A single solution jet was converted into a single electrospun nanofibre during the steady but slow needle electrospinning process.

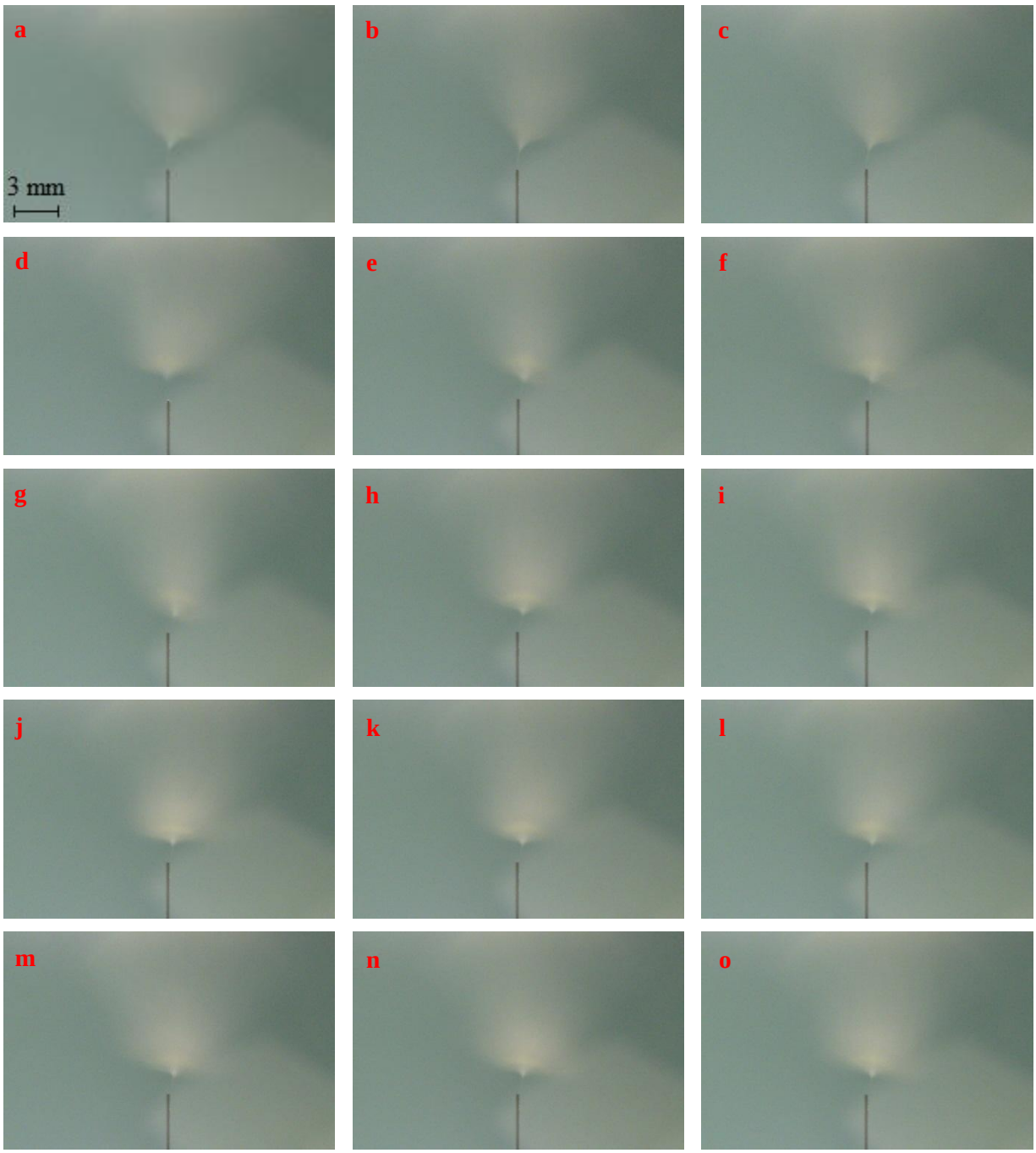

Figure 5.1 – Sequence of images from **(a)** to **(o)** showing needle electrospinning over a spin distance of 5 cm. The images were taken at a speed of three frames per second and the sequence was started ± 1 min after electrospinning was initiated.

The sequence of images in Figure 5.2 shows the 6 wt% PAN solution spun with the ball electrospinning process. The formation of multiple polymer jets were observed on the ball's surface. As the ball rotated from front to back (relative to the camera position of the images) the jets on the ball surface continuously moved from back to front, while some of the jets at the back of the ball were terminated and new jets were initiated on the front of the ball. These motions had the jets continuously moving close to the top section of the rotating ball as the spin distance was smallest and the electric field concentrated strongest in this area.

The jets in the centre of the ball followed relatively straight paths while the jets on the outer edges of the jetting area followed an arched trajectory towards the collector. This was due to the centremost jets experiencing charge repulsions from the surrounding jets, restricting the paths available and forcing them in a quasi-straight line toward the collector. The outermost jets experienced charge repulsions from jets on the inside of the spinning envelope, but had relative unrestricted space on the outside, allowing them to balloon outward while traveling toward the collector.

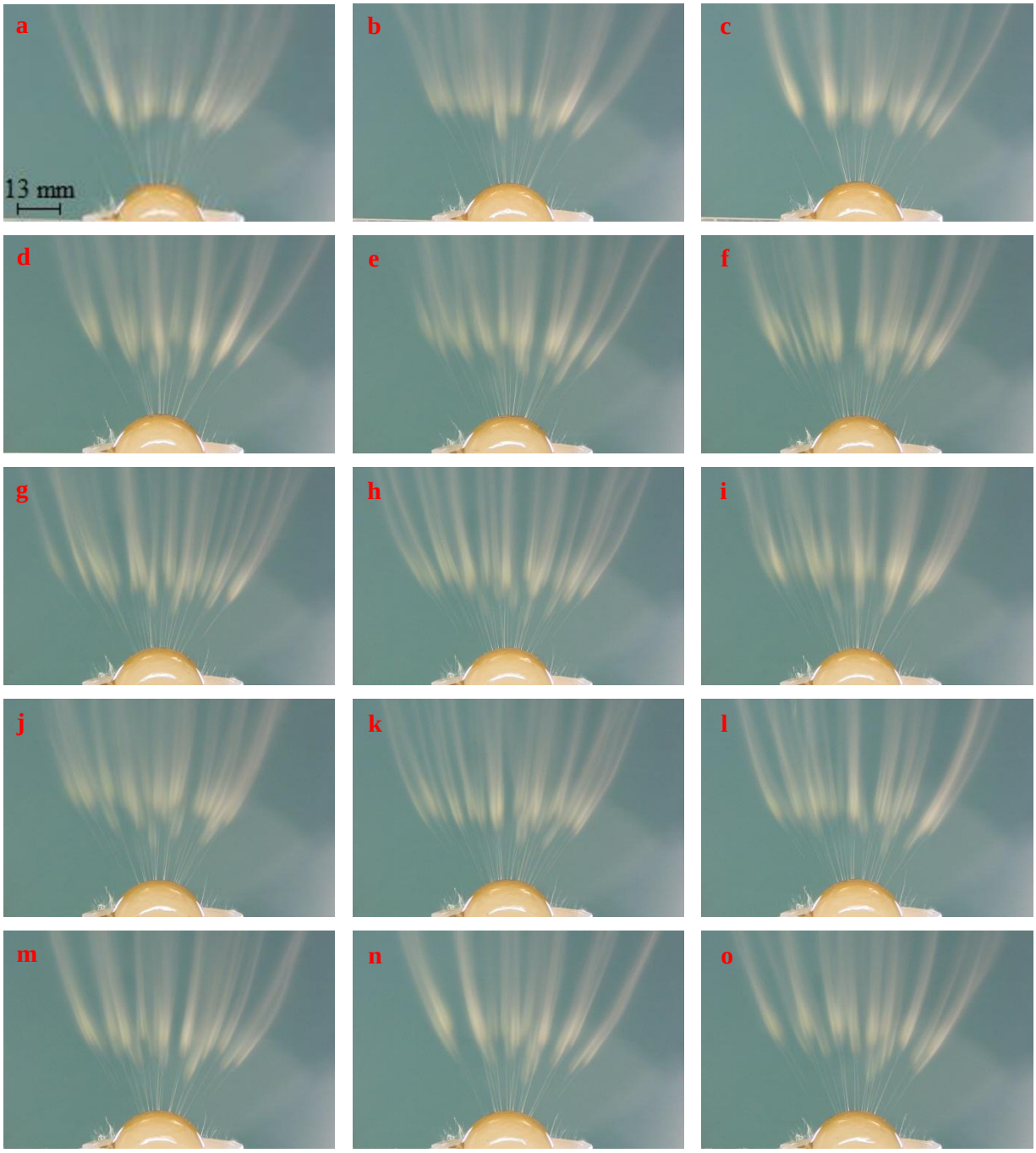

Figure 5.2 – Sequence of images from **(a)** to **(o)** showing ball electrospinning over a spin distance of 5 cm. The images were taken at a speed of three frames per second and the sequence was started ± 1 min after electrospinning was initiated.

5.1.2 Average fibre production rates

Nanofibre webs were produced at an average production rate of only 0.37 ± 0.06 mg/min when needle electrospinning the 6 wt% PAN solution, whereas ball electrospinning of the same solution produced nanofibre webs at an average production rate of 31.59 ± 0.70 mg/min. A more than 86 times greater mass of nanofibres was produced by ball electrospinning compared to needle electrospinning per unit time when an absolute comparison was done of the two processes' production rates.

5.1.3 Average nanofibre diameters

The nanofibres obtained from the needle and ball electrospinning processes were observed using scanning electron microscopy (SEM) and the images were used to measure the fibre diameters. The average diameter of the nanofibres electrospun with an applied positive voltage of 8 kV using the needle electrospinning process was 172 ± 35 nm while the average fibre diameter of the nanofibres electrospun with an applied positive voltage of 35 kV using the ball electrospinning process was 210 ± 49 nm. The fibre diameters of the ball electrospun nanofibres were on average only 38 nm larger than those produced by needle electrospinning. The fibre diameter distributions of the nanofibres produced by the two electrospinning processes are shown in Figure 5.3.

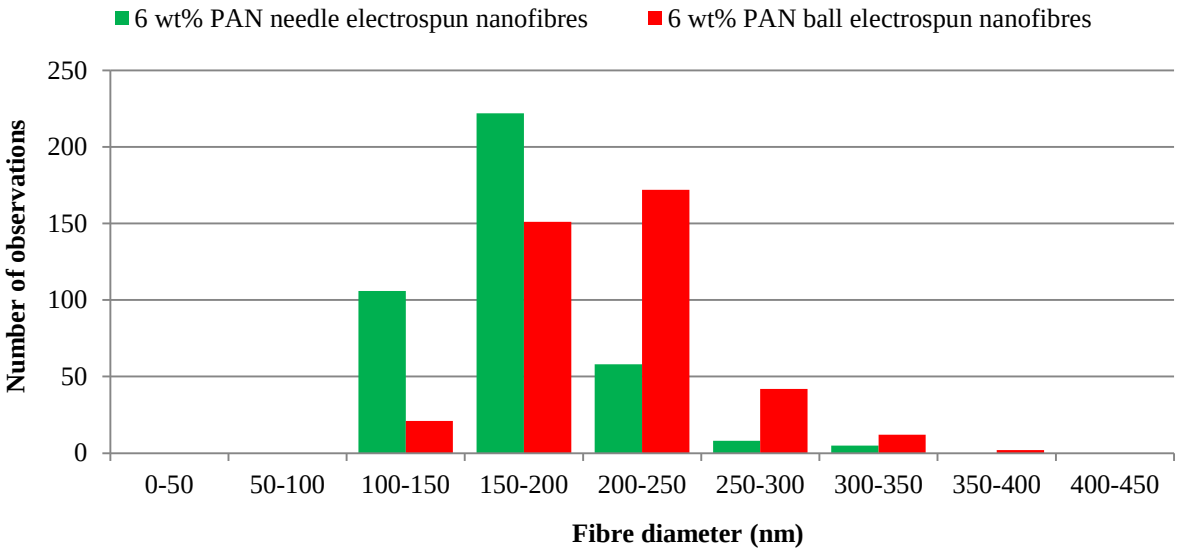

Figure 5.3 – The fibre diameter distributions of the nanofibres produced by the needle and ball electrospinning processes. Distributions were plotted using 400 measurements.

5.1.4 A visual comparison of the nanofibres

Representative and high resolution SEM images of the nanofibres obtained from needle electrospinning are shown in Figure 5.4(a) and (c), respectively, while representative and high resolution SEM images of the nanofibres obtained from ball electrospinning are shown in

Figure 5.4(b) and (d), respectively. There was an observed difference in fibre morphology between the nanofibres produced using needle electrospinning and those produced using ball electrospinning when comparing the lower magnification images (a) and (b). The nanofibres obtained with the needle electrospinning process (a) showed relatively smooth surfaces along the fibre length while the nanofibres obtained from the ball electrospinning process (b) showed sphere-like surface structures along the lengths of the fibres.

The high resolution images shown in Figure 5.4(c) and (d) revealed additional structures on the nanofibre surfaces that were not visible on the representative images. The sphere-like surface structures along with added surface roughness were observed on the ball electrospun nanofibres, while additional scale-like structures were visible on the needle electrospun nanofibres.

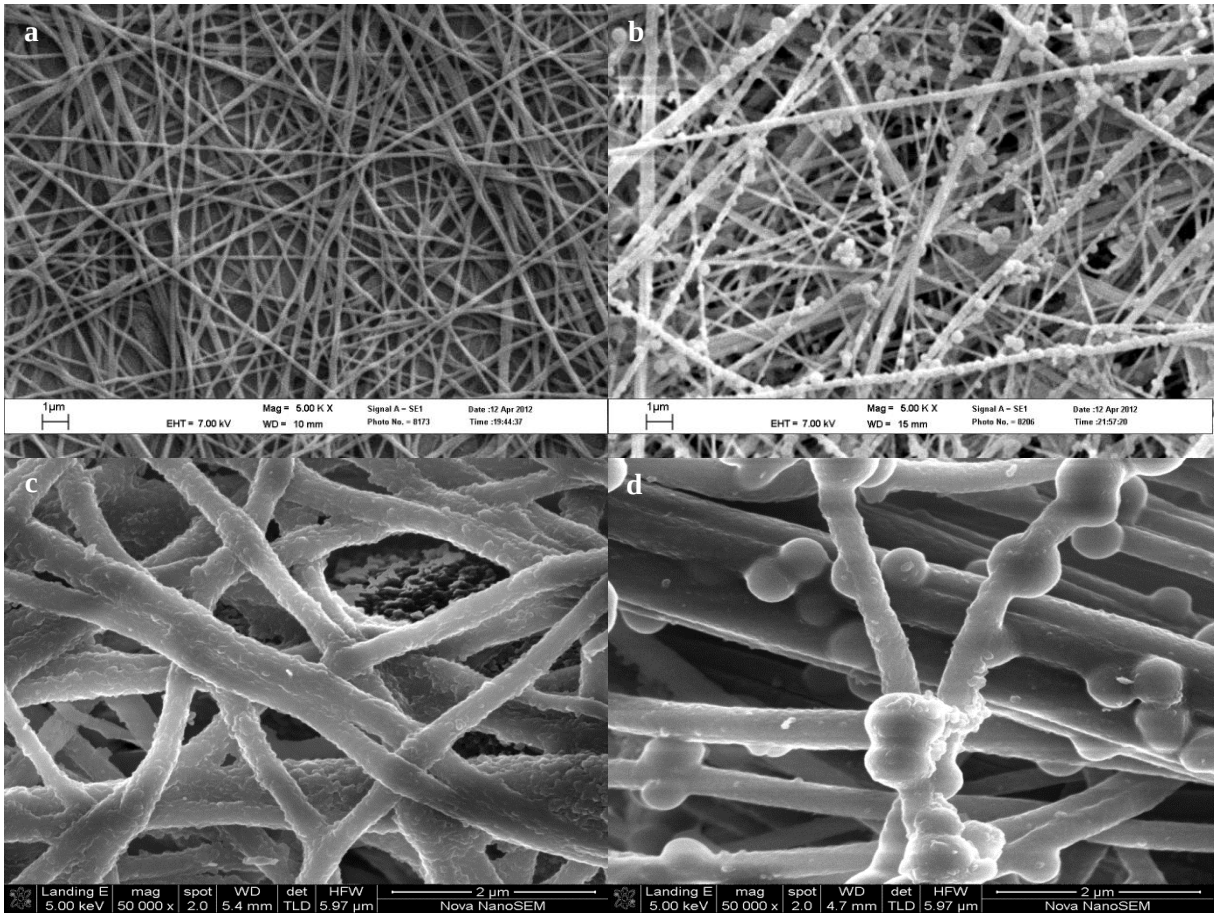

Figure 5.4 – Representative images of the nanofibre webs electrospun using **(a)** needle electrospinning and **(b)** ball electrospinning. High resolution SEM images of the same nanofibre webs are shown for **(c)** needle electrospinning and **(d)** ball electrospinning.

5.1.5 Surface structure analysis using sodium hydroxide (NaOH)

Previous experiences when electrospinning pure PAN produced nanofibres without the surface structures observed when the blended PAN and *Platisorb* solutions were electrospun. Other

researchers also produced nanofibres without the surface structures when needle electrospinning solutions of PAN in DMSO.[137] It was therefore postulated that the surface structures were formed by the *Platisorb* oligomers.

A range of NaOH concentrations and the effect they had on the *Platisorb* oligomer after 24 hours is shown in Figure 5.5 (NaOH concentration increasing from right to left). When the NaOH concentration was low (0.0125 M), the oligomer remained in a precipitated yellow powder form. As the concentration increased (0.075 M) the oligomer formed a murky yellow permanent suspension in solution. In a 0.25 M NaOH solution the *Platisorb* formed a dark yellow solution. While a 0.25 M NaOH solution degraded* the *Platisorb* powder, it had no effect (not shown) on PAN polymer after 24 hours of exposure.

Figure 5.5 – Solutions containing 10 mg *Platisorb* powder in different concentrations of NaOH, done in duplicate. As the concentration of NaOH increased from right to left: the *Platisorb* remained unaffected (rightmost two samples, 0.0125 M NaOH), formed a permanent suspension (middle two samples, 0.075 M NaOH) and when the concentration reached 0.25 M, the *Platisorb* degraded to form a yellow solution (leftmost two samples).

Needle and ball electrospun nanofibre webs were submerged in 0.25 M NaOH solutions for 24 hours, washed with distilled water and dried under ambient conditions. SEM was used to compare a NaOH treated nanofibre sample to an untreated sample for both the needle and ball electrospun samples, shown in Figures 5.6 and 5.7, respectively.

The SEM images showed the structures present on the surface of the nanofibres before NaOH treatment and absent from the surface after NaOH treatment. This confirmed that the *Platisorb* oligomer formed the structures on the surfaces of the nanofibres, as the *Platisorb* degraded in NaOH while the PAN remained unaffected.

---

* Note: The *Platisorb* oligomers are assumed to degrade rather than dissolve in the 0.25 M NaOH solution. This is proposed as gas bubbles were observed when the *Platisorb* powder was placed in the 0.25 M NaOH solution, indicating a reaction taking place. The treatment of *Platisorb* with NaOH is hence referred to as degradation.

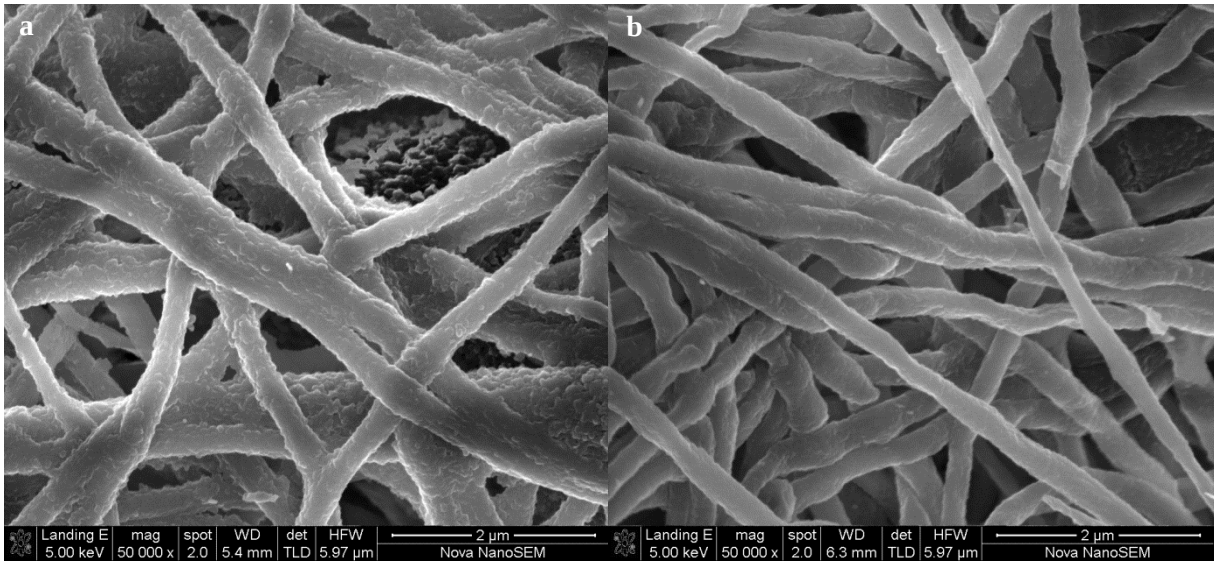

Figure 5.6 – Using 0.25 M NaOH solution to degrade the exposed *Platisorb* from the nanofibres. Shown here are the **(a)** untreated and **(b)** treated needle electrospun nanofibres.

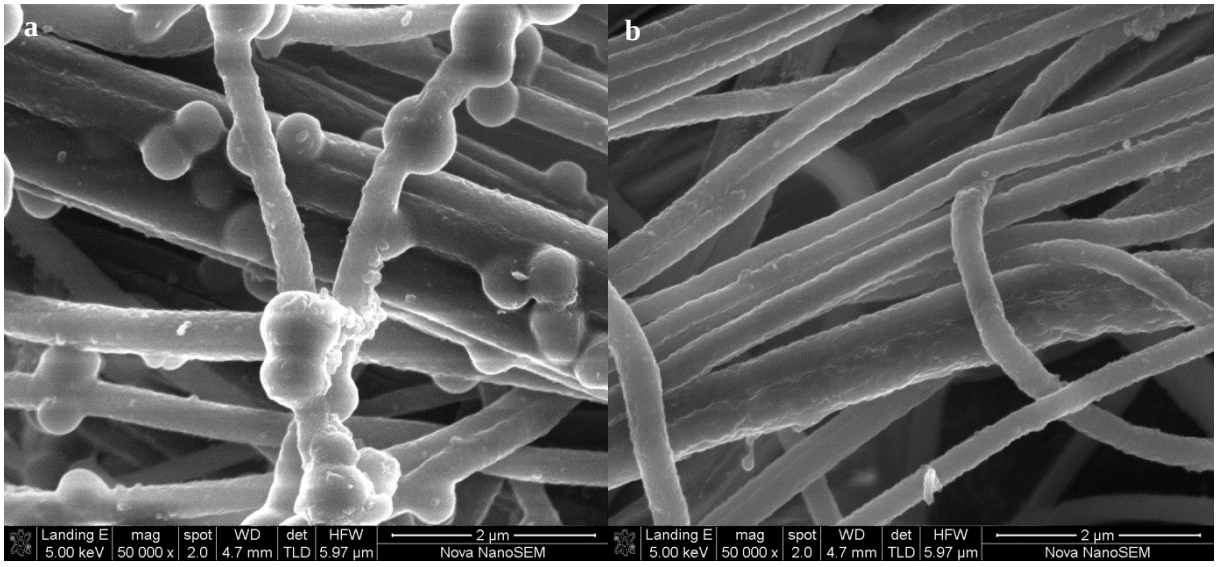

Figure 5.7 – Using 0.25 M NaOH solution to degrade the exposed *Platisorb* from the nanofibres. Shown here are the **(a)** untreated and **(b)** treated ball electrospun nanofibres.

The mass loss exhibited by the nanofibres due to NaOH degradation of the *Platisorb* was investigated as a second confirmation of the visual observations made in Figures 5.6 and 5.7. A mass loss of 21.1 ± 2.3 % was observed after treating three different 50 mg nanofibre webs with 0.25 M NaOH for 24 hours. This proved that it was the *Platisorb* oligomers that formed the structures on the surfaces of the nanofibres.

It was also interesting to note that not all of the *Platisorb* oligomers were removed from the nanofibres by NaOH treatment. While *Platisorb* made up 30 % of the electrospinning solution, only a 21.1 % reduction in mass was observed. It is therefore assumed (and confirmed in Chapter 6, section 6.2.2) that some of the *Platisorb* oligomeric chains are encapsulated within the PAN nanofibre structures.

The *Platisorb* oligomers form the surface structures on the PAN nanofibres during the post-electrospinning washing step due to partially separation of the PAN and *Platisorb* chains. The DMSO used as solvent is miscible with water, while both the PAN and *Platisorb* precipitate when in contact with water. When the wet nanofibre webs come into contact with water during the washing step, the DMSO on the surface of the nanofibres disperses into the water while the PAN and *Platisorb* on the surface precipitate. A solvent gradient between the inside of the nanofibres and their surfaces is formed, causing more of the DMSO inside of the nanofibres to migrate to the surface. Due to their low molecular weights (shown in Chapter 4, section 4.3.2), the *Platisorb* oligomeric chains migrate along with the solvent towards the surface of the nanofibres, past the entangled PAN polymer chains forming the nanofibre structure. When these oligomer chains come into contact with the water they precipitate, while the DMSO dispersed into the water, causing the observed *Platisorb* structures on the nanofibre surfaces.

The mechanism of *Platisorb* oligomer surface deposition is not explicitly known, but the explanation above can be used to describe its occurrence. The process was not studied any further as it falls outside the scope of this work. Nonetheless, it is advantageous that the *Platisorb* oligomer formed these structures on the surfaces of the electrospun nanofibres as the surface structures, containing the Pt ion coordination sites, were in close proximity with the $[PtCl_6]^{2-}$ in solution during the extraction experiments.

5.2 Differing nanofibre diameters produced by ball electrospinning 6 wt% and 8 wt% PAN solutions

There were only slight differences between the diameters of the nanofibres produced using the needle and ball electrospinning processes, with the ball electrospun nanofibres on average having 38 nm larger average fibre diameters than the needle electrospun nanofibres. Both the needle and ball electrospun nanofibres also had *Platisorb* surface structures, so comparable nanofibres were produced by both of the electrospinning processes. The ball electrospinning process, due to its high production rate, was therefore chosen to create all of the nanofibre webs used for the $[PtCl_6]^{2-}$ extraction experiments.

High specific surface area is an inherent property of nanofibres.[25] It was therefore decided to determine to what extent the specific surface area affected the Pt ion extraction efficiency of the

electrospun nanofibres. It is known from literature on the needle electrospinning process (and shown in our research group to hold true for ball electrospinning as well) that increasing the viscosity of the spin solutions produces nanofibres with increased fibre diameters, which can easily be achieved with an increase in polymer concentration added to the spin solution.[67,72,74,76] A 6 wt% and 8 wt% PAN solution, both with a 7:3 ratio of PAN to *Platisorb*, were ball electrospun to produce the nanofibres with different specific surface areas.

5.2.1 Ball electrospinning conditions and ambient conditions

The 6 wt% and 8 wt% PAN solutions had to be spun multiple times over multiple days to determine the reproducibility of the ball electrospinning process. The maximum spin distance for each solution was chosen before the backbuilding phenomenon (explained in Chapter 3, section 3.6.2) was observed. For this reason the 6 wt% PAN solutions were electrospun at a spin distance of 5 cm while the 8 wt% PAN solutions were electrospun at a spin distance of 6 cm.

The ambient conditions were controlled to ensure that variations in temperature and relative humidity did not affect the resultant nanofibre webs. The ambient conditions on the days of spinning are given in Table 5.1, all measured at 1 atm pressure.

Table 5.1 – Ambient conditions while ball electrospinning different 6 wt% PAN and 8 wt% PAN solutions on three different days.

	Temperature (°C)	**Relative humidity (%)**
6 wt% solutions	21.4 – 23.6	31 – 37
8 wt% solutions	21.6 – 23.6	32 – 34

The environment surrounding the electrospinning setup was controlled to have consistent temperature and relative humidity, so only small variations in the ambient conditions were observed on the different days of electrospinning. No variation in the fibre diameters was therefore caused by the ambient conditions. The solution properties (shown in the section 5.2.3) were also measured at these ambient conditions to ensure consistency.

Excess moisture had to be removed as the ball electrospinning process exposed the top layer of spin solution to the surrounding atmosphere. DMSO in the spin solution was miscible with water while both PAN and *Platisorb* were not. When the humidity was high, moisture in the atmosphere mixed with the surface of the spin solution, causing the polymer and oligomer to precipitate out and a film to form over the surface of the ball electrospinning setup.

5.2.2 Comparing the number of jets, current per jet and fibre production capacity

The number of jets and current per jet were investigated during the ball electrospinning of the 6 wt% and 8 wt% PAN solutions. It was difficult to accurately count the number of jets produced at any specific point in time due to the large quantity of jets as well as the three dimensional structure of the ball. In spite of this, distinct variations were observed with regard to the number of jets and current per jet when ball electrospinning the two different PAN solutions.

The average number of jets was 24 when ball electrospinning the 6 wt% PAN solution, while 38 jets were observed on average while electrospinning the 8 wt% PAN solution. Both solutions were electrospun with an applied voltage of positive 35 kV. The average current per jet measured during ball electrospinning the 6 wt% PAN solution was 0.35 ± 0.02 mA, while the average current per jet was 0.55 ± 0.04 mA when ball electrospinning the 8 wt% PAN solution.

The 6 wt% PAN solution had an average production rate of 31.59 ± 0.70 mg/min while the 8 wt% PAN solution had an average production rate of 67.92 ± 9.00 mg/min. This difference in fibre production was expected as an increase in the flow of electrical current leads to an increase in mass transfer. This increase in production capacity is also ascribed to the number of jets produced, with more jets formed when ball electrospinning the 8 wt% PAN solution than when ball electrospinning the 6 wt% PAN solution.

5.2.3 Viscosity, conductivity and surface tension of the 6 wt% and 8 wt% PAN solutions

The viscosity, conductivity and surface tension were measured for each of the 6 wt% and 8 wt% PAN solutions prior to ball electrospinning. The values obtained are reported in Table 5.2 with standard deviations calculated for three different solutions over three different days.

Table 5.2 – Solution properties of the 6 wt% and 8 wt% PAN solutions with standard deviations, determined using 9 measurements.

	6 wt% solution	**8 wt% solution**
Viscosity (cP)	361.2 ± 3.3	1161.0 ± 18
Conductivity (µS/cm)	147.8 ± 11	154.3 ± 11
Surface Tension (mN/m)	40.0 ± 0.78	40.2 ± 0.76

The statistical significance of the differences between the solution property values obtained for the 6 wt% and 8 wt% PAN solutions was determined using a paired-sample t-test. Both the conductivity ($t = -0.77$, $df = 16$, $p > 0.05$) and surface tension ($t = -0.58$, $df = 16$, $p > 0.05$) of the 6 wt% and the 8 wt% PAN solutions did not differ significantly. However, the viscosity of the 8wt% PAN solution was significantly higher than that of the 6wt% PAN solution ($t = 138.18$, $df = 16$, $p < 0.05$).

The conductivity and surface tension of the solutions would therefore not play a role in any average fibre diameter differences observed between the nanofibres produced from the 6 wt% and 8 wt% PAN solutions. The significant difference between the viscosities measured for the two solutions, with the 8 wt% PAN solution having a viscosity more than three times greater than that of the 6 wt% PAN solution, was expected to have an effect on the diameters of the nanofibres. It is known from literature that an increase in solution viscosity causes an increase in nanofibre diameter.[64] The nanofibres produced by the 8 wt% PAN solution were therefore expected to have larger diameters than those produced when electrospinning the 6 wt% PAN solution.

5.2.4 Average fibre diameters and reproducibility of ball electrospinning

The average fibre diameters along with standard deviations obtained from ball electrospinning the 6 wt% and 8 wt% PAN solutions are shown in Figure 5.8. The average fibre diameter of the nanofibres produced by the 6wt% PAN solution was 210 nm with a standard deviation of 35 nm, while the 8 wt % PAN solution produced nanofibres with an average fibre diameter of 351 nm and a standard deviation of 81 nm. Good reproducibility of both the nanofibres electrospun using the 6 wt% PAN solutions as well as the 8 wt% PAN solutions can also be seen in Figure 5.8. The fibre diameter distributions are shown in Figure 5.9.

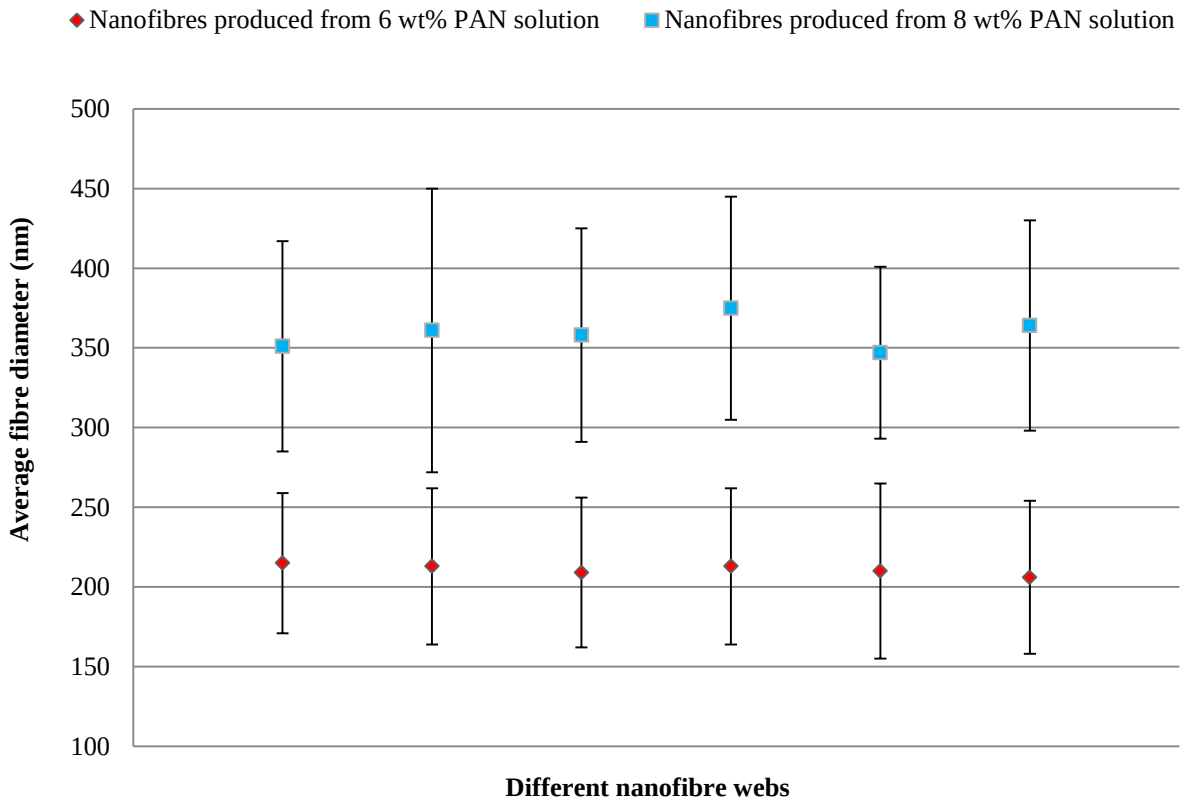

Figure 5.8 – The average fibre diameters of the nanofibres produced by ball electrospinning the 6 wt% and 8 wt% PAN solutions with a PAN to *Platisorb* ratio of 7:3. The standard deviations are indicated by the vertical error bars.

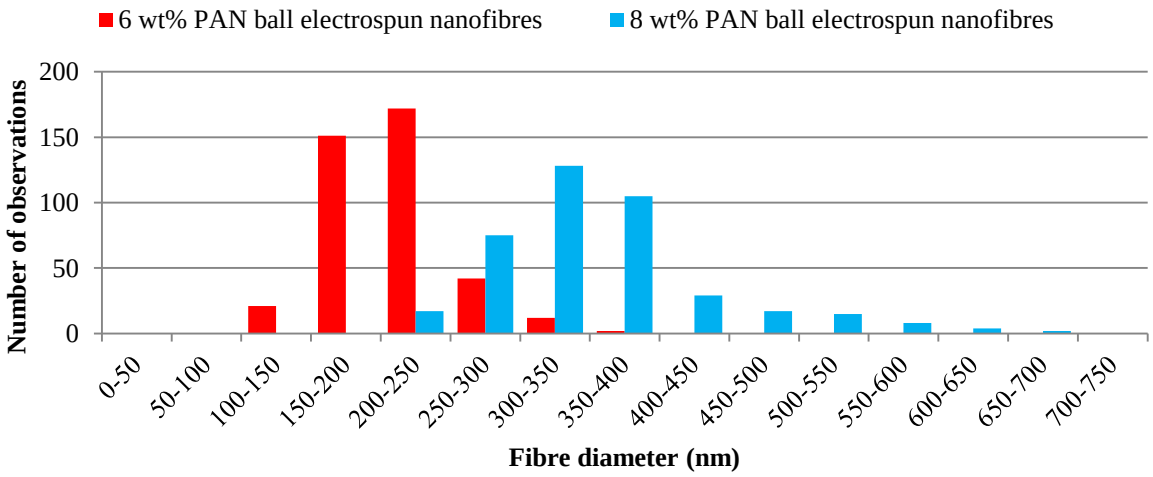

Figure 5.9 – The fibre diameter distributions of the nanofibres produced by the needle and ball electrospinning processes. Distributions were plotted using 400 measurements.

There were three factors affecting the resultant nanofibre diameters when ball electrospinning the 6 wt% and 8 wt% PAN solutions. The first was the effective spinning distance of the two solutions during ball electrospinning, the second was the effect of the current carried by each individual jet during the electrospinning process and the third was the difference in viscosity between the two solutions.

When the spin distance is shorter in which the polymer jets can stretch and elongate, thicker fibres are obtained.[67] The 6 wt% PAN solution had a 1 cm shorter spin distance and therefore shorter distance in which to stretch and elongate, which means that these fibres were expected to have slightly thicker fibres than those produced from the 8 wt% PAN solution.

The second factor affecting the fibre diameters was the current per jet during ball electrospinning of the two solutions. The jets formed during electrospinning whip due to instability caused by the electrical current. Because the current per jet was on average 0.20 mA less for the jets produced by the 6 wt% PAN solution, these fibres were expected to have larger fibre diameters.

The final factor that affected the average fibre diameters was the difference in viscosity between the 6 wt% and 8 wt% PAN solutions. More viscous solutions produces nanofibres with larger diameters, explaining why the 8 wt% PAN solution produced nanofibres with larger average fibre diameters than the 6 wt% PAN solution.

The dominant factor affecting the average fibre diameters was the viscosity (with the 8 wt% PAN solution having a viscosity more than three times greater than that of the 6 wt% PAN solution), which overshadowed the effects of the effective spinning distance (1 cm difference) and the current per jet (0.20 mA difference).

5.2.5 BET surface area analysis of the two nanofibre webs

BET surface area analysis was done on both of the 6 wt% and 8 wt% PAN solutions' ball electrospun nanofibre webs to determine their specific surface areas. The specific surface area of the nanofibre web produced by the 6 wt% PAN solution was 39.38 ± 0.05 m^2/g, while the specific surface area of the nanofibre web produced by the 8 wt% PAN solution was 29.34 ± 0.04 m^2/g. This showed that increasing the average fibre diameter from 210 ± 35 nm to 351 ± 81 nm caused a decrease in specific surface area of roughly 10.04 m^2/g (34.2 %).

CHAPTER 6

EXTRACTION OF HEXACHLOROPLATINATE USING PLATISORB-*CONTAINING NANOFIBRES*

Objective C:

*To study the electrospun nanofibre webs containing the poly(*N-*terephthaloylthiourea)*-N*',*N*'-*piperazine oligomer for the extraction of Pt(II/IV) ions in the form of* $[PtCl_6]^{2-}$ *from acidic solutions under varying conditions, including: varying specific surface area of the extractant, varying extraction temperatures, as well as varying solution hydrochloric acid concentrations.*

6.1 Pt(II/IV) ion mass balance using NaOH treatment of *Platisorb* powder

Platisorb powder was shaken in a $[PtCl_6]^{2-}$ and allowed to extract the Pt(II/IV) ions from solution. NaOH with a concentration of 0.25 M was then used to degrade (refer to Chapter 5, section 5.1.5) the *Platisorb*, after which ICP-AES analysis was done on the degraded *Platisorb* solution to determine the concentration of Pt ions extracted by the oligomer. ICP-AES was also used to determine the concentration of Pt ions in the solution before and after *Platisorb* extraction. Pt(II/IV) ion mass balance is shown in Figure 6.1 using the results from Table 6.1.

Table 6.1 –Concentrations of Pt(II/IV) ions in the different solutions. Standard deviation was determined using 9 measurements obtained from analysis of 3 different solutions.

	Pt(II/IV) concentration (mg/L)
Pt(II/IV) ion concentration in stock solution	231.1
Pt(II/IV) ion concentration in supernatant after extraction	29.6 ± 1.3
Pt(II/IV) ion concentration loaded onto *Platisorb* oligomer	197.5 ± 2.1
Pt(II/IV) ions unaccounted for	4.1 ± 0.8

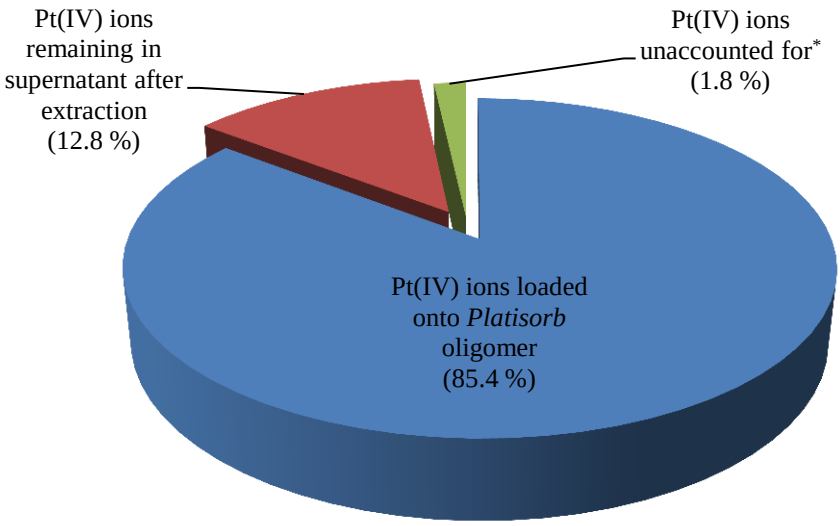

Figure 6.1 – A pie chart showing Pt(II/IV) ion mass balance. A small percentage of Pt(II/IV) ions were unaccounted for due to solution preparations. Experimental: 30 mg *Platisorb* powder was added to 10 mL of 231.1 mg/L $[PtCl_6]^{2-}$ stock solution in a 1 M HCl matrix and shaken. *Platisorb* powder was isolated after extraction and degraded in 10 mL 0.25 M NaOH solution for 24 hours.

* Note: The loss of Pt(II/IV) ions during the rest of the extraction investigations is believed to be much less than observed during the mass balance investigation, so the Pt(II/IV) ions unaccounted for due to solution preparation (1.8 % of the total Pt(II/IV) ions) are not taken into account for any of the results shown in the rest of the chapter. Less solution processing was required for the other extraction experiments, which meant less loss of Pt(II/IV) ions would affect the Pt(II/IV) ion concentrations.

All subsequent Pt(II/IV) ion concentrations extracted by both the *Platisorb* and *Platisorb*-containing nanofibres were obtained by subtracting the concentration of Pt(II/IV) ions after extraction from the concentration of the Pt(II/IV) ions in the stock solution using equation 2.

$$Pt_{extracted\ by\ \text{Platisorb}} = Pt_{in\ solution\ before\ extraction} - Pt_{in\ solution\ after\ extraction} \quad [2]$$

6.2 The effect of specific surface area and coordination site availability on the extraction of Pt(II/IV) ions

The first extraction experiment investigated the effects of varying specific surface area and the availability of coordination sites on the extraction of Pt(II/IV) ions from acidic solutions. Three different extraction media were used during the investigation:

- 15 mg pure *Platisorb* powder,
- 50 mg *Platisorb*-containing nanofibres spun using a 6 wt% PAN solution with a PAN to *Platisorb* ratio of 7:3, and
- 50 mg *Platisorb*-containing nanofibres spun using an 8 wt% PAN solution with a PAN to *Platisorb* ratio of 7:3.

The pure *Platisorb* oligomer samples as well as the *Platisorb*-containing nanofibre samples contained 15 mg of *Platisorb* to ensure comparable extraction results. All three extractants were used concurrently to determine which had the highest extraction efficiency of Pt ions as a function of time.

6.2.1 Time dependence study of Pt(II/IV) ion extraction

The results of the extraction are shown in Figure 6.2. The lowest extraction of Pt(II/IV) ions was obtained using the *Platisorb*-containing nanofibres spun from the 8 wt% PAN solution, with an average of 81.9 ± 2.3 % extraction after 120 hours. Comparable extraction was observed when using the *Platisorb*-containing nanofibres spun from the 6 wt% PAN solution, with an average extraction of 83.9 ± 0.3 % after 120 hours. The pure *Platisorb* oligomer showed the best extraction, with 100 ± 0.1 % after 120 hours.

The Pt(II/IV) ion extraction results of the 6 wt% and the 8 wt% PAN nanofibres* did not differ significantly, as determined by a paired-sample t-test ($t = 0.70$, $df = 52$, $p > 0.05$). However, the differences in Pt(II/IV) ions extraction between the 6wt% PAN nanofibres and *Platisorb* powder

* Note: During the rest of this chapter the nanofibres produced by electrospinning the 6 wt% PAN solution with a ratio of PAN to *Platisorb* of 7:3 are also referred to as 6 wt% PAN nanofibres. The nanofibres produced when electrospinning the 8 wt% PAN solution with a PAN to *Platisorb* ratio of 7:3 are also referred to as the 8 wt% PAN nanofibres.

(t = -5.87, df = 52, p < 0.05), as well as the 8 wt% PAN nanofibres and *Platisorb* powder (t = -6.97, df = 52, p < 0.05) showed that the powder's extraction was significantly higher.

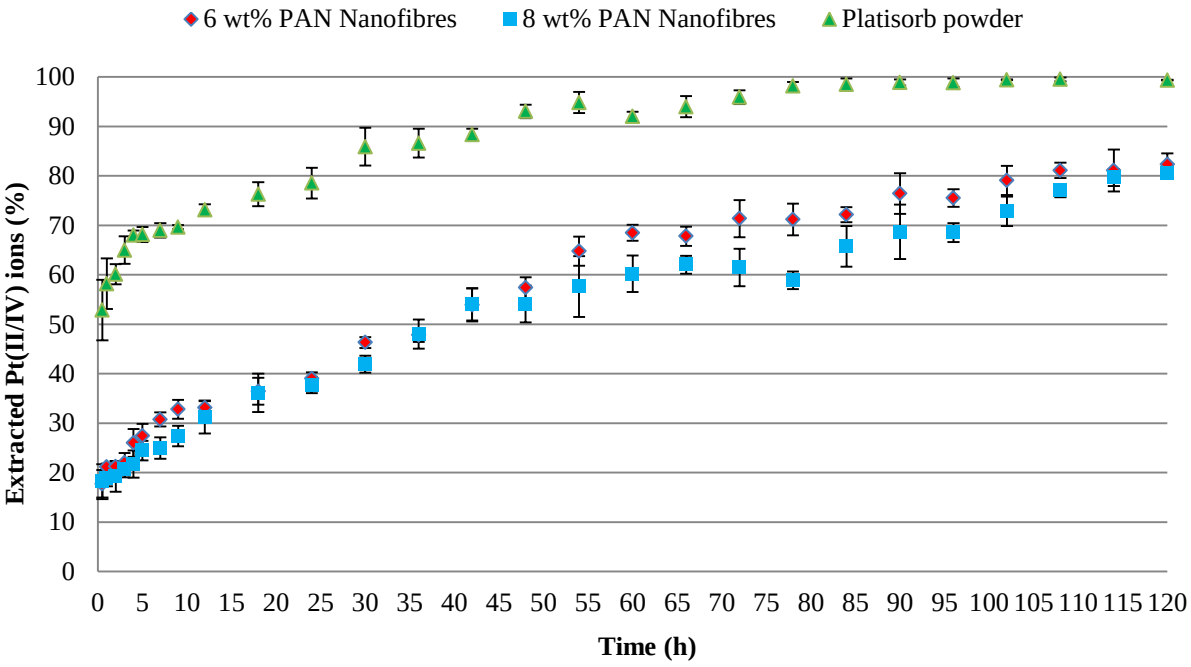

Figure 6.2 – Percentage extraction of Pt(II/IV) ions as a function of time. Experimental: Stock solution was 118.9 mg/L Pt(II/IV) in a 1 M HCl matrix. 10 mL stock solution containing the extractant material was shaken at 250 rpm at room temperature, after which the supernatant solution was analysed. Triplicate analyses were done and the error bars indicate the standard deviations.

6.2.2 Discussion of the observed Pt(II/IV) ion extraction trends

The specific surface areas of the 6 wt% and 8 wt% PAN nanofibres (reported in Chapter 5, section 5.2.5), as well as the specific surface area of the *Platisorb* powder, were measured using BET analysis. A larger specific surface area was expected to facilitate a greater degree of Pt(II/IV) ion extraction. Table 6.2 shows this correlation for specific surface area of each of the extractants used and the Pt(II/IV) ion extraction achieved.

Table 6.2 – The correlation between specific surface area and the percentage $[PtCl_6]^{2-}$ extracted after 120 hours for each of the extractants.

Extractant	Specific surface area (m^2/g)	Pt(II/IV) ions extracted after 120 hours (%)
Platisorb powder	61.69 ± 0.12	100.0 ± 0.1
6 wt% PAN nanofibres	39.38 ± 0.05	83.9 ± 0.3
8 wt% PAN nanofibres	29.34 ± 0.04	81.9 ± 2.3

A 22.31 m^2/g increase in specific surface area from the 6 wt% PAN nanofibres to the *Platisorb* powder correlated to a 16.1 % increase in Pt(II/IV) ion extraction, while a 32.35 m^2/g increase in specific surface area from the 8 wt% PAN nanofibres to the *Platisorb* powder correlated to only an 18.1 % increase in Pt(II/IV) ion extraction. From these results there appeared to be a correlation between specific surface area and Pt(II/IV) ion extraction. A specific surface area increase of 10.04 m^2/g from the 8 wt% PAN nanofibres to the 6 wt% PAN nanofibres, however, had an insignificant (see section 6.2.1) increase in Pt(II/IV) ion extraction. The conclusion was therefore, due to no clear correlation between the specific surface area and the Pt(II/IV) ion extraction, that the specific surface area of the extractant was not the only factor affecting Pt(II/IV) ion extraction.

Another factor which contributed to the Pt(II/IV) ion extraction was the availability coordination sites. An example of a postulated coordination site is shown in Figure 2.3. The amount of Pt(II/IV) ion that was removed from solution would directly be affected by the amount and availability of the coordination sites to which these ions bind. Some coordination sites were situated on the surfaces of the nanofibres and accessible, while other coordination sites were encapsulated within the PAN matrix of the nanofibre structures and inaccessible during Pt(II/IV) ion extraction. The extent to which the *Platisorb* oligomers were encapsulated within the nanofibres was determined using energy-dispersive X-ray spectroscopy (EDS) before and after 0.25 M NaOH treatment, as the NaOH removed all accessible *Platisorb* on the nanofibre surfaces and not the oligomer chains encapsulated within the nanofibre structures. Figure 6.3 shows the labelled EDS images obtained from analysis of the 6 wt% PAN nanofibres.

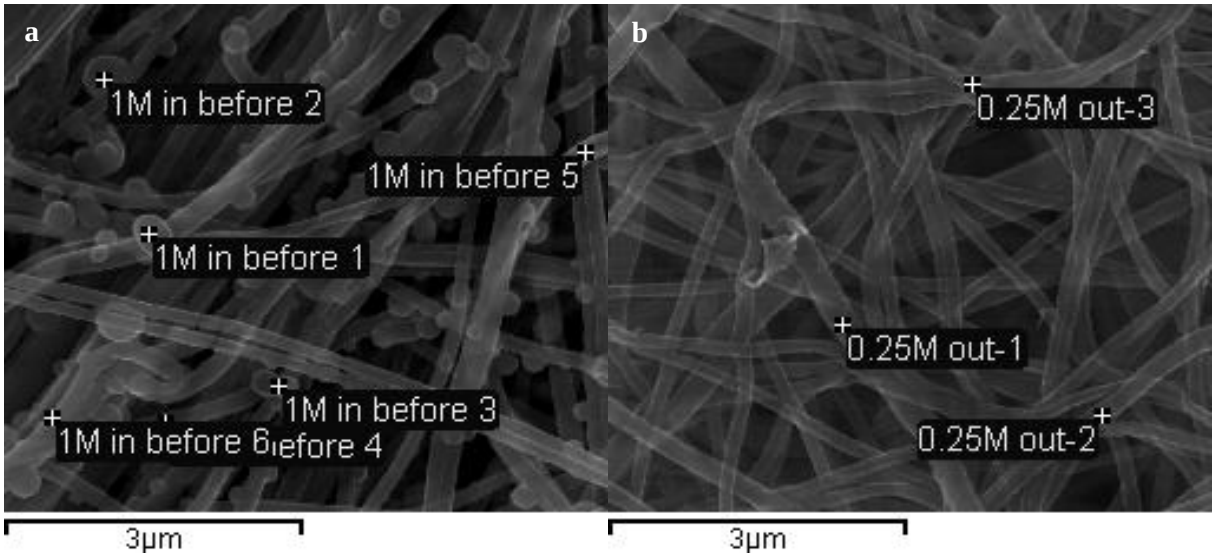

Figure 6.3 – Images obtained from EDS analysis of 6wt% PAN nanofibres which have been exposed to 100 mg/L Pt(II/IV) ions **(a)** before and **(b)** after 0.25 M NaOH treatment for 24 hours. Note that the points marked in image (a) with labels ending in "1" to "3" are on the *Platisorb* surface structures (discussed in Chapter 5, section 5.1.5), while the points with labels ending in "4" to "6" are on the nanofibres. Also note the transparent nature of the nanofibres in the images due to the high electron beam strength of 20 kV.

The transparency of the nanofibres in Figure 6.3 is ascribed to the high electron beam strength of 20 kV, which was required to obtain consistent EDS composition values. Due to its strength, the electron beam penetrated through the nanofibre web beyond the points being targeted and measured the compositions of subsequent layers, giving the average composition of all the penetrated layers. The electron beam strength therefore explains why no variation in composition was observed between the nanofibres and the nanofibre surface structures (shown in Table 6.3)

Table 6.3 – EDS results of the chemical composition of the 6 wt% PAN nanofibres before and after 0,25 M NaOH treatment, as well as the surface structures on the nanofibres before NaOH treatment. The results of the % oxygen and % sulphur are highlighted as being indicative of the presence of *Platisorb* oligomers.

		%C	%N	%O	%Na	%S	%Pt	%Total
Surface Structures Before NaOH Treatment	Average	62.9	28.7	5.1	0.0	2.6	0.8	100
	Std. Deviation	6.1	5.7	1.2	0.0	0.5	0.3	
Fibres Before NaOH Treatment	Average	62.1	29.3	5.3	0.0	2.6	0.8	100
	Std. Deviation	6.2	6.1	1.3	0.0	0.5	0.4	
Fibres After NaOH Treatment	Average	67.8	27.1	3.2	0.4	0.9	0.7	100
	Std. deviation	3.3	3.1	0.6	0.1	0.2	0.2	

The sulphur and oxygen measured by EDS are indicative of *Platisorb* oligomeric chains (see Figure 4.3), with the sulphur and oxygen originating from the thiocarbonyl and carbonyl moieties, respectively. EDS showed that the nanofibres after 0.25 M NaOH treatment still contained sulphur (0.9 %) as well as oxygen (3.2 %), even though the NaOH degraded the surface structures consisting of *Platisorb* oligomers (as shown in Figure 5.6(b)). Some of the oligomers were therefore encapsulated inside the nanofibre structure, inaccessible during NaOH treatment. The mass loss due to NaOH treatment supported this conclusion (Chapter 5, section 5.1.5).

The greater degree of Pt(II/IV) ion extraction of the *Platisorb* powder compared to the electrospun nanofibres can therefore also be attributed to the availability of coordination sites. A fine suspension was formed in solution when the powder was shaken at 250 rpm, exposing the coordination sites to the $[PtCl_6]^{2-}$ in solution and consequently exhibiting a greater degree of extraction. The nanofibres did not form a suspension when shaken and some of the coordination sites were encapsulated within the nanofibre structure, unable to interact with the $[PtCl_6]^{2-}$ in solution.

6.3 Temperature dependence investigation of Pt(II/IV) ion extraction

The effect of temperature on the extraction of Pt(II/IV) ions from acidic solutions was investigated for temperatures ranging from 20 °C to 60 °C while using the 6 wt% PAN ball electrospun nanofibres as extractant. Figure 6.4 shows an increase in percentage extraction as temperature increases from 20 °C to 60 °C. A steady increase in the percentage Pt(II/IV) ion extraction was observed from 20 °C to 40 °C, after which the percentage extraction plateaued and reached a maximum of 100 % between 55 °C and 60 °C. This clearly indicates that temperature has a substantial effect on the Pt(II/IV) ion extraction efficiency. A mass per mass extraction increase from 0.007 g to 0.023 g Pt per gram of nanofibres was observed when the temperature was increased from 20 °C to 60 °C during this investigation. It should be noted that these mass per mass extraction values can in no way be seen as the Pt(II/IV) ion extraction capacity of the *Platisorb*-containing nanofibres, as only trace amounts of Pt ions were available for extraction from solution.

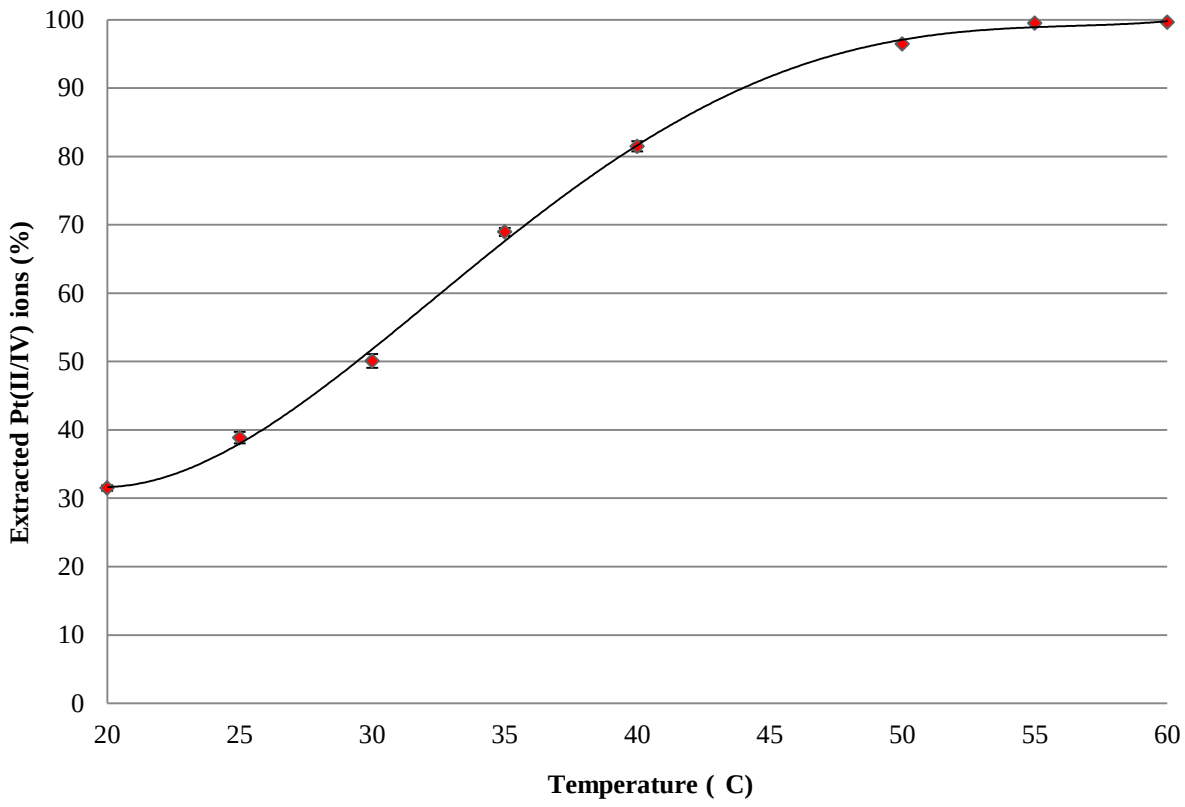

Figure 6.4 – The percentage extraction of Pt(II/IV) ions from solution as a function of temperature. Experimental: Stock solution was 114.0 mg/L Pt(II/IV) ions in a 1 M HCl matrix. 10 mL of stock solution containing a 50 mg 6 wt% PAN nanofibre web was shaken at 250 rpm in a temperature-controlled chamber for 24 hours, after which the supernatant solution was analysed. Triplicate analyses were done and the error bars indicate the standard deviations.

A thermodynamic investigation of the effect of temperature on Pt(II/IV) ion extraction was done using the extraction results obtained from 20 °C to 40 °C. Only the concentrations of Pt(II/IV) ions obtained

for temperatures 20 °C to 40 °C were used as the concentrations obtained for the higher temperatures were limited by the amount of $[PtCl_6]^{2-}$ in solution and caused deviations in the Van't Hoff plot.

Equations 3 and 4 were used to calculate the change in Gibbs free energy (ΔG^o):

$$\Delta G^o = \Delta H^o - T\Delta S^o \quad [3]$$

$$\Delta G^o = -RTlnK_e \quad [4]$$

where ΔH^o is the standard enthalpy change, T is the temperature in Kelvin, ΔS^o is the standard entropy change, R is the universal gas constant (8.314 J K^{-1} mol^{-1}), and K_e is the equilibrium constant. Equations 3 and 4, along with the Van't Hoff equation (Equation 5) were used to formulate Equation 6. This equation was subsequently used to draw the Van't Hoff plot shown in Figure 6.5. The Van't Hoff plot was in turn used to determine the thermodynamic parameters ΔH^o and ΔS^o and these values were then used to calculate ΔG^o.

$$\frac{dlnK_e}{dT} = \frac{\Delta H^o}{RT^2} \quad [5]$$

$$lnK_e = \frac{-\Delta H}{RT} + \frac{\Delta S}{R} \quad [6]$$

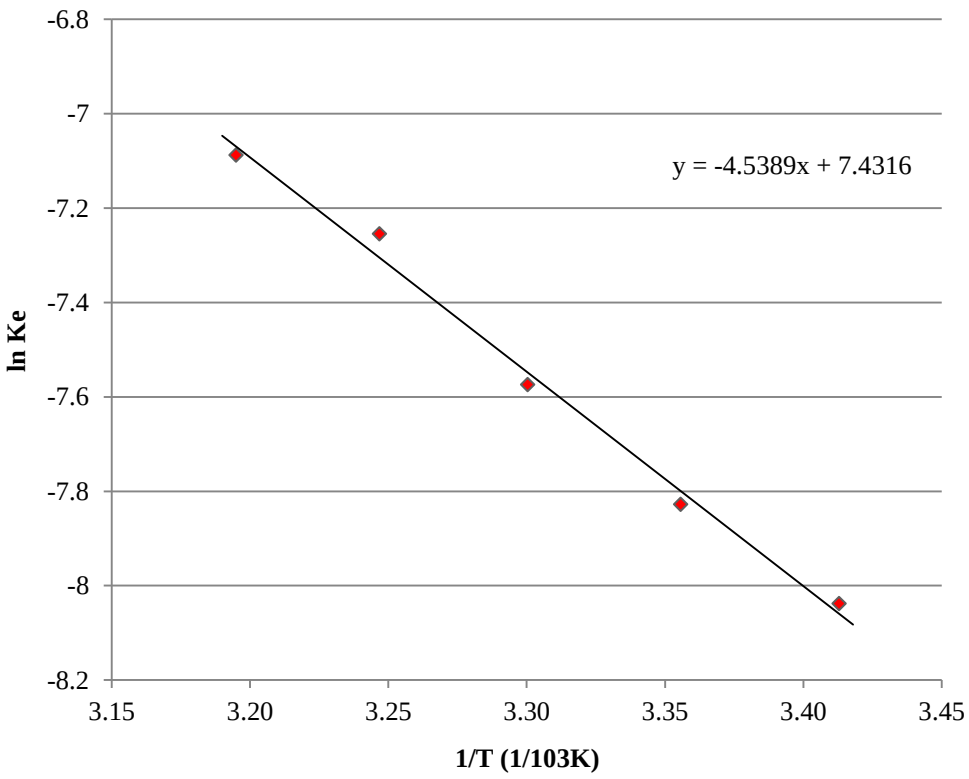

Figure 6.5 - The Van't Hoff plot, drawn using Equation 6. The formula y = -4.54x + 7.43 was obtained from the trendline fitted to the plot's data points.

The thermodynamic results obtained were only used to confirm the extraction mechanism and to determine whether the reaction's ΔG^o, ΔH^o and ΔS^o values were positive or negative. No further manipulations were done using the actual values obtained for ΔG^o, ΔH^o and ΔS^o, as it falls outside the scope of this study to prove whether or not the system was in equilibrium or not. It was found that all of ΔG^o, ΔH^o and ΔS^o were positive. These positive values obtained for ΔG^o and ΔH^o indicates the presence of an energy barrier in the $[PtCl_6]^{2-}$ extraction process and that the process is endothermic, while the positive ΔS^o obtained is attributed to increased randomness in the system due to the extraction process using the *Platisorb*-containing nanofibres.

6.3.1 The postulated *Platisorb* extraction mechanism

The extraction mechanism, whether chemisorption or physisorption, is an important indicator of the type of interaction taking place between the affinity sites present on the *Platisorb* oligomer and the $[PtCl_6]^{2-}$. A decrease in extraction with increasing temperature indicates a physisorption reaction such as ion-exchange while an increase in extraction with increasing temperature signifies a chemisorption reaction such as coordination. This is because chemisorption often involves activation energy while physisorption does not.

An increase in temperature resulted in an increase in extent of extraction efficiency of $[PtCl_6]^{2-}$ shown in Figure 6.4, suggesting that chemisorption, probably *via* a coordination mechanism, controlled the rate of the process of extraction. This correlates well with the complexation shown when reacting *N*,*N*-dialkyl-*N*-aroylthiourea or *N*,*N*-dialkyl-*N*-acyl-thiourea ligands with Pt(II) chloride ions.[45–47] It is thus reasonable to postulate a similar mode of complextation with the $[PtCl_6]^{2-}$, *via* the carbonyl and thiocarbonyl moieties with loss of halide ions, as a possible method of extraction in this work. This could occur either through the complexation of the Pt(IV) ions from the $[PtCl_6]^{2-}$, or by the reduction of Pt(IV) to Pt(II) followed by coordination of Pt(II) ions by a similar mechanism to the one shown in Figure 2.3. Establishing the detailed nature of the extraction or the binding mode of the Pt(II/IV) species to *Platisorb* was not within the scope of this project, and it is likely that the metal ions may be coordinated as a mixture of both Pt(II/IV) ions.

6.4 Effect of the HCl concentration on the extraction of Pt(II/IV) ions

The efficiency of $[PtCl_6]^{2-}$ extraction using the 6 wt% PAN electrospun nanofibres was investigated at six different HCl matrix concentrations ranging from 1.0×10^{-3} M to 6 M. Figure 6.6 shows the results obtained. No difference in $[PtCl_6]^{2-}$ extraction was observed when the matrix's HCl concentration was varied between 1.0×10^{-3} M to 1 M. The nanofibres did however exhibit a greater degree of $[PtCl_6]^{2-}$ extraction when the HCl concentration was increased from 1 M to 3 M, and again when the HCl concentration was increased from 3 M to 6 M.

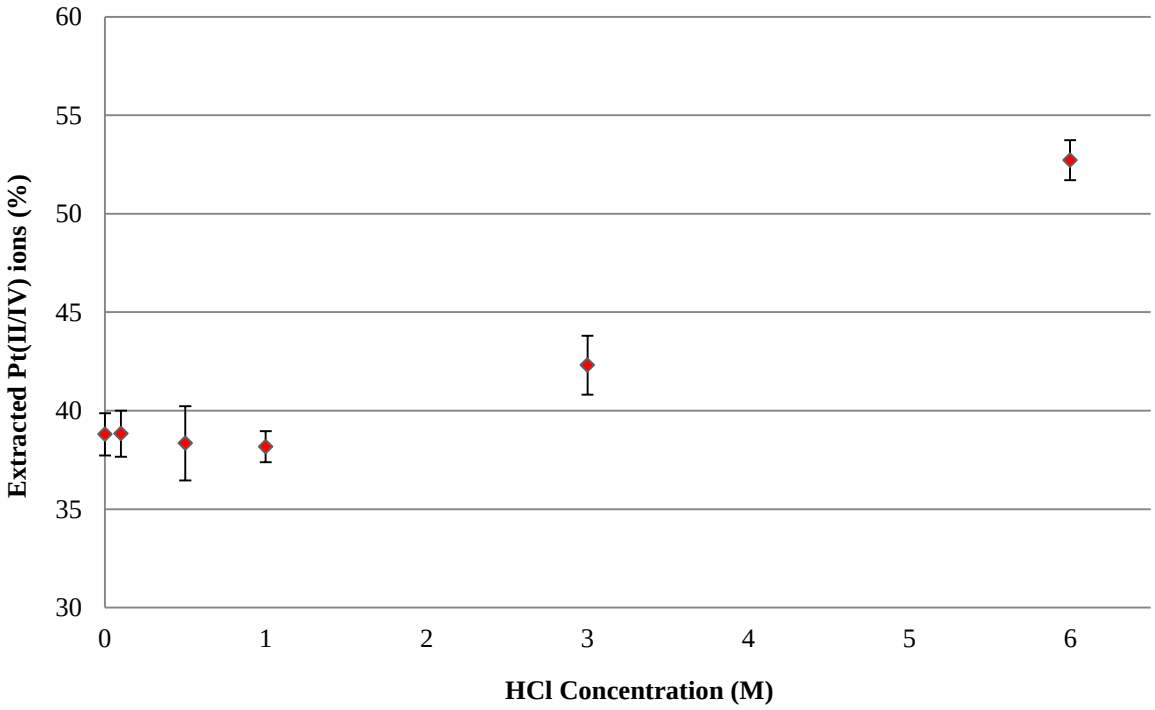

Figure 6.6 – The percentage extraction of $[PtCl_6]^{2-}$ from solution as a function of HCl concentration in the matrix. Experimental: Stock solution was 118.9 mg/L Pt(II/IV) ions in varied HCl matrix concentrations. 10 mL of stock solution containing a 50 mg 6 wt% PAN nanofibre web was shaken at 250 rpm at room temperature for 24 hours, after which the supernatant solution was analysed. Triplicate analyses were done and the error bars indicate the standard deviations.

The strong HCl concentrations of 3 M and 6 M were believed to cause fibre swelling and/or damage during the $[PtCl_6]^{2-}$ extraction investigations. 50 mg nanofibre samples were weighed before and after 24 hour contact with the different HCl solutions. A weight loss of 4.60 % was observed for the nanofibres exposed to the 3 M HCl solution for 24 hours, while the nanofibres exposed to the 6 M HCl solution exhibited a weight loss of 6.64 %. Nanofibre samples exposed to the lower concentrations (1.0×10^{-3} M to 1 M) of HCl showed negligible weight loss. The weight loss of the nanofibre samples exposed to the stronger acid concentrations indicated that fibre damage occurred during the extraction experiments.

The greater degree of $[PtCl_6]^{2-}$ extraction observed when using stronger HCl matrix concentrations is ascribed to damage caused to the nanofibres, exposing more of the *Platisorb* previously encapsulated within the nanofibre structure (see section 6.2.2) to the $[PtCl_6]^{2-}$ in solution, effectively facilitating greater extraction of Pt(II/IV) ions. The greater extraction capability was however offset by the fact that the nanofibre structures were damaged in the process.

CHAPTER 7

CONCLUSIONS AND RECOMMENDATIONS FOR FURTHER STUDY

7.1 Conclusions

This chapter details how the three specific objectives set in the beginning of this study were met and the recommendations are made for further study.

Objective A:

(i) *To prepare poly(*N-*terephthaloylthiourea)*-N*'*,N*'-piperazine oligomer, as reputed in the Patent Application WO 2000/53663,*[21]

Poly(*N*-terephthaloylthiourea)-*N*',*N*'-piperazine was successfully synthesised using a similar "one-pot" two step synthesis method to the one proposed by Douglass and Dains,[130] while using terephthaloyl chloride, NaSCN and piperazine as starting reagents.

A final product yield of 65.5 % was achieved, which was less than the yield of 76.2 % reported in the patent application.[21] The difference in yield obtained was ascribed to the much larger batch size, as well as the additional washing steps incorporated into the synthesis procedure for this work.

Objective A:

(ii) conducting analytical analyses on the produced substance for characterization purposes.

Multiple techniques were used to elucidate the chemical groups present in the synthesised oligomer, as well as to determine the oligomer's chemical composition and average molecular weight. Elemental analysis was used to determine the chemical composition, while GPC was used to determine the molecular weight of the oligomer. All of the moieties present in the postulated structure were accounted for using FTIR as well as ^{1}H and ^{13}C NMR, including the carbonyl, thiocarbonyl, secondary amine, six-membered aromatic ring, and piperazine groups. The M_n (3705 g/mol), M_w (6427 g/mol) and postulated molecular weight of the oligomer repeat unit (609.8 g/mol), were used to determine that the average oligomer chain had six repeat units. This value was expected to vary due to the oligomer's polydispersity of 1.73.

Five possible repeat units were postulated using the chemical composition of the synthesised oligomer. It was found that a combination of three of these repeat units had a comparable chemical composition to the oligomer, and these were proposed to be the repeat units making up the oligomeric chain.

It was difficult to completely characterise the oligomer described in the patent application as the oligomer that was produced was found to be heterogeneous. However, sufficient characterisation was done to show the presence of the postulated Pt(II/IV) ion coordination sites and to prove that an oligomeric structure was formed.

Objective B:

*To examine the process of needle as well as ball electrospinning of a bicomponent solution containing poly(*N-*terephthaloylthiourea)*-N*'*,*N*'*-piperazine oligomer and polyacrylonitrile into suitable nanofibres.*

Needle electrospinning the 6 wt% PAN solution over an effective spin distance of 5 cm produced nanofibres at an average production rate of 0.37 ± 0.06 mg/min, whereas ball electrospinning produced nanofibres at an average production rate of 31.59 ± 0.70 mg/min. The ball electrospinning process required an applied voltage of 35 kV to initiate solution jetting, while the needle electrospinning process only requires an applied voltage of 8 kV. The needle and ball electrospinning processes produced nanofibres with average fibre diameters of 172 ± 35 nm and 210 ± 49 nm, respectively. Structures observed on the surfaces of the nanofibres produced by both of the electrospinning processes were shown to consist of *Platisorb* oligomers and are believed to form during the water washing step after electrospinning.

Ball electrospinning is a new technique only patented in 2011,[29] compared to needle electrospinning which was already patented in 1902.[59,60] A comparison between the two processes was therefore important to determine whether similar results are obtained and whether the processes can be used interchangeably. The nanofibres from both processes appear to be interchangeable from the observations made during this work, with only minor differences in fibre diameters and fibre morphologies. However, the ball electrospinning process exhibited, *via* comparison of the absolute production rates, an 86 times increase in nanofibre production rate over that of needle electrospinning. Ball electrospinning is therefore a high throughput electrospinning process capable of creating comparable nanofibres to the needle electrospinning process.

Objective C:

*To study the electrospun nanofibre webs containing the poly(*N-*terephthaloylthiourea)*-N*'*,*N*'*-*piperazine oligomer for the extraction of Pt(II/IV) ions in the form of* $[PtCl_6]^{2-}$ *from acidic solutions under varying conditions, including: varying specific surface area of the extractant, varying extraction temperatures, as well as varying solution hydrochloric acid concentrations.*

The effect of specific surface area on $[PtCl_6]^{2-}$ extraction was determined by using pure *Platisorb* powder with a specific surface area of 61.69 ± 0.12 m^2/g, 6 wt% PAN nanofibres with specific surface area of 39.38 ± 0.05 m^2/g and 8 wt% PAN nanofibres with specific surface area of 29.34 ± 0.04 m^2/g. Specific surface area was not the only factor affecting Pt(II/IV) ion extraction, as a specific surface area increase of 22.31 m^2/g (from the 6 wt% PAN nanofibres to the *Platisorb* powder) caused a 16.1 % increase in Pt(II/IV) ion extraction while a specific surface area increase of 10.04 m^2/g (from the 8

wt% PAN nanofibres to the 6 wt% PAN nanofibres) had no significant increase in Pt(II/IV) ion extraction.

Another explanation for the extraction trends is the availability of coordination sites. The pure *Platisorb* oligomer had the most coordination sites available as it formed a fine suspension during the extraction process, while both sets of nanofibres had some of the coordination sites encapsulated within the nanofibre structures. EDS was used to show to a certain extent that some of the coordination sites were encapsulated within the PAN matrix of the nanofibres and this was verified by the mass loss observed when removing the Platisorb oligomers (with 0.25 M NaOH) from the surfaces of the nanofibres.

The temperature dependence study showed that faster $[PtCl_6]^{2-}$ extraction was achieved with increased extraction temperature. The Pt(II/IV) ion extraction increased from 0.007 g to 0.023 g Pt for each gram of added nanofibres as the temperature was increased from 20 °C to 60 °C. The thermodynamics were also investigated. Positive values of ΔG^o, ΔH^o and ΔS^o were attributed to the presence of an energy barrier in the extraction process, the endothermic nature of the extraction process, and an increased randomness in the system caused by $[PtCl_6]^{2-}$ extraction, respectively. The increase in extraction with an increase in temperature was used to verify coordination as the method of extraction.

The HCl concentration did not affect the $[PtCl_6]^{2-}$ extraction capacity when ranging from 1.0×10^{-3} M to 1 M. An increase from 1 M to 6 M HCl caused an increase in the Pt(II/IV) ion extraction due to swelling and/or damage of the nanofibre webs by the strongly acidic solutions. As a result of the change in the nanofibre webs, more of the *Platisorb* previously encapsulated inside the nanofibres were exposed to the surrounding solution, facilitating a greater degree of extraction.

Even though the *Platisorb* oligomer shows better $[PtCl_6]^{2-}$ extraction in powder form, the *Platisorb*-containing nanofibres are easier to handle and remove from solution after the extraction process. The HCl concentration study's findings place restrictions on the uses of the electrospun nanofibres for industrial Pt(II/IV) ion extraction applications, in that the acid concentration should not surpass 1 M HCl. Prolonged exposure to solutions with HCl concentrations above 1 M would compromise the integrity of the nanofibre webs. When working within these acid concentration restrictions, the *Platisorb*-containing nanofibre webs produced by the ball electrospinning process are very effective at extracting trace amounts of Pt(II/IV) ions from acidic solutions.

7.2 Recommendations for further study

This study only focuses on the extraction of Pt(II/IV) ions in the form of $[PtCl_6]^{2-}$ from acidic solutions which were carefully prepared in a laboratory. Ideally however, these *Platisorb*-containing nanofibres should be used on site at the platinum refineries that produces the effluent, to recover the Pt(II/IV) ions

directly from the effluent solutions. It would therefore be worthwhile to determine how the nanofibres interact with Pt(II/IV) ions in a more complex solution containing other components such as base metals and other PGM salts. It is recommended that the nanofibres should be used to determine the extraction efficiency of Pt(II/IV) ions from actual refinery effluent, to determine the selectivity towards the Pt(II/IV) ions in a complex solution.

A second important investigation would be to determine whether or not the Pt(II/IV) ions bound to the *Platisorb*-containing nanofibres can be recovered. The bonds that form between the *Platisorb* oligomers and the Pt(II/IV) ions need to be broken in order to recover the ions after the extraction process. The investigation should also determine whether or not the nanofibres could be used again for Pt(II/IV) ion extraction, for how many cycles the *Platisorb*-containing nanofibre web remains an effective extraction material, and what effect the desorption process has on the effectiveness of the nanofibres when used for subsequent extractions. When investigating possible desorption mechanisms it is important to determine both the costs and environmental impacts of the chemicals used.

REFERENCES

1. Wood, I., 2004. *Platinum*. New York: Marshall Cavendish

2. Rillema, D.P., 2004. *Platinum*. Chemistry: Foundations and Applications. [online] Available at: <http://www.encyclopedia.com/topic/platinum.aspx#3> [Accessed 03 November 2012]

3. Butler, J., 2010. *Platinum 2010 interim review*. Royston: Johnson Matthey.

4. Krebs, R.E., 2006. *The history and use of our earth's chemical elements: A reference guide*. 2nd ed. Westport, CT: Greenwood Publishing Group.

5. The Columbia Electronic Encyclopedia, 2012. *Platinum*. [online] Available at: <http://www.encyclopedia.com/topic/platinum.aspx#2> [Accessed 03 November 2012]

6. Uheida, A., Iglesias, M., Fontàs, C., Hidalgo, M., Salvadó, V., Zhang, Y., Muhammed, M. Sorption of palladium(II), rhodium(III), and platinum(IV) on Fe_3O_4 nanoparticles. *Journal of colloid and interface science* **301**(2) (2006) 402–408.

7. Fujiwara, M., Matsushita, T., Kobayashi, T., Yamashoji, Y., Tanaka, M. Preparation of an anion-exchange resin with quaternary phosphonium chloride and its adsorption behaviour for noble metal ions. *Analytica Chimica Acta* **274** (1993) 293–297.

8. Parajuli, D., Kawakita, H., Inoue, K., Funaoka, M. Recovery of gold(III), palladium(II), and platinum(IV) by aminated lignin derivatives. *Industrial & Engineering Chemistry Research* **45**(19) (2006) 6405–6412.

9. Kasaini, H., Mbaya, R.K. Continuous adsorption of Pt ions in a batch reactor and packed-bed column. *Hydrometallurgy* **97**(1-2) (2009) 111–118.

10. Park, C., Chung, J., Cha, K. Separation and preconcentration method for palladium, platinum and gold from some heavy metals using Amberlite IRC 718 chelating resin. *Bulletin of the Korean Chemical Society* **21**(1) (2000) 121–124.

11. Parajuli, D., Khunathai, K., Adhikari, C.R., Inoue, K., Ohto, K., Kawakita, H., Funaoka, M., Hirota, K. Total recovery of gold, palladium, and platinum using lignophenol derivative. *Minerals Engineering* **22**(13) (2009) 1173–1178.

12. Fujiwara, K., Ramesh, A., Maki, T., Hasegawa, H., Ueda, K. Adsorption of platinum (IV), palladium (II) and gold (III) from aqueous solutions onto L-lysine modified crosslinked chitosan resin. *Journal of Hazardous Materials* **146**(1-2) (2007) 39–50.

13. Zhou, L., Liu, J., Liu, Z. Adsorption of platinum(IV) and palladium(II) from aqueous solution by thiourea-modified chitosan microspheres. *Journal of Hazardous Materials* **172**(1) (2009) 439–446.

14. Vincent, T., Parodi, A., Guibal, E. Pt recovery using Cyphos IL-101 immobilized in biopolymer capsules. *Separation and Purification Technology* **62**(2) (2008) 470–479.

15. Wang, R., Liao, X., Shi, B. Adsorption Behaviors of Pt(II) and Pd(II) on collagen fiber immobilized bayberry tannin. *Industrial & Engineering Chemistry Research* **44**(12) 2005 4221–4226.

16. Jermakowicz-Bartkowiak, D., Kolarz, B.N., Serwin, A. Sorption of precious metals from acid solutions by functionalised vinylbenzyl chloride–acrylonitryle–divinylbenzene copolymers bearing amino and guanidine ligands. *Reactive and Functional Polymers* **65**(1-2) (2005) 135–142.

17. Shah, R., Devi, S. Preconcentration and separation of palladium(II) and platinum(IV) on a dithizone anchored poly(vinylpyridine)-based chelating resin. *Analytica Chimica Acta* **341**(2-3) (1997) 217–224.

18. Parodi, A., Vincent, T., Pilsniak, M., Trochimczuk, A.W., Guibal, E. Palladium and platinum binding on an imidazol containing resin. *Hydrometallurgy* **92**(1-2) (2008) 1–10.

19. Chassary, P., Vincent, T., Sanchez Marcano, J., Macaskie, L.E., Guibal, E. Palladium and platinum recovery from bicomponent mixtures using chitosan derivatives. *Hydrometallurgy* **76**(1-2) (2005) 131–147.

20. Yi-Yong, C., Xing-Zhong, Y. Synthesis and properties of 1-(2-aminoethyl)piperazine resin used in the sorption of the platinum group and gold ions. *Reactive Polymers* **23**(2-3) (1994) 165–172.

21. Koch, K.R., Miller, J.D.S., 2000. *A polymeric or oligomeric compound and its uses in absorption processes*. South Africa. PCT/WO2000/53663

22. Reneker, D.H., Chun, I. Nanometer diameter fibers of polymer, produced by electrospinning. *Nanotechnology* **7**(3) (1996) 216–223.

23. Ryu, Y.J., Kim, H.Y., Lee, K.H., Park, H.C., Lee, D.R. Transport properties of electrospun nylon 6 nonwoven mats. *European Polymer Journal* **39**(9) (2003) 1883–1889.

24. Chen, Z., Foster, M.D., Zhou, W., Fong, H., Reneker, D.H., Resendes, R., Manners, I. Structure of poly(ferrocenyldimethylsilane) in electrospun nanofibers. *Macromolecules* **34**(18) (2001) 6156–6158.

25. Chronakis, I.S., 2009. Micro-/nano-fibers by electrospinning technology: processing, properties and applications. In: Y. Qin, ed. 2009. *Micromanufacturing Engineering and Technology*. Boston: William Andrew Publishing. pp. 264–286.

26. Frenot, A., Chronakis, I.S. Polymer nanofibers assembled by electrospinning. *Current Opinion in Colloid & Interface Science* **8**(1) (2003) 64-75.

27. Pham, Q.P., Sharma, U., Mikos, A.G. Electrospinning of polymeric nanofibers for tissue engineering applications: A review. *Tissue engineering* **12**(5) (2006) 1197–1211.

28. Alamein, M.A., Liu, Q., Stephens, S., Skabo, S., Warnke, F., Bourke, R., Heiner, P., Warnke, P.H., 2012. Nanospiderwebs: Artificial 3D extracellular matrix from nanofibers by novel clinical grade electrospinning for stem cell delivery. *Advanced Healthcare Materials*, [online]. Available at: http://doi.wiley.com/10.1002/adhm.201200287 [Accessed 5 Novermber 2012].

29. Smit, A.E., Sanderson, R.D., 2011. *Method and apparatus for the production of fine fibres*. U.S. Pat. 2011/0156321 A1

30. Soldatov, V.S., Shunkevich, A.A., Elinson, I.S., Johann, J., Iraushek, H. Chemically active textile materials as efficient means for water purification. *Desalination* **124**(1-3) (1999) 181–192.

31. Saeed, K., Haider, S., Oh, T-J., Park, S-Y. Preparation of amidoxime-modified polyacrylonitrile (PAN-oxime) nanofibers and their applications to metal ions adsorption. *Journal of Membrane Science* **322**(2) (2008) 400–405.

32. Ki, C.S., Gang, E.H., Um, I.C., Park, Y.H. Nanofibrous membrane of wool keratose/silk fibroin blend for heavy metal ion adsorption. *Journal of Membrane Science* **302**(1-2) (2007) 20–26.

33. Cawthorn, R.G. The platinum and palladium resources of the Bushveld Complex. *South African Journal of Science* **95**(11/12) (1999) 481–489.

34. Swanepoel, E., 2009. Demand to outstrip platinum supply between 2010 and 2016 - Platinum Australia. *Mining Weekly.com*, [online], 03 September. Available at: <http://www.miningweekly.com/article/platinum-demand-to-outstrip-supply-between-2010-and-2016---platinum-australia-2009-09-03> [Accessed on 04 November 2012]

35. Royal Bafokeng Platinum, n.d. *Mining and processing of PGMs*, [online]. Available at: <http://www.bafokengplatinum.co.za/b/process.php> [Accessed 03 November 2012]

36. Johnson Matthey, n.d. *Production - South Africa*, [online]. Available at: <http://www.platinum.matthey.com/production/south-africa/> [Accessed 03 November 2012]

37. UNCTAD, n.d. *Platinum*, [online]. Available at: <http://r0.unctad.org/infocomm/anglais/platinum/chain.htm> [Accessed 03 November 2012]

38. Phetla, T., Muzenda, E., Belaid, M. A Study of the variables in the optimisation of a platinum precipitation process. *World Academy of Science, Engineering and Technology* **45** (2010) 248–254.

39. Bruce, J., 2005. *Potentially fluorescent ligands based on the N,N-dialkyl-N'-aroylthiourea motif and their Pt(II) and Pd(II) compexes*. M.Sc. University of Stellenbosch.

40. Zhang, H., Nie, H., Yu, D., Wu, C., Zhang, Y., White, C.J.B., Zhu, L. Surface modification of electrospun polyacrylonitrile nanofiber towards developing an affinity membrane for bromelain adsorption. *Desalination* **256**(1-3) (2010) 141–147.

41. Smith, B.F., 1993. *Actinide separations for advanced processing of nuclear waste: annual report 1993*. Los Alamos, N.M.: Los Alamos National Laboratory.

42. Asongwe, L.A.T., 2008. *Development of a synthetic affinity membrane for the purification of recombinant maltose binding proteins*. M.Sc. University of Stellenbosch.

43. Opitz, L., Lehmann, S., Reichl, U., Wolff, M.W. Sulfated membrane adsorbers for economic pseudo-affinity capture of influenza virus particles. *Biotechnology and Bioengineering* **103**(6) (2009) 1144–1154.

44. Kasaini, H., Goto, M., Furusaki, S. Adsorption performance of activated carbon pellets immobilized with organophosphorus extractants and an amine : A case study for the separation of Pt (IV), Pd (II), and Rh (III) ions in chloride media. *Separation Science and Technology* **36**(13) (2001) 2845–2861.

45. Bourne, S., Koch, K.R. Intramolecular hydrogen-bond controlled unidentate co-ordination of potentially chelating *N*-acyl-*N*'-alkyl-thioureas: Crystal structure of cis-bis(*N*-benzoyl-*N*'-propylthiourea)dichloroplatinum(II). *Journal of the Chemical Society, Dalton Transactions* **13** (1993) 2071–2072.

46. Mautjana, A.N., Miller, J.D.S., Gie, A., Bourne, S.A., Koch, K.R. Tailoring hydrophilic *N,N*-dialkyl-*N*'-acylthioureas suitable for Pt(II), Pd(II) and Rh(III) chloride pre-concentration from acid aqueous solutions , and their complex separation by reversed-phase HPLC. *Dalton Transactions* **10** (2003) 1952–1960.

47. Koch, K.R. New chemistry with old ligands: *N*-alkyl- and *N*,*N*-dialkyl-*N*'-acyl(aroyl)thioureas in co-ordination, analytical and process chemistry of the platinum group metals. *Coordination Chemistry Reviews* **216-217** (2001) 473–488.

48. Yoshimatsu, K., Ye, L., Lindberg, J., Chronakis, I.S. Selective molecular adsorption using electrospun nanofiber affinity membranes. *Biosensors and Bioelectronics* **23**(7) (2008) 1208–1215.

49. Adhikari, C.R., Parajuli, D., Inoue, K., Ohto, K., Kawakita, H., Harada, H. Recovery of precious metals by using chemically modified waste paper. *New Journal of Chemistry* **32**(9) (2008) 1634–1641.

50. Silva, R.F., Passerini, S., Pozio, A. Solution-cast Nafion®/montmorillonite composite membrane with low methanol permeability. *Electrochimica Acta* **50**(13) (2005) 2639–2645.

51. Klein, E. Affinity membranes: a 10-year review. *Journal of Membrane Science* **179**(1-2) (2000) 1–27.

52. Suresh, B.R., Ramaseshan, R., Liu, Y., Sundarrajan, S., Lala, N.L., Ramakrishna, S., 2007. Nanotechnology for protection from chemical and biological warfare agents: separation and decontamination aspects. In: J.V. Borrelli, ed. 2007. *Bioterrorism: prevention, preparedness and protection*. New York: Nova Science Publishers, pp83–123.

53. Fabbricante, A.S., Fabbricante, T.J., Najour, G.C., 1997. *Disposable extrusion apparatus with pressure balancing modular die units for the production of nonwoven webs*. U.S. Pat. 5,679,379.

54. Fabbricante, A.S., Ward, G.F., Fabbricante, T.J., 2000. *Micro-denier nonwoven materials made using modular die units*. U.S. Pat. 6,114,017.

55. Pike, R.D., Kimberly-Clark Worldwide International, 1999. *Superfine microfiber nonwoven web*. U.S. Pat. 5,935,883.

56. Hagewood, J., Wilkie, A., n.l. *Production of sub-micron fibers in non-woven fabrics*, [online]. Available at: <http://www.hillsinc.net/> [Accessed 22 September 2012]

57. Wilkie, A., n.l. *Multi-component fiber technology for medical and other filtration applications*, [online]. Available at: <http://www.hillsinc.net/> [Accessed 22 September 2012]

58. Formhals, A., 1934. *Process and apparatus for preparing artificial threads*. U.S. Pat. 1975504.

59. Cooley, J.F., 1902. *Apparatus for electrically dispersing fluids*. U.S. Pat. 692,631.

60. Morton, W.J., 1902. *Method of dispersing fluids*. U.S. Pat. 705,691.

61. Doshi, J., Reneker, D.H. Electrospinning process and applications of electrospun fibers. *Journal of Electrostatics* **35**(2-3) (1995) 151–160.

62. Taylor, G. Electrically Driven Jets. *Proceedings of the Royal Society of London A: Mathematical and Physical Sciences* **313**(1515) (1969) 453–475.

63. Yarin, A.L., Koombhongse, S., Reneker, D.H. Taylor cone and jetting from liquid droplets in electrospinning of nanofibers. *Journal of Applied Physics* **90**(9) (2001) 4836–4846.

64. Garg, K., Bowlin, G.L. Electrospinning jets and nanofibrous structures. *Biomicrofluidics* **5**(1) (2011) 013403/1–013403/19.

65. Feng, J.J. The stretching of an electrified non-Newtonian jet: A model for electrospinning. *Physics of Fluids* **14**(11) (2002) 3912–3926.

66. Carroll, C.P., Yong, L.J. Electrospinning of viscoelastic Boger fluids: Modeling and experiments. *Physics of Fluids* **18**(5) (2006) 53102–1– 53102–14.

67. Reneker, D.H., Yarin, A.L., Zussman, E., Xu, H. Electrospinning of nanofibers from polymer solutions and melts. *Advances in Applied Mechanics* **41** (2007) 43–195.

68. Laud, B.B., 1987. *Electromagnetics*, 2nd ed. New Delhi: New Age International Ltd.

69. Yarin, A., Koombhongse, S., Reneker, D.H. Bending instability of electrically charged liquid jets of polymer solutions in electrospinning. *Journal of Applied Physics* **89**(5) (2001) 3018–3026.

70. Mitchell, S.B., Sanders, J.E. A unique device for controlled electrospinning. *Journal of Biomedical Materials Research Part A* **78A**(1) (2006) 110–120.

71. Theron, S.A., Yarin, A.L., Zussman, E., Kroll, E. Multiple jets in electrospinning: experiment and modeling. *Polymer* **46**(9) (2005) 2889–2899.

72. Carnell, L.S., Siochi, E.J., Holloway, N.M., Stephens, R.M., Rhim, C., Niklason, L.E., Clark, R.L. Aligned mats from electrospun single fibers. *Macromolecules* **41**(14) (2008) 5345–5349.

73. Liu, C-K., Chen, M-Y., Sun, R-J., Zhang, W-H., Zhang, Z-H., Yao, M. Experimental investigation on the multiple jets from a single droplet by electrospinning. *Advanced Materials Research* **129-131** (2010) 365–369.

74. Fong, H., Reneker, D.H., 2001. Electrospinning and the formation of nanofibers. In: D.R. Salem, ed. *Structure formation in polymeric fibers*. Princeton, NJ: Hanser Gardner Publications, Inc., pp225–246.

75. Petrik, S., Maly, M. Production nozzle-less electrospinning nanofiber technology. *Materials Research Society Proceedings* **1240** (2009).

76. Chowdhury, M., Stylios, G. Effect of experimental parameters on the morphology of electrospun Nylon 6 fibres. *International Journal of Basic & Applied Sciences* **10**(6) (2010) 116–131.

77. Ding, W., Wei, S., Zhu, J., Chen, X., Rutman, D., Guo, Z. Manipulated electrospun PVA nanofibers with inexpensive salts. *Macromolecular Materials and Engineering* **295**(10) (2010) 958–965.

78. Hardick, O., Stevens, B., Bracewell, D. Nanofiber fabrication in a temperature and humidity controlled environment for improved fibre consistency. *Journal of Material Science* **46**(11) (2011) 3890–3898.

79. Kim, S.J., Lee, C.K., Kim, S.I. Effect of ionic salts on the processing of poly(2-acrylamido-2-methyl-1-propane sulfonic acid) nanofibers. *Journal of Applied Polymer Science* **96**(4) (2005) 1388–1393.

80. Mit-uppatham, C., Nithitanakul, M., Supaphol, P. Ultrafine electrospun polyamide-6 fibers: Effect of solution conditions on morphology and average fiber diameter. *Macromolecular Chemistry and Physics* **205**(17) (2004) 2327–2338.

81. Ebbing, D.D., Gammon, S.D., 2007. *General Chemistry*, 9th ed. Belmont, CA: Cengage Learning Inc.

82. Chawla, K.K., 1998. *Composite materials: science and engineering*, 2nd ed. New York: Springer Science & Business Media Inc.

83. Lim, Y., Gwon, H., Jeun, J.P., Nho, Y., 2010. Preparation of cellulose-based nanofibers using electrospinning. In: A. Kumar, ed. *Nanofibres*. Vukovar: InTech, pp179–188.

84. Ramakrishna, S., Fujihara, K., Teo, W-E., Lim, T-C., Ma, Z.. 2005. *An introduction to electrospinning and nanofibers*. Singapore: World Scientific Publishing Co.

85. Koombhongse, S., Liu, W., Reneker, D.H. Flat polymer ribbons and other shapes by electrospinning. *Journal of Polymer Science Part B: Polymer Physics* **39**(21) (2001) 2598–2606.

86. Fong, H., Chun, I., Reneker, D.H. Beaded nanofibers formed during electrospinning. *Polymer* **40**(16) (1999) 4585–4592.

87. Subbiah, T., Bhat, G.S., Tock, R.W., Parameswaran, S., Ramkumar, S.S. Electrospinning of nanofibers. *Journal of Applied Polymer Science* **96**(2) (2005) 557–569.

88. Lin, T., Wang, H., Wang, H., Wang, X. The charge effect of cationic surfactants on the elimination of fibre beads in the electrospinning of polystyrene. *Nanotechnology* **15**(9) (2004) 1375–1381.

89. Baumgarten, P.K. Electrostatic spinning of acrylic microfibers. *Journal of Colloid and Interface Science* **36**(1) (1971) 71–79.

90. Stanishevsky, A., Chowdhury, S., Chinoda, P., Thomas, V. Hydroxyapatite nanoparticle loaded collagen fiber composites: Microarchitecture and nanoindentation study. *Journal of Biomedical Materials Research Part A* **86A**(4) (2008) 873–882.

91. Sun, Z., Knopf, J., Deitzel, J.M., Gillespie, J.W.J. Drawing of spatially oriented electrospun fibers. *ASME Conference Proceedings* (43840) (2009) 333–337.

92. Toncheva, A., Spasova, M., Paneva, D., Manolova, N., Rashkov, I. Drug-loaded electrospun polylactide bundles. *Journal of Bioactive and Compatible Polymers* **26**(2) (2011) 161–172.

93. Sundaray, B., Subramanian, V., Natarajan, T., Xiang, R., Chang, C., Fann, W. Electrospinning of continuous aligned polymer fibers. *Applied Physics Letters* **84**(7) (2004) 1222–1224.

94. Medeiros, E.S., Mattoso, L.H.C., Offeman, R.D., Wood, D.F., Orts, W.J. Effect of relative humidity on the morphology of electrospun polymer fibers. *Canadian Journal of Chemistry* **86**(6) (2008) 590–599.

95. Wang, C., Chien, H-S., Hsu, C-H., Wang, Y-C., Wang, C-T., Lu, H-A. Electrospinning of polyacrylonitrile solutions at elevated temperatures. *Macromolecules* **40**(22) (2007) 7973–7983.

96. De Vrieze, S., Van Camp, T., Nelvig, A., Hagström, B., Westbroek, P., De Clerck, K. The effect of temperature and humidity on electrospinning. *Journal of Materials Science* **44**(5) (2009) 1357–1362.

97. Andrady, A.L., Ensor, D.S., 2010. *Electrospray/electrospinning apparatus and method*. U.S Pat. 7762801.

98. Demir, M.M. Investigation on glassy skin formation of porous polystyrene fibers electrospun from DMF. *eXPRESS Polymer Letters* **4**(1) (2010) 2–8.

99. McKee, M.G., Hunley, M.T., Layman, J.M., Long, T.E. Solution rheological behavior and electrospinning of cationic polyelectrolytes. *Macromolecules* **39**(2) (2006) 575–583.

100. Kong, C.S., Lee, T.H., Lee, S.H., Kim, H.S. Nano-web formation by the electrospinning at various electric fields. *Journal of Materials Science* **42**(19) (2007) 8106–8112.

101. MacDiarmid, A.G., Jones Jr., W.E., Norris, I.D., Gao, J., Johnson Jr., A.T., Pinto, N.J., Hone, J., Han, B., Ko, F.K., Okuzaki, H., Llanguno, M. Electrostatically-generated nanofibers of electronic polymers. *Proceedings of the International Conference on Science and technology of Synthetic Metals* **119**(1-3) (2001) 27–30.

102. Yang, C., Jia, Z., Xu, Z., Wang, K., Guan, Z., Wang, L. Comparisons of fibers properties between vertical and horizontal type electrospinning systems. *Electrical Insulation and Dielectric Phenomena*, *2009* (2009) 204–207.

103. Sun, Z., Zussman, E., Yarin, A.L., Wendorff, J.H., Greiner, A. Compound core-shell polymer nanofibers by co-electrospinning. *Advanced Materials* **15**(22) (2003) 1929–1232.

104. Kriel, H., Sanderson, R.D., Smit, A. Coaxial electrospinning of miscible PLLA-core and PDLLA-shell solutions and indirect visualisation of the core-shell fibres obtained. *Fibres and textiles in Eastern Europe* **20**(2) (2012) 28–33.

105. Teo, W.E., Ramakrishna, S. A review on electrospinning design and nanofibre assemblies. *Nanotechnology* **17**(14) (2006) R89–R106.

106. Zhou, F-L., Gong, R-H., Porat, I. Mass production of nanofibre assemblies by electrostatic spinning. *Polymer International* **58**(4) (2009) 331–342.

107. Yamashita, Y. Current state of nanofiber produced by electrospinning and prospects for mass production. *Journal of Textile Engineering* **54**(6) (2008) 199–205.

108. Ding, B., Kimura, E., Sato, T., Fujita, S., Shiratori, S. Fabrication of blend biodegradable nanofibrous nonwoven mats via multi-jet electrospinning. *Polymer* **45**(6) (2004) 1895–1902.

109. Yarin, A.L., Zussman, E. Upward needleless electrospinning of multiple nanofibers. *Polymer* **45**(9) (2004) 2977–2980.

110. Kishimoto, Y., 2008. *Process for producing microfiber assembly*. Japan. PCT/WO2008/010307.

111. Ren, Z-F., He, J-H. Single polymeric bubble for the preparation of multiple micro/nano fibers. *Journal of Applied Polymer* Science **119**(2) (2011) 1161–1165.

112. Liu, Y., He, J-H. Bubble electrospinning for mass production of nanofibers. *International Journal of Nonlinear Sciences and Numerical Simulation* **8**(3) (2007) 393–396.

113. Jirsak, O., Sanetrnik, F., Lukas, D., Kotek,V., Martinova, L., Chaloupek, J., 2009. *A method of nanofibers production from a polymer solution using electrostatic spinning and a device for carrying out the method*. U.S. Pat. 7,585,437 B2.

114. Petrik, S., Maly, M., Rubacek, L., Macak, J., Stranska, D., Duchoslav, J., Coppe, A., 2009. Electrospun nanofiber: The tiny layers that add great value to nonwovens. *Stockholm: International Nonwovens Symposium*, [online]. Available at: <http://www.elmarco.cz/upload/soubory/dokumenty/76-1-3-nw-symp-stockholm-09.pdf> [Accessed 04 November 2012].

115. Duchoslav, J., Rubacek, L., Kavan, L., Zukalova, M., Prochazka, J., 2008. Electrospun TiO_2 fibers as a material for dye sensitized solar cells. *Boston: NSTI BioNano: Bio-Nanotechnology Conference and Trade Show*, [online]. Available at: <http://www.elmarco.com/upload/soubory/dokumenty/105-1-4-electrospun-tio2-fibers-as-a-material-for-dye-sensitizied-solar-cells.pdf> [accessed 04 November 2012]

116. Sambaer, W., Zatloukal, M., Kimmer, D. 3D modeling of filtration process via polyurethane nanofiber based nonwoven filters prepared by electrospinning process. *Chemical Engineering Science* **66**(4) (2011) 613–623.

117. Cengiz, F., Jirsak, O. The effect of salt on the roller electrospinning of polyurethane nanofibers. *Fibers and Polymers* **10**(2) (2009) 177–184.

118. Niu, H., Wang, X., Lin, T., 2011. Needleless electrospinning: developments and performances. In: T. Lin, ed. *Nanofibers - Production, Properties and Functional Applications*. Rijeka:InTech. pp17–36.

119. Jia, H., Zhu, G., Vugrinovich, B., Kataphinan, W., Reneker, D.H., Wang, P. Enzyme-carrying polymeric nanofibers prepared via electrospinning for use as unique biocatalysts. *Biotechnology Progress* **18**(5) (2002) 1027–1032.

120. Demir, M.M., Gulgun, M.A., Menceloglu, Y.Z., Erman, B., Abramchuk, S.S., Makhaeva, E.E., Khokhlov, A.R., Matveeva, V.G., Sulman, M.G. Palladium nanoparticles by electrospinning from poly(acrylonitrile-co-acrylic acid)−$PdCl_2$ solutions. Relations between

preparation conditions, particle size, and catalytic activity. *Macromolecules* **37**(5) (2004) 1787–1792.

121. Graham, K., Gogins, M., Schreuder-Gibson, H. Incorporation of electrospun nanofibers into functional structures. *International Nonwovens Journal* **13**(2) (2004) 21–27.

122. Chronakis, I.S., Jakob, A., Hagström, B., Ye, L. Encapsulation and selective recognition of molecularly imprinted theophylline and 17β-estradiol nanoparticles within electrospun polymer nanofibers. *Langmuir* **22**(21) (2006) 8960–8965.

123. Pinto, N.J., Johnson Jr., A.T., MacDiarmid, A.G., Mueller, C.H., Theofylaktos, N., Robinson, D.C., Miranda, F.A. Electrospun polyaniline/polyethylene oxide nanofiber field-effect transistor. *Applied Physics Letters* **83**(20) (2003) 4244–4246.

124. Kim, C., Yang, K.S. Electrochemical properties of carbon nanofiber web as an electrode for supercapacitor prepared by electrospinning. *Applied Physics Letters* **83**(6) (2003) 1216–1218.

125. Kim, J., Reneker, D.H. Mechanical properties of composites using ultrafine electrospun fibers. *Polymer Composites* **20**(1) (1999) 124–131.

126. Bergshoef, M.M., Vancso, G.J. Transparent nanocomposites with ultrathin, electrospun Nylon-4,6 fiber reinforcement. *Advanced Materials* **11**(16) (1999) 1362–1365.

127. Gibson, P., Schreuder-Gibson, H., Rivin, D. Transport properties of porous membranes based on electrospun nanofibers. *Colloids and Surfaces A: Physicochemical and Engineering Aspects* **187–188** (2001) 469–481.

128. Li, D., Xia, Y. Electrospinning of Nanofibers: Reinventing the Wheel? *Advanced Materials* **16**(14) (2004) 1151–1170.

129. Chemindustry.ru., n.l. *Sodium thiocyanate*. [online], Available at: < http://chemindustry.ru/Sodium_Thiocyanate.php> [Accessed 11 December 2012].

130. Douglass, I.B., Dains, F.B. Some derivatives of benzoyl and furoyl isothiocyanates and their use in synthesizing heterocyclic compounds. *Journal of the American Chemical Society* **56**(3) (1934) 719–721.

131. Seo, J.M., Arumugam, G.K., Khan, S., Heiden, P.A. Comparison of the effects of an ionic liquid and triethylbenzylammonium chloride on the properties of electrospun fibers, 1 - poly(lactic acid). *Macromolecular Materials and Engineering* **294**(1) (2009) 35–44.

132. Nalas Engineering Services, Inc., n.l. *Reaction Engineer*, [online]. Available at: <http://nalasengineering.com/customers/reaction-engineer/> [Accessed 11 December 2012].

133. Crawley, M.L., Trost, B.M., 2012. *Applications of transition metal catalysis in drug discovery and development: An industrial perspective*. Hoboken, NJ:John Wiley & Sons.

134. Miller, J.D., 2000. *Synthesis of* N-*alkyl and* N,N-*dialkyl*-N*'-acyl and* N*'-aroylthioureas, and aspects of their coordination chemistry with Pt(II) and Pd(II)*. M.Sc. University of Cape Town.

135. Whelan, T., 1994. *Polymer Technology Dictionary*. London: Chapman & Hall. p256.

136. Chemicalland21, n.l. *Terephthaloyl chloride*, [online]. Available at: < http://www.chemicalland21.com/specialtychem/perchem/TEREPHTHALOYL%20CHLORIDE.htm> [Accessed 11 December 2012].

137. Cengiz, F., Krucińska, I., Gliścińska, E. Comparative analysis of various electrospinning methods of nanofibre formation. *Fibres and textiles in Eastern Europe* **17**(1) (2009) 13–19.

APPENDIX A

^{1}H and ^{13}C NMR spectra of the reagents used during the *Platisorb* synthesis

The terephthaloyl chloride showed a multiplet in the ^{1}H NMR spectrum observed at 8.00 ppm, which was assigned to the protons on the aromatic ring (shown in Figure A.1). A small amount of moisture in the DMSO-d_6 solvent caused some carboxylic acid groups to form and these groups were the origin of the multiplicity seen in the spectrum. Terephthaloyl chloride showed three peaks in the ^{13}C NMR spectrum: a single peak at 166.7 ppm assigned to the carbonyl, peaks around 135.0 ppm assigned to the aromatic carbons and a peak at 129.6 ppm assigned to the aromatic CH carbons. The spectrum is shown in Figure A.2.

The H^{1} NMR spectrum of piperazine showed two peaks: a sharp peak at 2.59 ppm assigned to the CH_2 protons and a broad peak at 1.99 ppm assigned to the NH protons. The ^{13}C NMR of piperazine showed a single sharp peak at 46.95 ppm, assigned to the chemically equivalent CH_2 carbons.

A ^{13}C NMR analysis of the NaSCN showed a single peak at 130.4 ppm, assigned to the lone carbon of the SCN group.

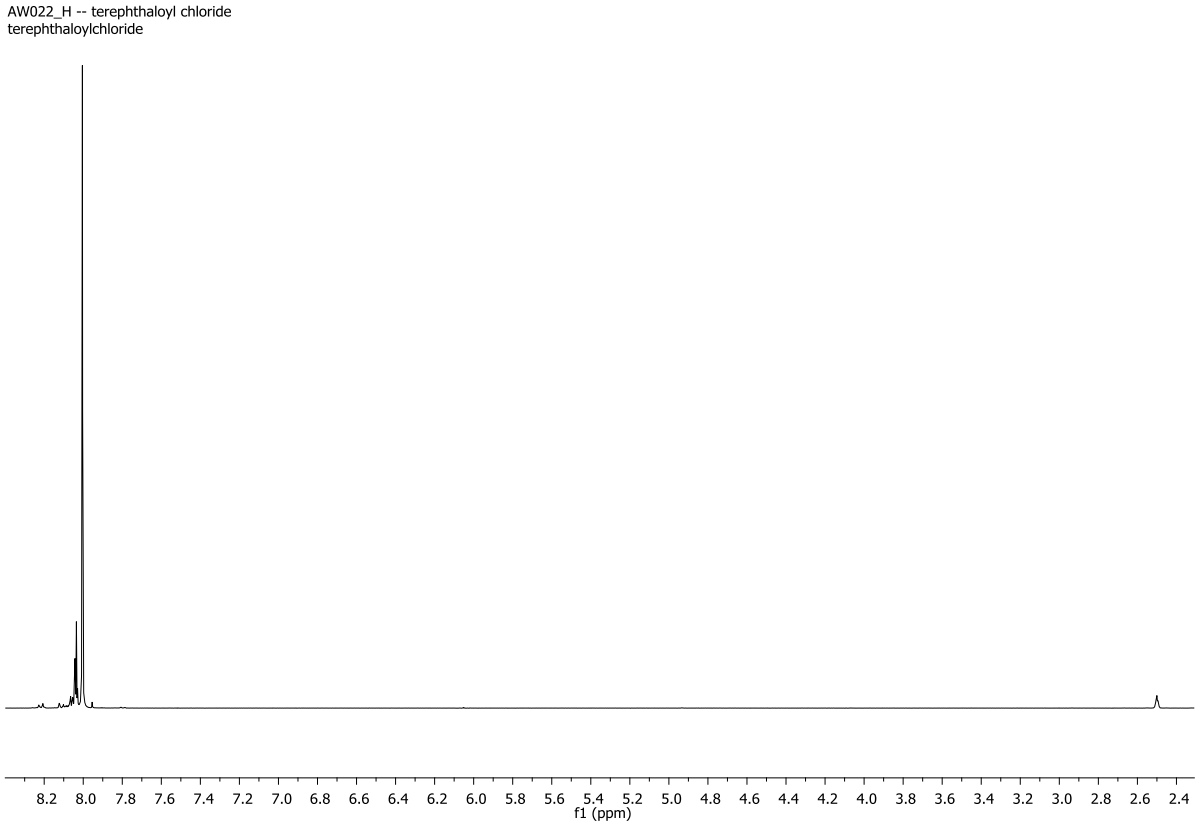

Figure A.1 - ^{1}H NMR spectrum of terephthaloyl chloride.

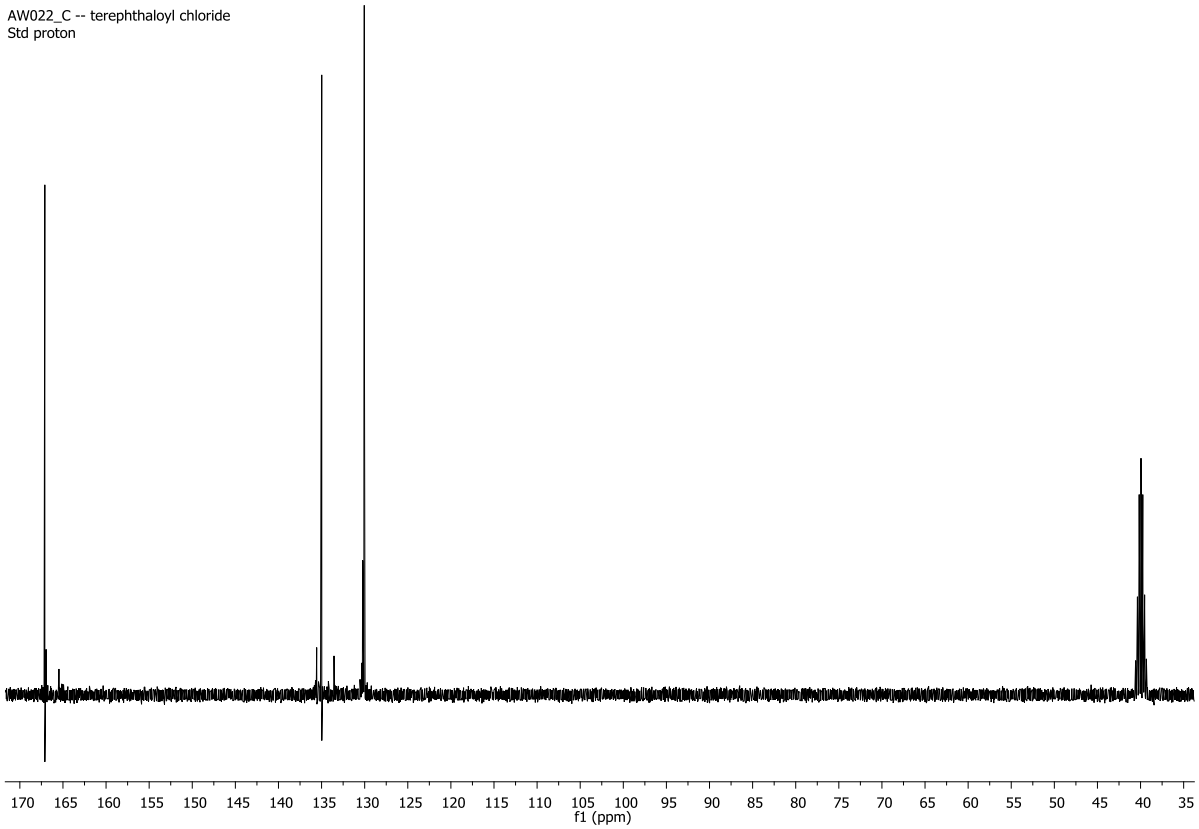

Figure A.2 – ^{13}C NMR spectrum of terephthaloyl chloride.

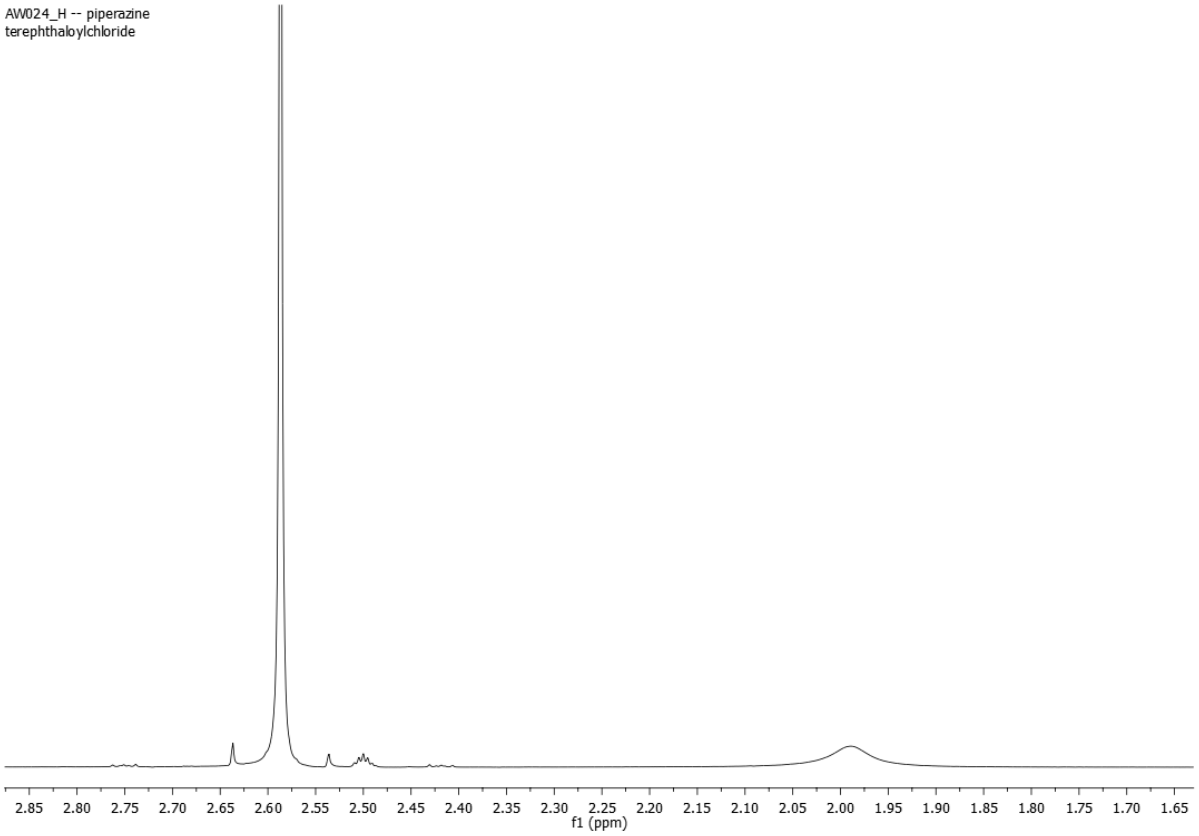

Figure A.3 - ^{1}H NMR spectrum of piperazine.

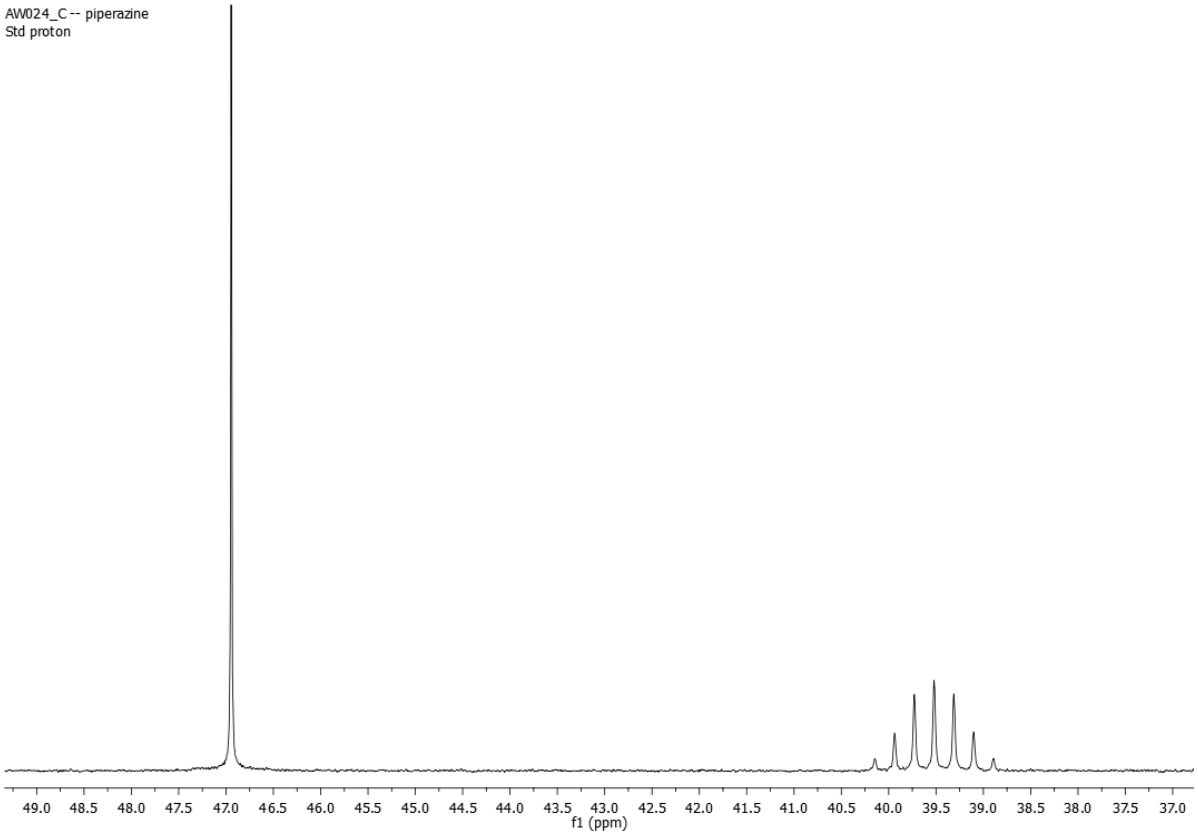

Figure A.4 – ^{13}C NMR spectrum of piperazine.

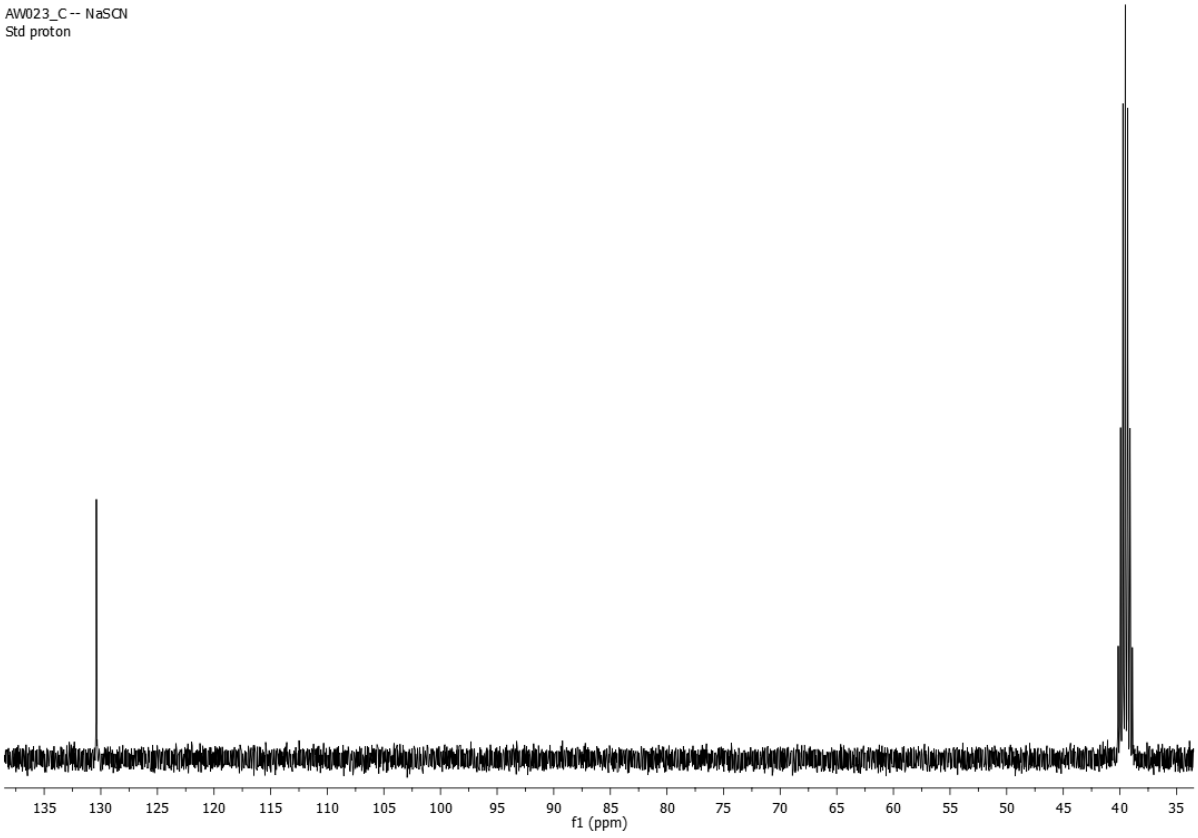

Figure A.5 – ^{13}C NMR spectrum of NaSCN.

APPENDIX B

Sequence of images showing backbuilding during ball electrospinning

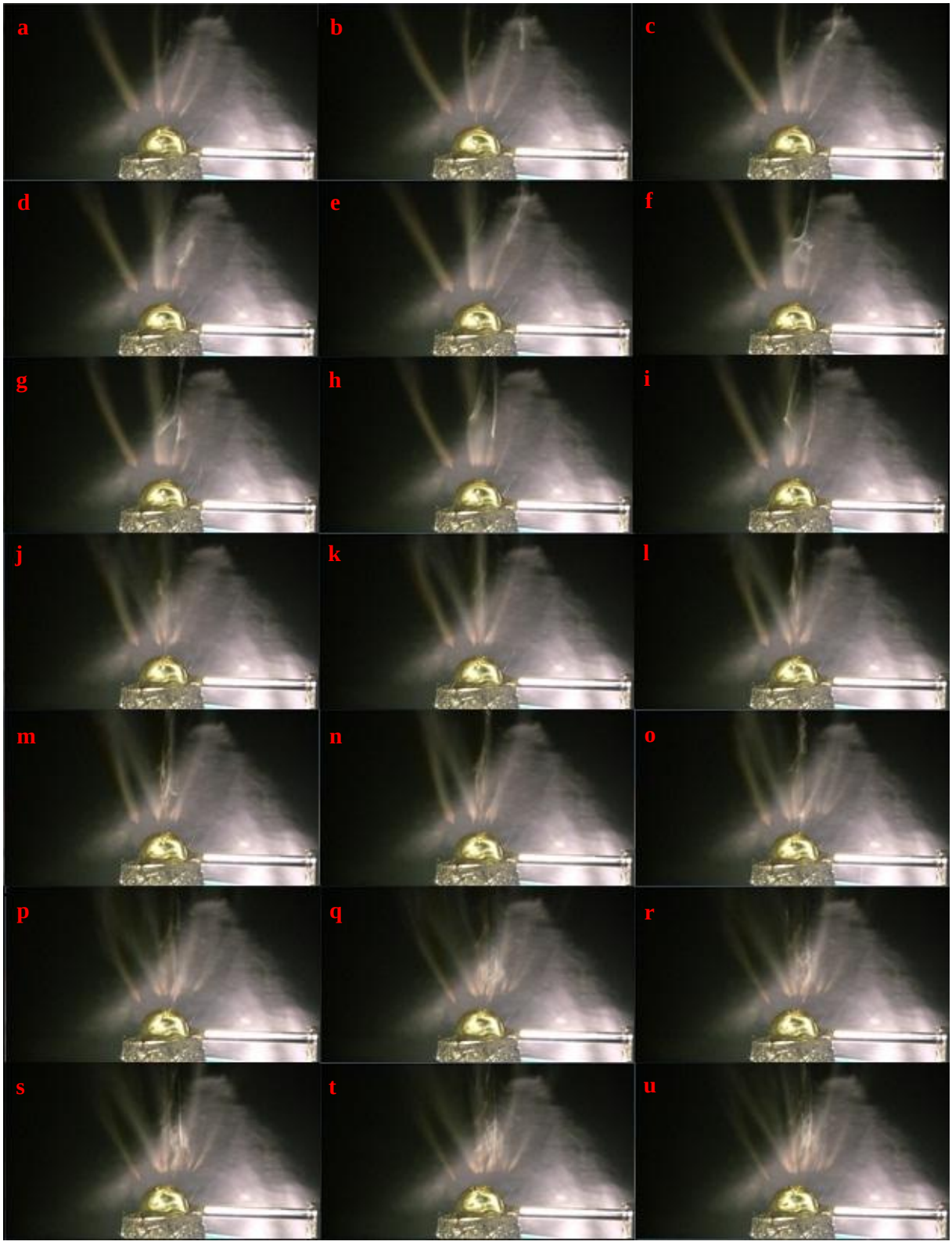

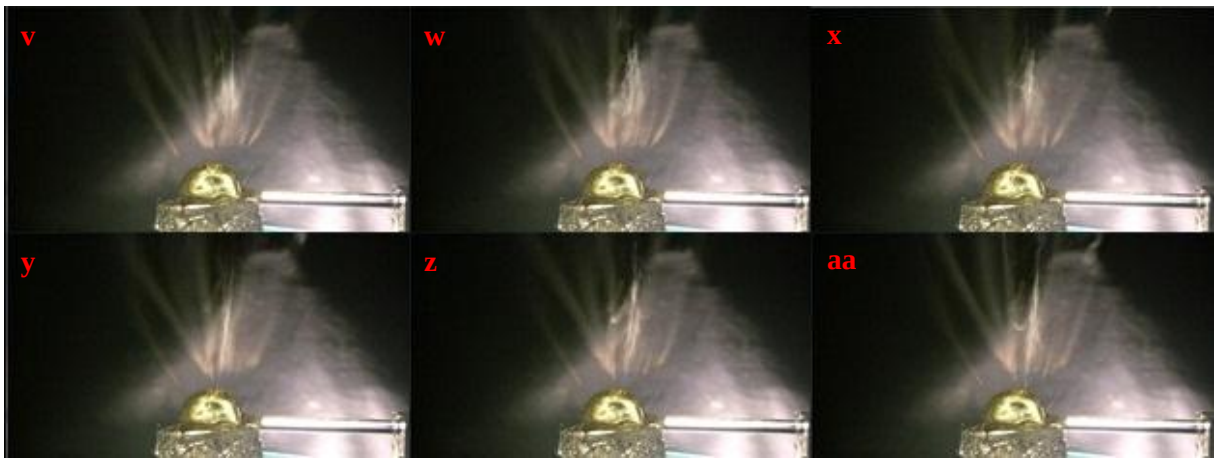

Figure B.1 - Sequence of 27 images **(a** to **aa)** of backbuilding during ball electrospinning. Images were taken at a frame rate of three frames per second and the sequence was taken roughly 3 minutes after the ball electrospinning was initiated. Experimental: Spin solution was 6 wt% PAN with a PAN to *Platisorb* ratio of 7:3. Effective spin distance was 10 cm to a collector rotating with a surface speed of 200 m/min.